Distributed dynamics of influx during MPD operations : modelling and estimation

Naveen Velmurugan

PSL UNIVERSITÉ PARIS

THÈSE DE DOCTORAT
DE L'UNIVERSITÉ PSL

Préparée à MINES ParisTech

Modélisation et estimation de la dynamique des flux du réservoir dans les opérations de forage

Distributed dynamics of influx during MPD operations : modelling and estimation

Soutenue par
Naveen VELMURUGAN
Le 30 juin 2020

École doctorale n°621
Ingénierie des Systèmes, Matériaux, Mécanique, Energétique (ISMME)

Spécialité
Mathématique et Automatique

Composition du jury :

M. Gildas BESANÇON Professeur, GIPSA Lab, Grenoble-INP	*Président*
M. Jan Tommy GRAVDAHL Professeur, Dept of Cybernetics, NTNU	*Rapporteur*
Mme. Sihem TEBBANI Professeur, CentraleSupélec	*Examinateur*
Mme. Liv Almås CARLSEN Ingénieur de recherche, NORCE	*Examinateur*
M. Florent DI MEGLIO Maître-assistant, MINES ParisTech	*Co-directeur de thèse*
M. Nicolas PETIT Professeur, MINES ParisTech	*Directeur de thèse*

MINES ParisTech | PSL

MINES PARISTECH

DOCTORAL THESIS

Distributed Dynamics of Influx During MPD Operations : Modelling and Estimation

Author:
Naveen VELMURUGAN

Supervisors:
Florent DI MEGLIO
Nicolas PETIT

A thesis submitted in fulfillment of the requirements for the degree of Philosophiae Doctor

Mathematics and Control

Centre Automatique et Systèmes

30 June, 2020

MINES PARISTECH

DOCTORAL THESIS

Distributed Dynamics of Influx During MPD Operations : Modelling and Estimation

Author:
Naveen VELMURUGAN

Supervisors:
Florent DI MEGLIO
Nicolas PETIT

This research has been carried out in the HYDRA[1] project, which has received funding from the European Union's Horizon 2020 research and innovation programme under grant agreement Nº 675731.

The consortium included Eindhoven University of Technology (TUe), MINES ParisTech and an industrial partner Kelda Drilling Controls AS.

[1] **HY**draulic modelling for **DR**illing **A**utomation

"Jarvis, sometimes you gotta run before you can walk."

Tony Stark

"Change alone is unchanging."

Heraclitus

To my parents, my brother
and me.

Abstract

Naveen VELMURUGAN

Distributed Dynamics of Influx During MPD Operations :
Modelling and Estimation

Lors du forage d'un puits de pétrole, il est courant de subir un influx non désiré de fluides provenant du réservoir. Ce manuscrit porte sur l'étude de la dynamique de l'écoulement en résultant dans le réservoir et le puits, pendant les opérations de forage à pression contrôlée (MPD en Anglais). La modélisation repose sur des équations de conservation, qui débouchent sur un modèle d'écoulement biphasique appelé modèle à dérive de flux. Celui-ci prend la forme d'un système hyperbolique d'équations de transport, alors que l'évolution de la pression dans le réservoir suit une dynamique gouvernée par une équation parabolique de diffusion. Nous proposons des schémas numériques permettant d'approcher les solutions de ces deux systèmes dynamiques. Nous synthétisons ensuite des observateurs permettant d'estimer le débit entrant depuis le réservoir. Ces observateurs du système couplé puits-réservoir prennent des formes différentes selon que le caractère distribué de chacune des dynamiques (puits ou réservoir) est négligé ou non. Nos estimateurs reposent sur la mesure de la pression en tête du puits, où un capteur est systématiquement installé dans les opérations de forage à pression contrôlée. L'existence d'un capteur de pression installé au fond du puits, plus rare, modifie la synthèse d'observateurs, d'une manière que nous détaillons. Pour chaque observateur, nous montrons la convergence des estimations de pression et de débit distribués vers leurs valeurs théoriques.

While drilling an oil and gas well, unwanted influx of fluids from the reservoir may occur. This manuscript studies the dynamics of the resulting fluid flow in the wellbore and the reservoir, during managed pressure drilling (MPD) operations. We study the phenomena using first-principle approach that leads to a modified two phase flow model called the drift-flux model (DFM). The model takes the form of a hyperbolic system of transport equations, whereas the reservoir pressure dynamics is given by a parabolic diffusion equation. We propose appropriate numerical schemes for both. Then, we propose different observer designs to estimate the influx from the reservoir into the wellbore. The observers for the coupled wellbore-reservoir system take different forms, as we combine the distributed and the reduced order models for each system. We propose to use the choke pressure as a measurement that is typically available on a MPD operational site, i.e., topside sensing. However, availability of the bottom hole pressure modifies the observer design, in ways we detail. We show convergence of the observers to the true values of reservoir pore pressure and influx, in each case.

Acknowledgements

I would like to extend my deepest gratitude to my advisor Florent Di Meglio, for his unparalleled support and teachings through these years of the project. I'm greatly indebted to the profound belief and the confidence he entrusted on me. His patience and consideration for the learning process cannot be overstated. He has played a monumental role in recognizing and nurturing the (tiny bit of a) researcher in me. I fail to express by words the admiration I have for him in multitude ways. This manuscript would not have been possible without the consistent guidance, the uplifting conversations and the ethic of working with an intellectual rigour that Florent has instilled in me. It has been an immensely pleasureful experience working with him, and I would dearly miss it being the routine. I would not miss a chance to collaborate with him again.

I would like to express my deepest appreciation to the defense committee that comprised of Gildas Besançon, who kindly agreed to be the president and provided valuable remarks to improve this manuscript; Jan Tommy Gravdahl who has given constructive feedback about the manuscript; Sihem Tebbani and Liv Almås Carlsen who have provided their support and participation. Though the defense presentation took place under a special arrangement (i.e., via video conferencing), the committee has left me with a whole-sum experience. I'm grateful for the enthusiastic discussions with the committee that has helped bring the best in me to reflect upon this work.

I'm extremely grateful to Nicolas Petit, for being a part of the defense committee and also to have provided an amazing ecosystem at the Centre Automatique et Systèmes (CAS) of MINES ParisTech. I cannot express enough how much the accommodating, kind and flexible work culture that he maintains at CAS has helped me be at ease and comfortable. My sincere thanks to all the members of CAS. My special thanks to Jean and Charles-Henri (Chucky), whom I look forward to in the academia and the entrepreneurial world respectively. Many thanks to Pierre-Olivier, Aurélien and Nils for the innumerous coffee sessions. Thanks should also go to Delphine Bresch-Pietri, Pauline Bernard, Philippe Martin and Pierre-Cyril for all the wonderful (and sometimes, scientific) conversations. I very much appreciate the company of Matthieu, Mona and Dilshad at work and during the travel to conferences. A very special thanks to Pierre Six for not only being the first to teach me French during my early days in Paris but for also to become my associate in the journey of entrepreneurship. I would like to extend my sincere thanks to Leobardo with whom I had the pleasure of working, initiated during his visit to CAS. *J'aimerais exprimer ici mes plus sincères remerciements pour les merveilleux moments que j'ai passés au CAS. A tous les membres de l'équipe : j'ai profondément aimé travailler avec chacun de vous.*

I cannot begin to express my thanks to all the members of HYDRA project. A seamless coordination and research organization of this project would not have been possible without the calm, composed and poised leadership of Nathan van de Wouw. He has played a vital role in managing the team and I'm grateful for the the knowledge and the experience he has shared in multiple fronts. I'm extremely greateful to Wil Schilders, Bart Basselink, Laura Iapichino and Ulf Jakob for sharing

their insights, thoughtful advices and constructive criticisms during this project. I would like to extend my gratitude to my colleagues Mohammad and Sajad. It has been a joyful experience and a pleasure to have known them, their culture; travel, learn and work with them. I very much appreciate the synergy that we established to bring this project to a fruitful conclusion. My thanks to Harshit for his collaboration during various phases of this project. I would also like to thank the well control instructor Jan Willem Flamma. My sincere thanks to Yann Le Gorrec and Emmanuel Witrant for their courses.

I would also like to express my deepest gratitude to Glenn-Ole Kaasa. He has been an aspiration for me to become the type of CEO who has an unwavering knowledge of the advanced technical concepts; can envision commercialising products from translational research projects and can manage a great team, all in parallel. My sincere thanks to Christian and Jon Åge. I have had the great pleasure of working with them and I gratefully acknowledge all the support they have provided me in understanding various scientific concepts and industrial practices. Thanks also to Geir Arne, Vinicius, Louis, Pål and Martin for their support. I would like to recognize the assistance of Linn and Marcela in all the administrative matters. I cannot thank enough the team at Kelda for the warm reception they offered me during each secondment to Norway. Thanks should also go to Hassan and all the interns at Kelda, who have shared cordial moments; a special mention to Micheal. *Norge ligger tett til mitt hjerte. Det har gitt meg så mange gode opplevelser gjennom årene. Jeg takker alle som har vært med på reisen min i de siste årene. Tusen hjertelig takk alle på Kelda. Tusen takk til Norge, du er vakker! Og endlig, takk for meg.*

I would always rejoice my stay in Paris and the people who particularly made that possible were my friends Gautham and Yamini. A special and heartfelt thanks to Particia, who played a part. Similarly, my stay in Porsgrunn wouldn't have been as exciting without the invaluable company of Abdul, for which I'm always indebted to him and his dear family. A special thanks to Maria the baby girl, for the cute bond and all the fond memories together. Trondheim has always been close to my heart and also the place where this journey has begun, many thanks to Meenu (Mami), Aravinth (Aafa) and Mani (MK) for sharing my joy and excitement. I cannot close without mentioning, Mirka who has been greeting me with her smile and coffee since my first day at CAS. Many thanks to Florence as well.

Last but not least, I thank dearly my mom Suzatha, my dad Velmurugan and my brother Dhacsheen. They have been extremely supportive of all my pursuits in life. They have shown me and stood by what it means to be a family, I'm always deeply indebted to all of them. I'm extremely grateful to our efforts and sacrifices through all these years that has made it possible to write this note to them while concluding my terminal degree.

Finally, I'm also grateful to the events, opportunities, situations, decisions and forfeits that have influenced my life. I would like to express my sincere thanks to the people whom I met in this journey and have helped me directly or indirectly to achieve this feat.

Naveen Velmurugan

Contents

List of Abbreviations

MPD	**M**anaged **P**ressure **D**rilling
BHCP	**B**ottom **H**ole **C**irculating **P**ressure
NPT	**N**on- **P**roductive **T**ime
HWDP	**H**eavy **W**eight **D**rill **P**ipe
OBM	**O**il **B**ased **M**ud
WBM	**W**ater **B**ased **M**ud
RCD	**R**otating **C**irculation **D**evice
PPT	**P**ore **P**ressure **T**est
FIT	**F**ormation **I**ntegrity **T**est
DST	**D**rill **S**tem **T**est
RFT	**R**epeat **F**ormation **T**ester
PI	**P**roductivity **I**ndex
CTRS	**C**onstant **T**erminal **R**ate **S**olution
LOT	**L**eak- **O**ff **T**est
DFM	**D**rift **F**lux **M**odel
BHA	**B**ottom **H**ole **A**ssembly
EOS	**E**quations **O**f **S**tate
PDE	**P**artial **D**ifferential **E**quation
CFL	**C**ourant **F**reidrichs **L**ewy
FVS	**F**lux **V**ector **S**plitting
HYDRA	**HY**draulic Modelling for **DR**illing **A**utomation
EOR	**E**nhanced **O**il **R**ecovery
GE	**G**rid **E**lements
ODE	**O**rdinary **D**ifferential **E**quation
DAE	**D**ifferential **A**lgebraic **E**quation
TDD	**T**est **D**riven **D**evelopment
GUI	**G**raphical **U**ser **I**nterface
API	**A**pplication **P**rogramming **I**nterface
OOP	**O**bject **O**riented **P**rogramming
SIL	**S**oftware **I**n **L**oop
HIL	**H**ardware **I**n **L**oop
SAT	**S**ite **A**cceptance **T**est
DLL	**D**ynamically **L**oading **L**ibrary
KPI	**K**ey **P**erformance **I**ndicator
ESR	**E**arly **S**tage **R**esearcher

List of Symbols

Area of annulus	A_a	m^2
Area of drillbit nozzles	A_n	m^2
Area of drillstring	A_d	m^2
Bit discharge coefficient	c_d	[-]
Bulk modulus	β	Pa
Choke characteristic function	$G(.)$	[-]
Choke constant	K_c	[-]
Choke opening	Z_c	[-]
Choke pressure, downstream	p_{ds}	Pa
Choke pressure, ODE state	p_c	Pa
Compressibility, for the reservoir system	c	Pa^{-1}
Compressibility / Z - Factor	Z	[-]
Critical pressure	p_c	Pa
Critical temperature	T_c	K
Density of gas	ρ_g	$\mathrm{kg\,m}^{-3}$
Density of liquid	ρ_l	$\mathrm{kg\,m}^{-3}$
Density of mixture	ρ_m	$\mathrm{kg\,m}^{-3}$
Diameter of annulus	D_a	m
Diameter of drillstring	D_d	m
Fanning friction factor	ν	[-]
Length of the wellbore	L, h_L	m
Mass flow rate of backpressure pump	J_{bpp}	$\mathrm{kg\,s}^{-1}$
Mass flow rate of pump	J_p	$\mathrm{kg\,s}^{-1}$
Mass flow rate of reservoir gas	J_f^g	$\mathrm{kg\,s}^{-1}$
Mass flow rate of reservoir liquids	J_f^l	$\mathrm{kg\,s}^{-1}$
Mass flow rate through the choke	J_c	$\mathrm{kg\,s}^{-1}$
Molecular weight	M_g	$\mathrm{g\,mol\,mol}^{-1}$
Number of choke	n_c	[-]
Number of pump strokes per minute	$n(t)$	[-]
Permeability	κ	m^2
Porosity	ϕ	[-]
Pressure	p	Pa
Reference density	ρ_0	$\mathrm{kg\,m}^{-3}$
Reference pressure	p_o	Pa
Reservoir pressure at infinite extent	p_e	Pa
Spatial discretization	Δx	m
Speed of sound in the liquid medium	C_l	$\mathrm{m\,s}^{-1}$
Speed of sound in the gas medium	C_g	$\mathrm{m\,s}^{-1}$
Speed of sound in the mixture	C_m	$\mathrm{m\,s}^{-1}$
Subscript for annulus	a	[-]
Subscript for drillstring	d	[-]
Temporal discretization	Δt	s

Thickness of the reservoir	h	m
Universal gas constant	R_g	$\mathrm{m^3\,Pa\,K^{-1}\,mol^{-1}}$
Velocity of gas	v_g	$\mathrm{m^3\,s^{-1}}$
Velocity of liquid	v_l	$\mathrm{m^3\,s^{-1}}$
Velocity of mixture	v_m	$\mathrm{m^3\,s^{-1}}$
Viscosity of gas	μ_g	Pa s
Viscosity of liquid	μ_l	Pa s
Volume fraction, gas	α_g	[-]
Volume fraction, liquid	α_l	[-]
Volume swept per pump stroke	V_p	$\mathrm{m^3}$
Volumetric flow rate from the pump	q_p	$\mathrm{m^3\,s^{-1}}$
Volumetric flow rate through the bit	q_{bit}	$\mathrm{m^3\,s^{-1}}$

Introduction

Dans ce chapitre, nous présentons le procédé forage dans sa généralité, ansi que les spécificités du forage à pression contrôlée (MPD en Anglais). Nous présentons une revue de la littérature portant sur la modélisation du processus de forage et l'état-de-l'art des techniques d'automatisation.

In this chapter, we introduce the basic terminologies used to describe a drilling process, followed by a description of Managed Pressure Drilling (MPD) operations. We present a literature review on the modelling of drilling processes and the state-of-the-art automation technologies.

Drilling window. Drilling for oil and gas is the process of creating a borehole in the ground that may extend unto several thousand meters. The goal is to create a path for the fluids (oil, gas and water) to flow from a particular section of rocks (called reservoir) to the surface. While doing so, an engineered fluid called the drilling mud is circulated. The main component of the mud is water for a water-based mud (WBM) and diesel (sometimes, crude oil) for oil-based mud (OBM). Various factors in the well plan, like the required temperature and type of the formation, dictate the choice between WBM and OBM. The foremost function of the mud is to maintain the required pressure at the bottom of the wellbore during circulation, referred to as the Bottomhole Circulating[2] Pressure (BHCP). It is required that the BHCP respects certain pressure constraints given by :

Pore pressure : the pressure at which the fluids are confined within the pore space of the reservoir ;

Collapse pressure : the minimum pressure required to hold the surrounding rock structure from collapsing into the borehole ;

Fracture pressure : the minimum pressure required to fracture through the reservoir.

A schematic of these pressure gradients along the depth of a wellbore is shown in Figure 1. Indeed, for any *drilling* operation, we maintain the BHCP between the collapse and the fracture pressure, to create a stable wellbore. However, with respect to the pore pressure, if the BHCP is [1]

- lower, then the operation is referred to as *under-balanced* ;
- higher, then the operation is referred to as *over-balanced* or *conventional* ;
- equal, then the operation is referred to as *at-balanced*.

The difference between BHCP and pore pressure is referred to as the *drawdown*. The operational limit set by the immediate pressure constraints with respect to the BHCP is called the *drilling window.*

[2]accounts for an additional factor due to frictional forces of the flow. For the given flow direction in schematic 2, circulating pressure in the annulus is higher than the static pressure. A common malpractice, i.e. not accounting the friction in the fluid flow, fractures the reservoir at the pump start.

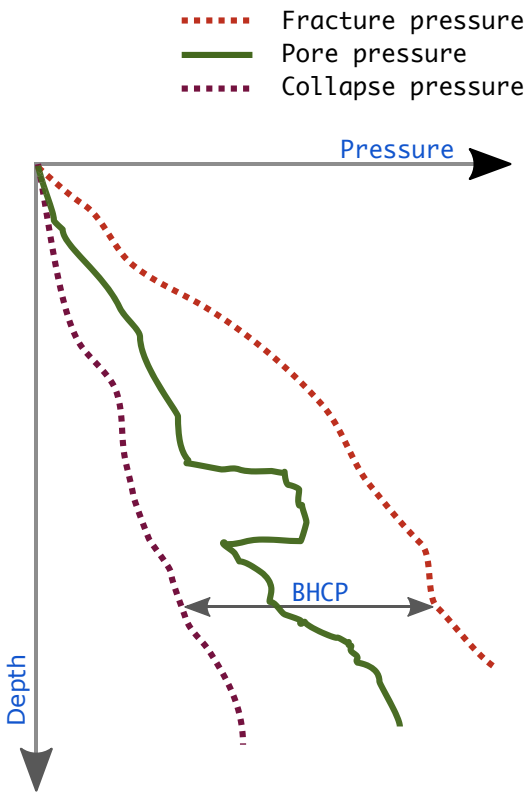

FIGURE 1: Schematic trend of various pressure gradients in the subsurface along the depth of the wellbore. During *normal* drilling operations, BHCP is maintained between the collapse and the fracture pressure limit. An over-pressured zone—deviation above the normal trend line—could potentially lead to a reservoir influx.

Kick. When the BHCP is maintained below the pore pressure (un-) intentionally, the fluids within the reservoir will flow into the wellbore. An undesired influx of the reservoir fluids is called a kick. The situation is severe if the influx is gas. An uncontrolled kick may lead to a *blowout*; causing potential loss to human lives and equipment. The ability to handle a kick is dependent on the type of drilling operation and the relevant equipment available. MPD is an established drilling technique to prevent and / or control small kicks with a limited non-productive time (NPT) [2].

Managed pressure drilling. In conventional drilling operations, density of the drilling mud is the main factor affecting the BHCP. It may take up to several hours to re-engineer. In the case of MPD operation, a choke valve that restricts the flow at the surface outlet is present — providing a closed-loop circulation system — as opposed to an open flow channel in conventional operations [3]. The choke valve opening (or restriction) provides an additional and a faster degree of freedom to control the BHCP (in a few minutes, see, e.g. [2], [4]). During MPD operations, the mud flows out from the annulus through a rotating circulation device (RCD), followed by a choke manifold. Figure 2 depicts a schematic view of the facilities and the flow path

of the fluid. During conventional MPD operations, the choke is manually operated[3], in which cases the efficiency of the BHCP control is, in general, proportional to the experience of the bloke on the choke.

Such operations are increasingly replaced by automation solutions [5]–[7]. In automated MPD operations, the choke valve in the manifold of the rig site is actuated using a closed-loop feedback controller. Various control designs have been proposed in the literature (see, e.g. [8]–[11]) with an increasing effort to tackle multiphase flow situations. Different approaches include using a distributed fluid flow models in the wellbore to using a lumped low-order models where certain dynamics are neglected; coupled with feedback and feedforward control approaches [12]. Automation solutions to control the choke during a MPD operations are commercially available, e.g. Leidar® from Kelda drilling controls AS.

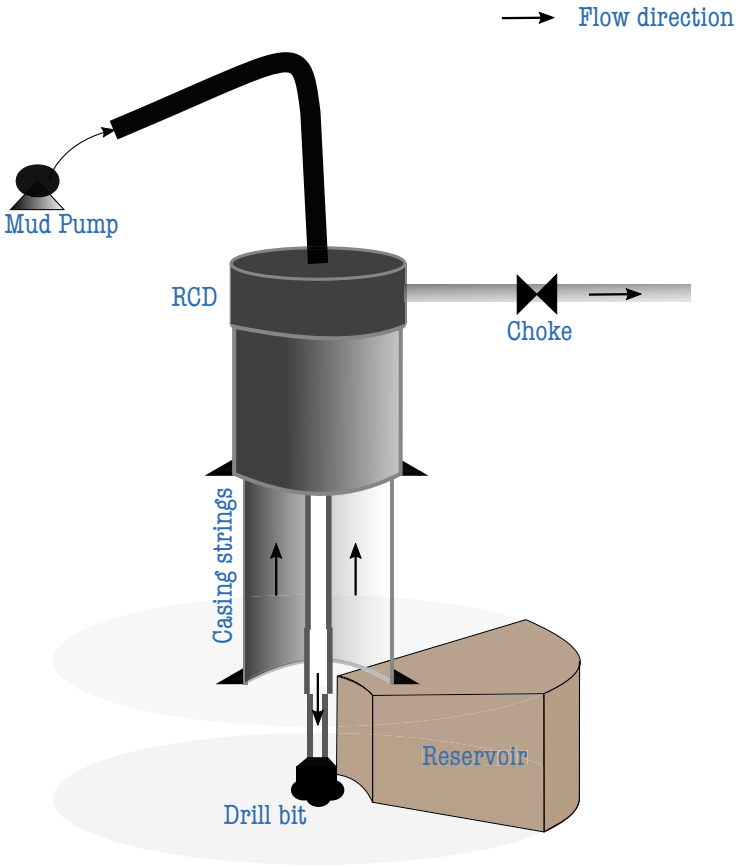

FIGURE 2: Schematic of the general setup in a MPD operation. The RCD equipment provide a closed-loop mud circulation system. The choke valve is the control actuator for automated solutions. Variation in the flow geometry is due to the BHA and latest casing string in the annulus. A radial reservoir section is used to model the influxes into the annulus.

Reservoir data collection technology. An influx from the reservoir occurs when the BHCP is reduced below the reservoir pore pressure, creating a drawdown. The occurrence, severeness, composition of the influx must, to the extent possible, be

[3] in the oilfield, the operator is referred to as 'bloke on the choke'.

anticipated, which requires some knowledge of the reservoir properties. We now review some of the technologies available in the industry to collect information on the reservoir. The following methods provide information regarding the rock constituting the reservoir :

- Prior to the drilling, seismic data and offset well data[4] provide a largely inaccurate estimate of the pore pressure gradient.
- A highly expensive operation—coring—and a laborious process of collecting drill-cuttings at the drilling rig-site are the only direct evidence to understand the subsurface rocks.
- In a production setting, a method referred to as well testing is used [13], [14]. It consists of temporarily shutting down the production and analyzing the subsequent evolution of pressure at the well-head. This generates information regarding the near-wellbore properties of the reservoir.
- In a drilling setting, wireline logging has evolved to provide an indirect measurement but with a high NPT cost. The drilling process is stopped and an array of logging tools are lowered into the wellbore and measure various physical quantities : sonic velocity, resistivity, radioactivity, etc.
- Recently, logging-while-drilling techniques aim at reducing the NPT by collecting the same measurements as wireline tools without stopping the drilling operation. Typically, sensors are installed in the BHA and their data is transmitted to the surface using mud-pulse telemetry, which is prone to delay and noise.

The main obstacle to characterizing the reservoir while drilling is the necessity to guarantee a safe interaction between reservoir and wellbore. In conventional drilling, the slow adjustment of the BHCP by varying mud density does not enable accurate control of the drawdown. Yet, the presence of an influx is a necessary condition to gather information on the reservoir via the flow properties. For this reason, various procedures consist in stopping the drilling process and crate conditions of an interaction with the reservoir. Pore pressure test (PPT) and formation integrity test (FIT) aim at understanding the pressure profiles at a particular section; drill stem test (DST) and repeat formation tester (RFT) aim at gathering information about the contained fluids, in addition. All of these generate NPT, since they cannot be realized as-drilling in conventional drilling.

Conversely, the MPD technique, by enabling fast and more accurate control of the BHCP, makes it possible to create safe interaction with the reservoir by generating small, controlled influxes [15]. This allows the operator to carry out the abovementioned tests dynamically, thus reducing NPT. The main goal of the work presented in this manuscript is to estimate some of the reservoir properties in real-time during MPD by relying solely on surface measurements.

Fluid flow modelling in the wellbore. As noted earlier, mud is circulated to maintain the required BHCP during the drilling operations. Drilling muds exhibit a non-Newtonian behaviour, making it challenging to mathematically model its flow dynamics. An influx from the reservoir alters the flow behavior of the mud in the annulus, primarily affecting the BHCP. The effect is more pronounced in case of a gas

[4] i.e., historical data from previously drilled wells in the same field.

influx, especially in rather long wells where gas dissolution[5] can occur. Such effects, when left unnoticed, may lead to an unstable feedback loop between the wellbore dynamics and the influx, leading to a riser-gas unloading or at worst, a blowout. Due to such inherent risks in the process of drilling for oil and gas, several efforts have been taken to understand the multiphase (liquid and gas) fluid flow. Different approaches range from the first principle mathematical models to experimental flow-loop tests (see, e.g. [8], [16]–[32]).

Primarily, such studies are useful to better understand the process so as to mitigate the risk of a blowout; used in well control simulations and training purposes. However, we envision that such models, when coupled with the reservoir models could be used to better understand the reservoir in *realtime*. The advantages of such an approach are multifold : understand the reservoir properties with a lower NPT, than the current state-of-the-art ; optimize drilling as a result of better estimate of the operating envelope and influx- (gas-) handling [2]. There is wide range of dynamical models of single-phase and multiphase flow used in the context of oil and gas. Commercial software such as OLGA provide high-fidelity models for simulation purposes [33], [34] (other software products are available, e.g. LedaFlow and DrillBench). In [35], a comprehensive drilling simulation environment, taking into account mechanical and hydrodynamic phenomena and their interaction, as well as cuttings transport is described. At the other end of the accuracy vs. tractability spectrum, the Kaasa model [36], while retaining only the main features of the pressure dynamics inside the wellbore, has been used for commercially implemented real-time estimation and control solutions [12]. For an extensive review of multiphase flow models, we refer the reader to [4]. In this manuscript, we rely on a model, described in Chapter 1 that retains main features of the transport phenomena in the wellbore, while simplifying the fluid rheology and thermodynamic aspects.

Reservoir characterization. Reservoir characterization typically relies on the fusion of measurement data with reservoir models. Reservoir modelling is a scientific field of its own, where complex, three dimensional, multiscale, multiphase models of the diffusion, transport, thermodynamic and chemical phenomena are studied. Here, we focus on models of the near-wellbore diffusion dynamics and their coupling with the wellbore transport dynamics.

Traditionally, simplified models of the reservoir-wellbore interaction inspired by production engineering [13] have been used for reservoir characterization. Several contributions [37]–[40] assume a linear, static relation between drawdown and influx flow rate. The proportionality constant is referred to as the Productivty Index (PI).

Other approaches consist in deriving approximate representations of the diffusion dynamics near the wellbore (see, e.g. [13], [41]–[44]). These can then be used along with models of the wellbore to estimate, e.g. permeability, porosity, or steady-state pore pressure. In [37], [45], [46], a linear time-varying relation between drawdown and influx rate, referred to as Constant Terminal Rate Solution (CTRS) is combined with measurements of the BHCP and influx rate to estimate pore pressure and sometimes permeability. In [38], [39], distributed models of the reservoir are used, along with downhole pressure and flow rate data.

While these approaches focus on the sole reservoir, other contributions analyze the impact of an influx on wellbore dynamics. In [47], nonlinear regression is used to interpret FIT and Leak-Off Test (LOT) data. In [9], [48], the CTRS is used along

[5] when BHCP is higher than the bubble-point pressure, i.e. the minimum pressure required for the first gas bubble to dissolve in the given liquid phase.

with distributed models of the wellbore and Kalman filters to estimate pore pressure. In [49], dynamical well testing is performed and the pore pressure is estimated from a BHCP sensor as a specific point in the pressure build-up curve. In [50], a least-square fitting of reservoir parameters is applied to a multiphase flow model along with a PI influx relation, requiring only surface data. An observer for a single-phase flow model and a linear, dynamic model of the reservoir is derived in [34].

In this manuscript, we investigate various combinations of distributed and simplified models, both for wellbore and reservoir, described in Chapters 1 and 2. Our estimation strategies rely on the backstepping approach, which is a "late lumping" [51] approach to observer design, i.e., the observer gains are derived for the distributed models rather than after discretization. The main contributions of this manuscript can be listed as below :

Contribution 1 A comprehensive modelling of the wellbore and the annulus during two-phase flow conditions in the annulus, a tailored treatment of the boundary conditions and a tailored numerical scheme to account for the varying flow geometry in the drilling operations.

Contribution 2 Modelling of the distributed dynamics of reservoir pressure and treatment of the coupling boundary conditions between the wellbore and the reservoir dynamics.

Contribution 3 Observer designs for the coupled wellbore–reservoir models that results in the following types of system : hyperbolic PDEs coupled with a time varying reflection coefficient, finite dimensional ODE system coupled with a parabolic PDE and hyperbolic PDEs coupled with a parabolic PDE. Theoretical proofs of the stability conditions for each of the observer designs are presented.

Publications

The work presented in this manuscript has resulted in the following publications :

Journals.

- M. Abbasi, S. N. Lordejani, **N. Velmurugan**, C Berg, L. Iapichino, W. Schilders, and N. van de Wouw, "A godunov-type scheme for the drift flux model with variable cross section", *Journal of Petroleum Science and Engineering*, vol. 179, pp. 796–813, 2019.
- C. Berg, G. A. Evjen, **N. Velmurugan**, and M. Culen, "The influx-management envelope considering real-fluid behavior", *SPE Drilling & Completion*, 2019.
- S. Naderi Lordejani, M. H. Abbasi, **N. Velmurugan**, C. Berg, J. Å. Stakvik, B. Besselink, L. Iapichino, F. Di Meglio, W. H. Schilders, and N. van de Wouw, "Modeling and numerical implementation of managed-pressure-drilling systems for the assessment of pressure-control systems", *SPE Drilling & Completion*, 2020.

Conferences.

- **N. Velmurugan** and F. Di Meglio, "Transient modelling of influx and observer implementation for estimation while drilling", in *2018 IEEE Conference on Decision and Control (CDC)*, IEEE, 2018, pp. 2623–2628.

- L. Camacho-Solorio, **N. Velmurugan**, F. Di Meglio, and M. Krstic, "Observer design for a coupled ODE-PDE system from a wellbore reservoir drilling model", in *2019 IEEE 58th Conference on Decision and Control (CDC)*, IEEE, 2019, pp. 3086–3091.

Outline

The rest of the thesis is organised as follows.

Part I focuses on the description of the wellbore and reservoir models used for simulation and estimation purposes.

Chapter 1 introduces the mathematical modelling of multiphase fluid flow within the drillstring and the annulus. We present a modification to current models to account for the variation in the flow geometry, and the required tools solve them numerically. We also present simulation case studies that are compared with the field data. Content of this chapter has partially appeared in [52] and [53].

Chapter 2 introduces various models to calculate the influx from a reservoir. We present analytical solutions using simplifying assumptions. However, a general solution for the transient model is also presented. We argue the requirement of transient model by comparing their results. We also present a numerical scheme to solve diffusion equations, with necessary tools to adapt for liquid and gas reservoirs.

Part II focuses on the design of observers for various combination of distributed and reduced-order models of the wellbore and reservoir.

Chapter 3 presents an observer design for a coupled system given by a distributed model for the fluid flow in the wellbore and an approximate solution for the influx of the reservoir. The system is decoupled from the reservoir dynamics and present pressure wave propagation in the wellbore with a time-dependent reflection coefficient at the wellbore-reservoir boundary. We present the well-posedness of the kernels as an extension of the results in the literature [54], [55].

Chapter 4 presents an observer design for the coupled wellbore and reservoir dynamics. We present a modification to the existing lumped low-order model for the wellbore dynamincs [36], to account for the the distributed pressure dynamics for the reservoir. We present a choice of observer design that results in a particular cascade structure that allows us to guarantee the stability of the error system. Content of this chapter has appeared in [56].

Chapter 5 presents an observer design by retaining the distributed nature of both the wellbore and the reservoir dynamics. We present the designs that consider two measurements : one at the topside and one hidden ; and only using topside sensing. This novel approach allows us to guarantee stability of the error system. Contents of this chapter has partially appeared in [57].

Chapter 6 concludes the discussions presented in this manuscript. We present the current advancements and the possible future prospects, that the author seems fit in this field of research.

Part I

Mathematical modelling

Chapter 1

Wellbore model

Dans ce chapitre, nous détaillons les équations du modèle décrivant la dynamique de l'écoulement dans le puits. Le modèle est basé sur des équations de conservation de la masse et de la quantité de mouvement dans la tige de forage et le puits. Les conditions frontières sont cohérentes avec les installations industrielles typiquement rencontrées dans les opérations de type MPD. Comme illustré en Section 1.2, le modèle reproduit fidèlement le comportement de l'écoulement pendant les opérations industrielles standards, telles que les connections, ou les évènements fréquents, comme l'obstruction de vannes de contrôle. Ce modèle reste toutefois suffisamment simple pour pouvoir servir de base aux synthèses d'observateurs de la Partie II de ce manuscrit.

In this chapter, we detail the model describing the dynamics of the flow inside the wellbore. The model is based on first principles – conservation of mass and momentum – written for the drillstring and annulus. It incorporates boundary conditions corresponding to the industrial facilities typically encountered on MPD operations. As illustrated in Section 1.2, the model is able to reproduce the behavior of drilling systems during standard industrial operations, such as connections, or frequent contingencies, such as MPD choke plugging. However, it remains mathematically tractable, to serve as the basis for observer design in Part II.

1.1 MPD model description

1.1.1 System description and modelling assumptions

Consider the facilities schematically depicted on Figure 2. A drilling fluid (typically liquid) is pumped at the top of the drillstring. The fluid passes through the nozzles of the drillbit, then travels back up the annulus. When the bottom of the annulus in in contact with the reservoir, fluids (oil, gas and water) may flow in. The nozzle acts as a one-way valve and multiphase flow can only occur in the annulus. We make the following assumptions :

A1 The flow is one-dimensional; radial and angular variations of all physical quantities are neglected, We denote $x \in [0, L]$ the curvilinear coordinate along the main axis of the pipe, where L is a pipe length.

A2 The temperature of the flowing fluid is constant — isothermal; not affected by the temperature gradient of seawater or/and the subsurface rocks.

A3 When two phases are present, they instantaneously reach their mechanical equilibrium at any given location x, i.e. both phases are at the same pressure $p(t, x)$, where $t > 0$ denotes time.

A4 There is no mass exchange between the two phases.

1.1.2 Conservation laws

The proposed model is a classical Drift-Flux Model (DFM) [58] incorporating variations of the cross-sectional area. Indeed, it is usual that, in any well design, the bottom-hole assembly (BHA) consists of drill collars that are used to provide weight to the drill bit. Heavy-weight drill pipes (HWDP) help the transition into the normal drill pipes. Such an arrangement yields variations of the inner and outer diameter of the drillstring, which we take into account here by assuming that the cross-sectional area $A(x)$ is space-dependent. Omitting the space and time dependence of the variables for clarity purposes, the mass conservation law for each phase and a combined momentum conservation law read [26]

$$\frac{\partial(A\alpha_l\rho_l)}{\partial t} + \frac{\partial(A\alpha_l\rho_l v_l)}{\partial x} = 0 \tag{1.1}$$

$$\frac{\partial(A\alpha_g\rho_g)}{\partial t} + \frac{\partial(A\alpha_g\rho_g v_g)}{\partial x} = 0 \tag{1.2}$$

$$\frac{\partial(A\alpha_l\rho_l v_l + A\alpha_g\rho_g v_g)}{\partial t} + \frac{\partial(A\alpha_l\rho_l v_l^2 + A\alpha_g\rho_g v_g^2 + Ap)}{\partial x} = AS + \frac{\partial A}{\partial x}p \tag{1.3}$$

where α_i is the volume fraction, v_i the velocity and ρ_i the density of the phase $i = l$ (liquid) and g (gas). Here, p is the pressure, A is the cross-sectional area and S is the momentum source term, which are detailed in Section 1.1.6.

Remark 1. *The indices g and l denote here liquid and gas, but Equations (1.1)–(1.3) are valid for any two phases for which Assumption A3 is valid.*

1.1.3 Closure relations

System (1.1)–(1.3) has seven unknowns and only three equations. The missing four equations are algebraic relations between the physical quantities, that we now detail.

Equations of state. The fluid densities and pressure are assumed to satisfy the following relations, referred to as the Equations of State (EOS) of liquid and gas, respectively

$$p - p_0 - C_l^2(\rho_l - \rho_0) = 0 \tag{1.4}$$

$$p - C_g^2\rho_g = 0 \tag{1.5}$$

where C_i is the velocity of sound in the medium i. Here ρ_0 is a known value of density at the reference pressure p_o.

Volume fractions. Besides, one has the following geometric condition on the volume fraction

$$\alpha_l + \alpha_g - 1 = 0. \tag{1.6}$$

Slip law. A consequence of Assumption A3 and of writing a combined momentum conservation law is that an empirical relation between the fluid velocities must be added to close the system. We assume the following form, commonly referred to as the slip law [59]

$$v_g - v_l = \Phi(\alpha_g), \qquad \Phi(\alpha_g) = C_0(\alpha_g)v_m + V_d(\alpha_g) - v_l \tag{1.7}$$

where $C_0(\alpha_g)$ is the distribution parameter and $V_d(\alpha_g)$ the slip velocity. The dependence of these parameters on the flow regimes is widely studied in the literature (see, for instance [60], [61]). Here v_m is the mixture velocity (see Equation 1.31b).

Drillstring and annulus – notations. In the next section, we detail the boundary conditions and in particular the one connecting the drillstring and the annulus. To avoid heavy notations, we rely on the fact that the drillstring contains liquid only. This allows us to use the following conventions :

- Subscripts d and a refer to drillstring and annulus, respectively, e.g. p_a is the pressure inside the annulus.
- Subscripts g and l refer *specifically to the annulus* and denote gas and liquid, respectively.
- No subscript refers to the liquid inside the drillstring, e.g. $v(t,x)$ is the velocity of the liquid at location x and time t inside the drillstring.

Further, we define the following *conservative variables* q_d and q_a as

$$q_d = [\rho, \quad \rho v]^\top \tag{1.8}$$
$$q_a = [\alpha_l\rho_l, \quad \alpha_g\rho_g, \quad \alpha_l\rho_l v_l + \alpha_g\rho_g v_g]^\top \tag{1.9}$$

along with the following *flux* function f and *source term* $\mathcal{S}$ as

$$f_d(q) = [\rho v, \quad \rho v^2 + p_d]^\top \tag{1.10}$$
$$f_a(q) = [\alpha_l\rho_l v_l, \quad \alpha_g\rho_g v_g, \quad \alpha_l\rho_l v_l^2 + \alpha_g\rho_g v_g^2 + p_a]^\top \tag{1.11}$$
$$\mathcal{S}_d = [0, \quad S_d]^\top \tag{1.12}$$
$$\mathcal{S}_a = [0, \quad 0, \quad S_a]^\top. \tag{1.13}$$

This enables us to write the equations for drillstring and annulus in the following compact form

$$\frac{\partial(A_d q_d)}{\partial t} + \frac{\partial f_d(A_d q_d)}{\partial x} = A_d\mathcal{S}_d + \frac{\partial A_d}{\partial x}p_d \tag{1.14}$$
$$\frac{\partial(A_a q_a)}{\partial t} + \frac{\partial f_a(A_a q_a)}{\partial x} = A_a\mathcal{S}_a + \frac{\partial A_a}{\partial x}p_a \quad . \tag{1.15}$$

Using the algebraic relations (1.4)–(1.7), one can determine the expression of the physical variables[1] $(\alpha_g, \alpha_l, v_g, v_l, \rho_g, \rho_l, p)$ as a function of the conservative variables q_a by following the procedure below[2] :

1. Solve for presssure using

$$p_a = \frac{-b + \sqrt{b^2 - 4d}}{2} \tag{1.16}$$

where $b = \rho_0 C_l^2 - p_0 - q_1 C_l^2 - q_2 C_g^2$ and $d = -(\rho_0 C_l^2 - p_0)C_g^2 q_2$. It is straightforward to derive from Equation (1.6).

2. Obtain the densities of each phase ρ_l and ρ_g by solving the EOS's (1.4) and (1.5).

[1] a vector of any combination of the physical variables is denoted by u.
[2] elements q_i, $i \in \{1,2,3\}$ are defined in the same order as Equation 1.9.

3. Find the velocity of liquid using

$$v_l = \frac{q_3\left(1 - C_0\alpha_g\right) - q_2 V_d}{q_1 + C_0\alpha_g q_2} \quad . \tag{1.17}$$

4. From the slip law[3] (1.7), obtain the gas velocity using

$$v_g = \frac{C_0\alpha_l v_l + V_d}{1 - C_0\alpha_g} \quad . \tag{1.18}$$

1.1.4 Boundary conditions

Systems (1.14),(1.15) along with (1.4)–(1.7) still require boundary conditions to be well-posed. For MPD operations we have conditions imposed at three locations

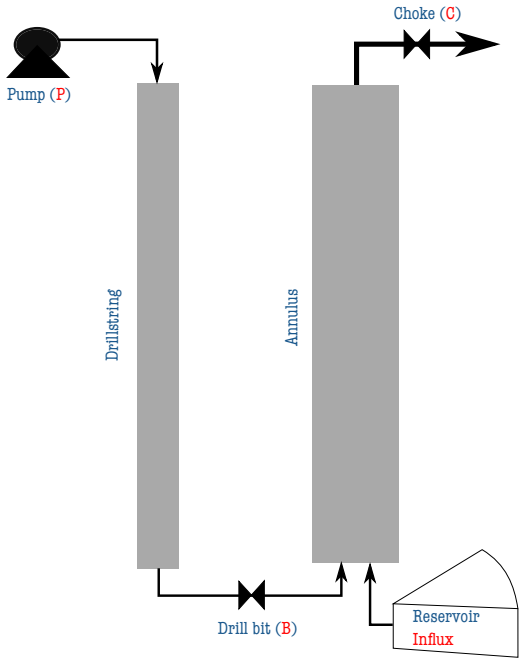

FIGURE 1.1: A schematic representation of fluid flow path in the drillstring and the annulus. The boundary conditions are specified at the locations of: the mud pump (P), the drill bit (B) and the choke (C). Influxes from the reservoir are coupled at the bit (B) boundary condition. $[P, B] \equiv [0, L]$ for drillsting and $[B, C] \equiv [0, L]$ for annulus.

indicated on Figure 1.1 — pump (P), drillbit (B) and choke (C) — as follows:

P Single-phase drilling mud is pumped into the drillstring. Then, the mass balance is given by

$$A_d\left(0\right)\rho\left(t,0\right)v\left(t,0\right) - J_p\left(t\right) = 0 \tag{1.19}$$

[3]The choice of $C_0(u)$ and $V_d(u)$ can make the Equations (1.17) and (1.18) nonlinear equations that need to be solved simultaneously using non-linear solvers.

where A_d denotes the cross-sectionnal area of the drillstring, J_p is the mass flow rate provided by the pump. At the rig site, pump stroke per minute $n_p(t)$ is generally available rather than the mass flow rate, in which case volume swept by the pump per stroke V_p is known. Then the mass flow rate is calculated as

$$J_p\left(\rho(t,0),t\right) = V_p n_p(t)\rho(t,0). \tag{1.20}$$

B At the drillstring-annulus connection, we model the flow through the nozzles using a one-way valve equation. Besides, we write the mass conservation laws of liquid and gas over the drillstring-annulus-reservoir interconnection. These yield

$$A_d(L)\rho(t,L)v(t,L) - C_d A_n\sqrt{2\rho(t,L)\mathcal{R}\left(p_d(t,L) - p_a(t,0)\right)} = 0 \tag{1.21}$$

$$A_d(L)\rho(t,L)v(t,L) + J_f^l(p_a(t,0),p_r) - A_a(0)\alpha_l(t,0)\rho_l(t,0)v_l(t,0) = 0 \tag{1.22}$$

$$J_f^g(p_a(t,0),p_r) - A_a(0)\alpha_g(t,0)\rho_g(t,0)v_g(t,0) = 0 \tag{1.23}$$

where c_d is the discharge coefficient and A_n the effective area of the bit nozzles. J_f^i is the mass flow rate of the liquid $(i = l)$ and the gas $(i = g)$ from the formation, i.e., reservoir section (detailed in Chapter 2). Here, the function $\mathcal{R}$ defined

$$\mathcal{R}(x) = \begin{cases} x & \text{if } x \geq 0 \\ 0 & \text{if } x < 0 \end{cases} \tag{1.24}$$

represents the non-return valve used to prevent backward flow of fluids from the annulus into the drillstring.

C At the top of the annulus, the boundary condition is determined by the valve equation describing the mass flow rate of the mixture through the MPD choke [62] that reads

$$J_c(t,q_a(t,L)) - J_{bpp}(t) - J_c^u(q_a(t,L)) = 0 \tag{1.25}$$

with

$$J_c(t,u_a(t,L)) = \sum_{i=1}^{n_c} K_{c,i}G_i(Z_{c,i}(t))\sqrt{2\rho_m(t,L)\mathcal{R}\left(p_a(t,L) - p_0\right)} \tag{1.26}$$

where $K_{c,i}$, $Z_{c,i}$ and $G_i(\cdot)$ are the choke flow factor, the choke opening and the choke characteristic of the choke valve i, respectively. Here, n_c is the number of choke valves in the MPD set up and $J_{bpp}(t)$ is the mass flow rate from the back-pressure pump. Moreover,

$$J_c^u = A_a(L)\alpha_l(t,L)\rho_l(t,L)v_l(t,L) + A_a(L)\alpha_g(t,L)\rho_g(t,L)v_g(t,L) \tag{1.27}$$

is the mass flow rate upstream the choke whereas J_c is that downstream the choke.

1.1.5 Single-phase liquid flow

In the case of single-phase liquid flow, which occurs in the drillstring and in the annulus in the absence of influx from the reservoir, the model can be simplified provided the following two additional simplifying assumptions are made.

A5 The cross-sectional area of the pipe A is constant.

A6 The velocity of the fluid is negligible with respect to the speed of sound, i.e., $v(t,x) \ll C_l, \quad \forall (t,x)$.

With these assumptions, Equations (1.1),(1.3), along with (1.4) and $\alpha_g \equiv 0$ rewrites as the following *semilinear* hyperbolic PDE

$$q_t + \mathcal{A} q_x = \mathcal{S} \tag{1.28}$$

where the *constant* matrix $\mathcal{A}$ and the source terms $\mathcal{S}$ are given by

$$\mathcal{A} = \begin{bmatrix} 0 & 1 \\ C_l^2 & 0 \end{bmatrix}, \qquad \mathcal{S} = \begin{bmatrix} 0 \\ S \end{bmatrix}. \tag{1.29}$$

This model will serve as the basis for the design of observers estimating liquid influx in Part II.

1.1.6 Source terms

The momentum source term comprises of pressure losses due to gravity and frictional flow. We present here their general form as a function of the physical variables u that reads

$$S(t,u) = \rho_m g \sin(\theta) - \frac{2\nu(u)\rho_m v_m}{D_h} \tag{1.30}$$

where g and θ are the gravitational acceleration and the inclination of the fluid transmission line with respect to the horizontal. D_h is the hydraulic diameter — for drillstring $D_h = D_{i,d}$; for annulus $D_h = D_{i,a} - D_{o,d}$; the subscripts i for inner diameter and o for outer diameter. The mixture density ρ_m and the mixture velocity v_m take the form

$$\rho_m = \alpha_l \rho_l + \alpha_g \rho_g \tag{1.31a}$$
$$v_m = \alpha_l v_l + \alpha_g v_g. \tag{1.31b}$$

The Fanning friction factor $\nu(u)$ is in general challenging to determine; first-principle based approach can be used, e.g. using non-newtonian models in [63] or obtained as a solution of an estimation problem, e.g. [36].

Single-phase laminar liquid flow. By setting $\alpha_g \equiv 0$ in the mixture relations (1.31) and assuming laminar flow, source terms (1.30), generally used to model the fluid flow in the drillstring, reduce to the following linear expression

$$S(t,x) = \rho(t,x) g \sin(\theta) - \frac{32\mu}{D_h^2} v(t,x). \tag{1.32}$$

1.2 Numerical simulations

In this section, we describe the numerical scheme used to compute the solution to Equations (1.14),(1.15),(1.19),(1.21)–(1.23),(1.25), before illustrating the approach on industrial test cases.

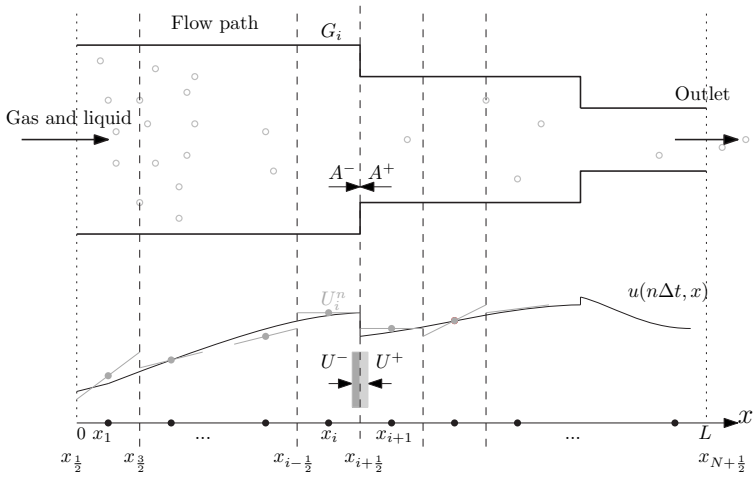

FIGURE 1.2: Stencil for the modified, model based approach to use FVM scheme to account for the variation in the flow area. The variables U^- and U^+ are calculated using a Godnov-type scheme assuming $A^- = A^+$, then update the *starred* variables using the algorithm 1. Flux limiters may be used to approximate the average of the variables U over the cell G_i.

1.2.1 Numerical scheme

General approach. Finite-volume discretization is commonly used to solve systems of partial differential equations (PDEs) such as the DFM [64]. We use the Finite-Volume methods to find the solution within the spatial computational domain $x \in \Omega = [0, L]$ and the temporal computational domain $t \in I = [0, T]$. Referring to the stencil in Figure 1.2, we

- discretize the spatial domain Ω into N cells, with length Δx ;
- discretize the time domain with a step-size[4] of Δt ; determined based on the Courant-Freidrichs-Lewy (CFL) condition [65] ;
- denote each discretized cell as $G_i = [x_{i-1/2}, x_{i+1/2}]$ with $x_{i+1/2} = i\Delta x$, the i^{th} cell interface. The center of the grid cell is given by $x_i = (i - 1/2)\Delta x$;
- denote Q_i^n as the spatial average of the conservative variable q over the i^{th} cell at the time instant $t^n = n\Delta t$;

and use a finite volume Godunov-type numerical scheme that takes the following form [66]

$$Q_i^{n+1} = Q_i^n - \frac{\Delta t}{\Delta x}\Big(F(Q_i^n, Q_{i+1}^n) - F(Q_{i-1}^n, Q_i^n)\Big) + \Delta t\, S(Q_i^n, t^n, x_i) \tag{1.33}$$

where F is the numerical flux function to be determined. Classically, one would use a conservative[5] scheme, such as the Rusanov scheme described in [67]. Here, however, the variations in the geometry imply that (1.14),(1.15) are not in conservative form, prompting the need for an adapted scheme. Further, we present a specific way to deal with the boundary conditions.

[4] We use a constant time step over the domain I.

[5] conservative schemes ensure that the numerical solution satisfies the mass and momentum conservation laws despite the discretization process [66].

A model-based approach for the numerical scheme

The additional derivative term $p_i \partial_x A_i$, for $i \in \{d, a\}$ in the systems (1.14) and (1.15) accounting for the variable geometry requires a numerical scheme with a non- conservative approach ; several methods have been proposed for the Euler equations (see [68]–[71]). We present here the numerical method proposed by [70] for the Euler equations (1.14) and the numerical method proposed by [52] for the DFM (1.15).

To accommodate the non-conservative terms, we present the numerical flux as a function of the primitive variables $U_i^n(Q_i^n)$: vector of an approximation of the physical variables u over the cell G_i^n. Representing U_j^- and U_j^+ as the approximate variables at the left and the right side of the interface j, the modified scheme to treat the variable geometry takes the form [53]

$$Q_i^{n+1} = Q_i^n - \frac{\Delta t}{\Delta x}\Big(F(U_{i+1/2}^{+*}, U_{i+1/2}^-) - F(U_{i-1/2}^+, U_{i-1/2}^{-*})\Big) + \Delta t\, S(U_i^n, t^n, x_i) \quad (1.34)$$

and the *starred* variables $U_{i+1/2}^*$ and $U_{i-1/2}^*$ have yet to be computed. In [53], a second-order flux-vector-splitting (FVS) scheme [72] is used to calculate the numerical flux function F in (1.34) for the DFM in the annulus and a first-order upwind scheme [66] for the same in the drillstring. In what follows we make the following assumption :

A7 The geometry of the flow path has piece-wise continuous cross-section, i.e. the area $A(x)$ is constant within each cell G_i and discontinuity occurs only at the cell interfaces $x_{i\pm1/2}$ for $i \in 1, 2, \ldots, N$.

the approach is as follows [52] : assume that the cells G_{i-1}, G_i and G_{i+1} all have the same area and calculate the variables ; use the Algorithm 1 to obtain the *starred* variables and calculate the variables for the next timestep. We present here the nonlinear coordinate transformation for the Euler equation (1.14) and the DFM (1.15) to calculate the $U^{\pm *}$ at the cell interface $x_{i\pm1/2}$ as (with the superscripts † and # defined in Algorithm 1)

For drillstring :

$$(\rho v)^{\dagger *} A_d^{\#} = (\rho v)^{\dagger} A_d^{\dagger} \quad (1.35a)$$

$$(v^{\dagger *})^2 + 2C_l^2 \ln(\rho^{\dagger *}) = (v^{\dagger})^2 + 2C_l^2 \ln(\rho^{\dagger}) \quad (1.35b)$$

For annulus :

$$(\alpha_l \rho_l v_l)^{\dagger *} A_a^{\#} = (\alpha_l \rho_l v_l)^{\dagger} A_a^{\dagger} \quad (1.35c)$$

$$(\alpha_g \rho_g v_g)^{\dagger *} A_a^{\#} = (\alpha_g \rho_g v_g)^{\dagger} A_a^{\dagger} \quad (1.35d)$$

$$\left(\frac{\alpha_l \rho_u^2}{2\rho_g} + \frac{\alpha_g u_g^2}{2} + C_g^2 \ln \rho_g\right)^{\dagger *} = \left(\frac{\alpha_l \rho_u^2}{2\rho_g} + \frac{\alpha_g u_g^2}{2} + C_g^2 \ln \rho_g\right)^{\dagger} \quad (1.35e)$$

Remark 2. *For a given cell interface, A^- represent the area of the cell immediately left to the interface and A^+ to its immediate right.*

Remark 3. *Variations in the pressure profile $p_d(t, x)$ in the drillstring due to the changes in the cross-sectional area can be neglected — as a result of the assumption A6. This will reduce the Equation (1.35b) to a linear setting.*

Remark 4. *Let $\check{u}_j^n$ be the variables averaged over the cell G_i, then for a first order scheme $\check{u}_j^n = U_i^n$ for $j = i \in (x_{i\pm1/2})$. For a second order scheme, we use the linear interpolation $\check{u}_j^n = U_i^n + (u_x)_i^n(x - x_i)$, where $(u_x)_i^n$ is the approximation of the exact derivative of the variables; computed using a flux limiter (see, e.g. [73]).*

Input: $Q_{i-1}^n, Q_i^n, Q_{i+1}^n, A_{i-1}, A_i, A_{i+1}$
Output: Q_i^{n+1}
Compute primitive variables, $U_{i-1}^n, U_i^n, U_{i+1}^n$, from conservative variables, $Q_{i-1}^n, Q_i^n, Q_{i+1}^n$,
if $A_{i+1} \neq A_i$ **then**
  Set † $= +$ and # $= -$
  Solve (1.35) for the interface $x_{i+1/2}$, obtain $U_{i+1/2}^{+*}$
else
  $U_{i+1/2}^{+*} = U_{i+1/2}^{+}$
end
if $A_i \neq A_{i-1}$ **then**
  Set † $= -$ and # $= +$
  Solve (1.35) for the interface $x_{i-1/2}$, and obtain $U_{i-1/2}^{-*}$
else
  $U_{i-1/2}^{-*} = U_{i-1/2}^{-}$
end
Compute Q_i^{n+1} via (1.34).

Algorithm 1: Algorithm for the model-based modification [52]

Treatment of the boundary conditions

The numerical scheme (1.34), for $i = 1$ and $i = N$, has explicit dependency on U_0 and U_{N+1} for first-order schemes and, in addition, implicit dependency on U_{-1} and U_{N+2} for second-order schemes. These values are, *a priori*, not defined since they lie outside of the solution grid. One way of dealing with this issue is to extrapolate the solution, e.g. using polynomial approximations at the boundaries. However, extrapolation methods are only accurate in the absence of source terms [74]. Here, we rely on a characteristic-based method, more suited to the presence of source-terms [75]. For clarity purposes, we first detail the method for the case of the single-phase liquid flow occuring in the drillstring.

Characteristic-based method for the drillstring. Consider the system (1.14). Denoting $\lambda_{d,1} = v - C_l$ and $\lambda_{d,2} = v + C_l$, one can rewrite the system in the following form

$$\frac{\partial\left(p_d - C_l\rho v\right)}{\partial t} - \lambda_{d,1}\frac{\partial\left(p_d + C_l\rho v\right)}{\partial x} = C_l S_d \tag{1.36}$$

$$\frac{\partial\left(p_d + C_l\rho v\right)}{\partial t} + \lambda_{d,2}\frac{\partial\left(p_d + C_l\rho v\right)}{\partial x} = -C_l S_d \tag{1.37}$$

where (1.36) corresponds to the pressure wave travelling upstream the flow with a velocity of $\lambda_{d,1}$, while (1.37) corresponds to the pressure wave travelling along the flow direction with a velocity of $\lambda_{d,2}$. In what follows, we refer to (1.36),(1.37) as the characteristics-based formulation of the equations. At each boundary, the method

consists in solving a set of two nonlinear equations to determine the values of the solution U_0 and U_{N+1} outside of the stencil. These equations consist of

- the physical boundary condition, as described in Section 1.1.4 ;
- the propagation forward in time of the characteristic-based equation corresponding *to the boundary leaving the spatial domain*. This means that Equation (1.36) is used at the topside (P) boundary, while Equation (1.37) is used at the bit (B) boundary.

This yields the following nonlinear system at the pump boundary,

$$A_d(0)\,\rho(t,0)\,v(t,0) - J_p(t) = 0 \tag{1.38a}$$

$$\frac{\partial p_d}{\partial t} - \lambda_{d,1}\frac{\partial p_d}{\partial x} - C_l\rho\frac{\partial v}{\partial t} - C_l\rho\lambda_{d,1}\frac{\partial v}{\partial x} = C_l S_d. \tag{1.38b}$$

Finding an analytical solution for the partial differential algebraic equation (1.38) is challenging. Thus, the system (1.38) is numerically solved for the next timestep $t = n+1$ using a first-order finite difference upwind scheme yielding

$$A_{d,0}\rho_0^{n+1}v_0^{n+1} - {J_p}^{n+1} = 0 \tag{1.39a}$$

$$\begin{aligned}\frac{p_{d,0}^{n+1} - p_{d,0}^n}{\Delta t} - C_l\rho_1^n\frac{v_0^{n+1} - v_0^n}{\Delta t} = &-(\lambda_{d,1})_1^n\frac{p_{d,0}^n - p_{d,1}^n}{\Delta x}\\ &- C_l(\rho\lambda_{d,1})_1^n\frac{v_0^n - v_1^n}{\Delta x} + C_l S_d\left(U_{d,1}^n\right)\end{aligned} \tag{1.39b}$$

Similarly, at the bit side, Equation (1.37) is discretized using a forward Euler scheme.

Characteristic-based method for two-phase flow. No exact characteristic-based form for (1.15) could, unfortunately, be derived. To apply the method, we make additional simplifying assumptions that enable such a formulation.

A8 the liquid is incompressible, i.e., $\dfrac{\partial C_o(u)}{\partial u} = 0$ and $\dfrac{\partial V_o(u)}{\partial u} = 0$

A9 the mass fraction of the gas is much lower than the liquid, i.e., $\alpha_g\rho_g \ll \alpha_l\rho_l$

Note that these assumptions are *solely used at the boundary*[6]. Under these assumptions, the characteristic equations represent the fast dynamics (pressure waves on either directions of the fluid transmission) and the slow dynamics (migration of the gas phase) and take the form [64]

$$\alpha_g\left(1 - C_0\alpha_g\right)\frac{d_1 p_a}{d_1 t} + p_a\frac{d_1}{d_1 t}\alpha_g = 0 \tag{1.40}$$

$$\frac{d_2 p_a}{d_2 t} - \rho_l C_m\left(v_g - v_l\right)\frac{d_2\alpha_g}{d_2 t} - \rho_l\alpha_l\left(v_g - v_l + C_m\right)\frac{d_2 v_l}{d_2 t} = \left(v_g - v_l + C_m\right)S_a \tag{1.41}$$

$$\frac{d_3 p_a}{d_3 t} + \rho_l C_m\left(v_g - v_l\right)\frac{d_3\alpha_g}{d_3 t} - \rho_l\alpha_l\left(v_g - v_l - C_m\right)\frac{d_3 v_l}{d_3 t} = \left(v_g - v_l - C_m\right)S_a \tag{1.42}$$

where C_m is the sound velocity (for details see, e.g. [36], [76]–[79]) in the mixture and the directional derivative along the vector $V = [1, \lambda_{a,i}]^T$ of eigenvalues[7] of the

[6] Other simplifying assumptions are considered inside the computational domain, see [53], [52] and the citations therein.

[7] see, e.g. [80] for the eigenvalue analysis of the DFM. The standing wave due to the variable geometry corresponding to $\lambda_4 = 0$ is analysed in [52]. At the boundary, it is reasonable to assume a constant area.

DFM $\lambda_{a,i}$ defined as

$$\frac{d_i}{dt} := \frac{\partial}{\partial t} + \lambda_{a,i}\frac{\partial}{\partial x}, \quad i = 1,2,3. \tag{1.43}$$

For subsonic flow, the characteristic velocities satisfy

$$\lambda_{a,1} > 0, \qquad \lambda_{a,2} > 0, \qquad \lambda_{a,3} < 0 \tag{1.44}$$

which is consistent with the number of boundary conditions at each boundary. Indeed, there is a single physical boundary condition (1.25) at the outlet of the annulus, with two outgoing characteristics, while there are, in total, three physical boundary conditions (1.21)–(1.23) with one outgoing characteristic in the drillstring and one in the annulus. This situation is schematically depicted on Figure 1.3. Similar to the

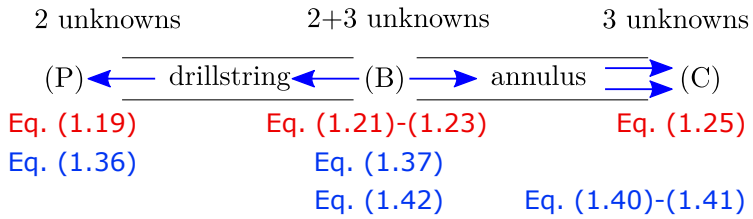

FIGURE 1.3: Schematic representation of the characteristic-based treatment of the boundary conditions. The equations in red represent the physical boundary conditions, while the blue ones correspond to outgoing characteristics.

case of single-phase flow, the characteristic equations (1.40)–(1.42) are discretized using a first-order finite-difference upwind scheme yielding, along with the physical boundary condition, a nonlinear system that is solved using Newton's algorithm. Due to the presence of a non-return valve that introduces a non-differentiable nonlinearity, the bit boundary condition (B) requires a slightly different treatment, which is detailed in [53]. In the next section, we apply this method on several test cases representing realistic industrial scenarios.

1.2.2 Simulation of industrial scenarios

An important aspect of the proposed model and numerical scheme is their ability to reproduce the behaviour of single and multiphase flow during typical industrial situations. In view of using the code developed within the HYDRA[8] project both for training and testing of control algorithm at Kelda Drilling Controls AS, an important effort has been devoted to integrate the simulator within the company's development framework, thus facilitating the transfer of knowledge to the industry. A description of this procedure is given in Appendices A and B.

The numerical simulation of Section A.3 is performed within this framework. Besides, the simulation scenarios presented in this section have been elaborated in collaboration with Kelda Drilling Controls to reflect situations encountered while drilling actual wells. The description of these scenarios, along with appropriate simulations is envisioned to become benchmarks for observer, controller and model testing within the industry. We present the results obtained from a study to evaluate the pressure control systems for MPD operations, that led to the publication [53]. A schematic of the wellbore profile used in the simulations is show in Figure 1.4 and

[8] HYdraulic modelling for DRilling Automation.

the simulation parameters are defined in Table 1.1. We study the results for both *open-loop*[9] and *closed-loop* simulations and are described for each of the scenarios.

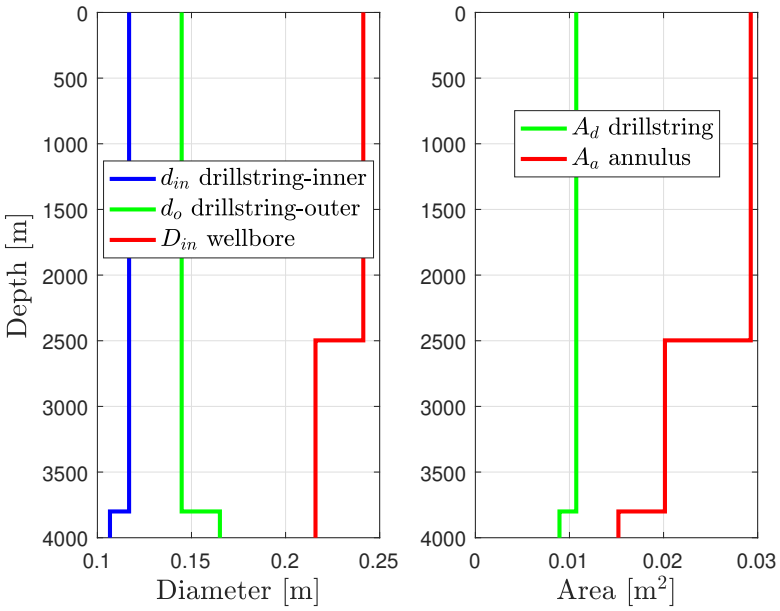

FIGURE 1.4: Wellbore profile with realistic variations in the flow geometry, used in the simulation of industrial scenarios.

Choke plugging. Choke plugging is a contingency likely to occur during an MPD operation. Indeed, during the drilling process, the drilled rock cuttings are transported up in the annulus. It is one of the functions of drilling mud to clean the wellbore and transport the cuttings. The average size of drilled cuttings depend on the type of the drill bit. However, for some physical and chemical properties of the rocks or a poorly engineered mud, big lumps of the cuttings may be transported up in the annulus. In such scenarios, the masses of drilled cuttings can plug the choke opening entirely. It is an operational requirement that two chokes aligned in parallel are present at the manifold. But, the pressure surge created at the choke due to the plugging, creates a pressure wave reflection phenomenon. The presented model illustrates the impact of such an event on the pressure and flow dynamics.

Open-loop. Effects on the choke pressure p_c and the BHCP p_{dh}, when the choke opening Z_c is plugged, can be seen in Figure 1.5. If unnoticed or not reacted in-time, pressure build-up in the wellbore may fracture the reservoir, initiating a chain of unwanted actions. The wave reflection and delay of the effect at each boundary are clearly seen because of the use of distributed models presented in this section.

Closed-loop. We now present the simulation results obtained by using a controller to maintain the required BHCP during a choke plugging scenario. Controller actuation is the choke value opening and the controller design is detailed in [53]. We implement the proposed controller on the design model, i.e., Kaasa model [36], and the distributed model discussed in Section 1.1. The results are shown in Figure 1.6 and depict two important characters : pressure wave

[9] i.e., without any controller.

TABLE 1.1: The simulation parameter values used to obtain the simulations of the industrial scenarios.

Parameter	Symbol	Value	Unit
Length of the well	L	4000	m
Well inclination	$\theta(x)$	$\pi/2$	rad
Liquid bulk modulus	β_l	1.1e+09	Pa
Sound speed in gas	C_g	316	$\mathrm{m\,s^{-1}}$
Reference pressure	p_0	1e+05	Pa
Liquid density at p_0	ρ_0	1500	$\mathrm{kg\,m^{-3}}$
Number of chokes	n_c	1	[-]
Choke flow factor	$K_{c,1}$	0.0025	$\mathrm{m^2}$
Average velocity	V_d	0.5	$\mathrm{m\,s^{-1}}$
Liquid viscosity	μ_l	0.04	Pa s
Gas viscosity	μ_g	5e-06	Pa s
Bit nozzles area	A_n	5.77e-04	$\mathrm{m^2}$
Space discretization step length	Δx	12.5	m
Gas production index	κ_g	8e-07	$\mathrm{kg\,Pa^{-1}\,s^{-1}}$
Bit discharge coefficient	c_d	0.8	[-]
Profile parameter	C_0	1.1	[-]
Number of discretization cells	N	320	[-]
CFL condition	-	0.9	[-]

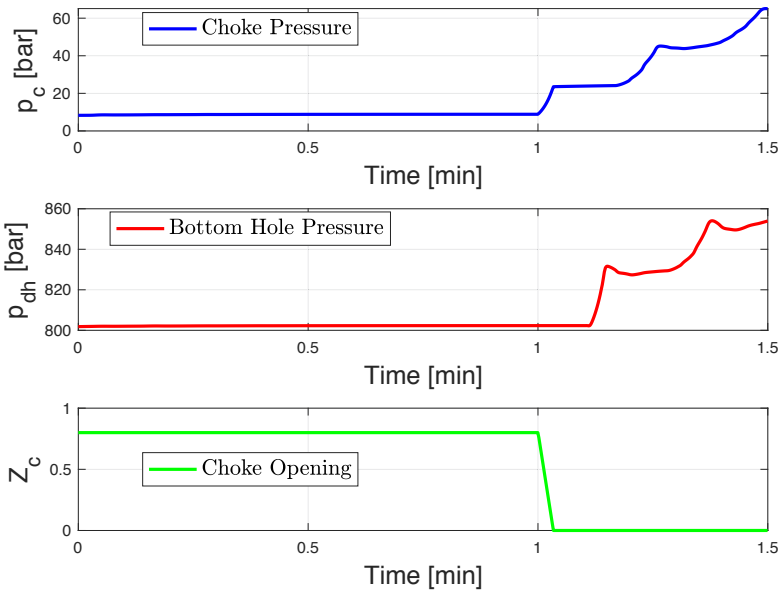

FIGURE 1.5: Open-loop choke plugging simulations. Results shows the pressure surge in an event of a blockage at the choke valve.

reflections at the choke and bottom of the wellbore in the simulation model, i.e., the distributed model, that are not seen in the design model which is a lumped low-order dynamical model; steady-state solution for the choke pressure p_c and the pump pressure p_p are different for both the models—the design model does not account for the compressibility of the fluid. The second part (right) of the Figure 1.6 shows the velocity profile of the liquid along the wellbore v and in the annulus v_l. We notice that the steady-state profiles are

perturbed due to the choke plugging and the discontinuities in the area acts as reflecting points for the pressure waves that are also showcased by the velocity profiles.

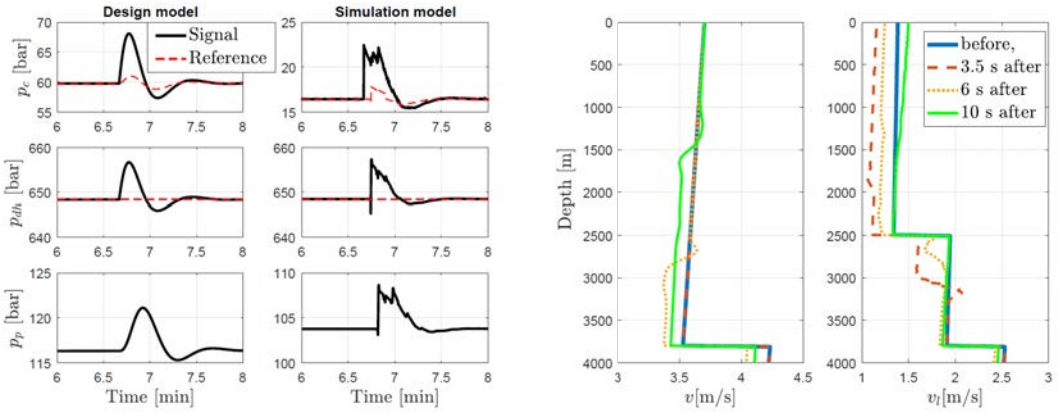

FIGURE 1.6: Choke plugging scenario with a controller to maintain the BHCP. *Left:* shows the comparison of the dynamics obtained by low-order and distributed model in an even of choke plugging. *Right:* shows the snapshots of the velocity profiles during different times, influenced by the pressure wave reflections in the wellbore.

Connections. One of the most common and repetitive operations on a drilling rig is *connection*. Drillpipes—$\approx 10m$—attached to their joints constitute a drillstring. To drill further, or to remove the drillstring out of the wellbore, it is required to (dis-) connect the drillpipe. We describe the connection process as follows :

1. Stop the drilling process.
2. Reduce the flow rate of the mud from the pump to zero.
3. Mechanically (dis-) connect the drillpipe from the drillstring on the rig floor.
4. Increase the flow rate of the mud from zero to an operational value.
5. Resume drilling.

We now present the simulations for a connection operation.

Open-loop. Both the choke opening Z_c and the pump flow J_p are manually operated (a back-pressure pump at the surface is not considered here) and the simulation result is shown in Figure 1.7. The changes created by such operation at one end, i.e., choke, generates a pressure pulse that reflects at the bottom. Indeed, the choke set-point changes create pressure pulses at the choke that travels to the bottom of the wellbore. It was observed that there is an offset between the pressure changes at the choke p_c to be reflected at the bottom of the wellbore p_{dh}. This time difference is dictated by the velocity of sound in the liquid—at which the pressure wave travels in the medium. The pressure wave reflections sustain even at zero flow and dissipates only due to the frictional losses. We note that during manual connection operations, the BHCP may exceed the reservoir pressure and create fractures.

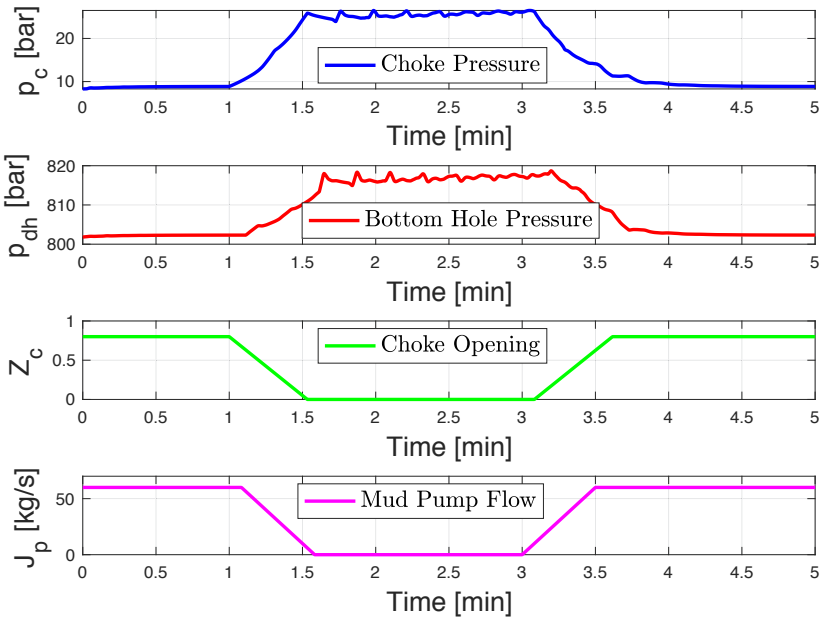

FIGURE 1.7: Open loop Connection operation. When the choke and pump are manually operated, it leads to pressure oscillations within the wellbore. They are captured here when the pump flow is zero. Reflecting waves sustain until dissipated by frictional forces.

Closed-loop. Using a closed-loop choke set-point changes can provide a better control of the BHCP. The flow rate of the mud pump and the back-pressure pump is changed as shown in Figure 1.8. Now, a controller is used to manipulate the choke opening to maintain the required BHCP. We again present the simulation case study comparing the controller performance using the design model and the distributed model. We present the results as a comparison between the design model and the distributed model but with two different set of control parameters [53]. Their performances are summarized as follows :

1. Parameter set for simulations in Figure 1.9 is designed to lead a gentle control signal, a slow closed-loop system to recover from system disturbances, e.g. changes in pump flow. In this case, the results are similar for both the models. We argue that the distributed model reduces to the design model when the operations are rather smooth—no dynamics are excited.
2. Parameter set for simulations in Figure 1.10 is designed to create a faster closed-loop performance. Naturally, rapid set-point changes excites the faster dynamics in the system such as the pressure wave propagation. This leads to a poor controller performance than that achieved using the parameter set 1.

We argue that distributed models must be considered while designing a controller as faster dynamics of the system deteriorate the controller performance.

Gas influx. An influx occurs when the BHCP is lower than the reservoir pore pressure creating a drawdown. We present a scenario when the well is drilled into a high pressure gas pocket. Flow through the mud pump J_p is maintained at $40\,\mathrm{kg\,s^{-1}}$,

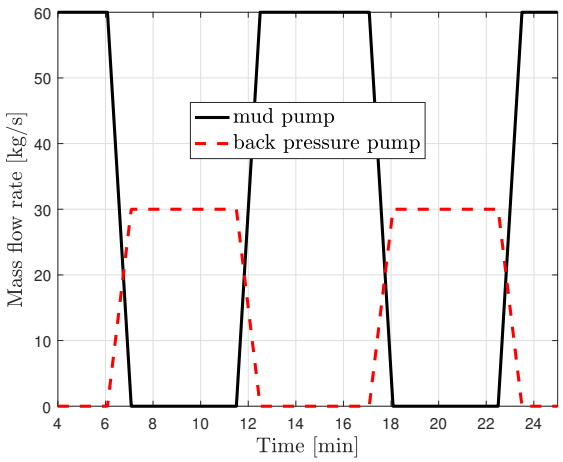

FIGURE 1.8: Mass flow rate changes for the mud pump and the back-pressure pump to simulate a closed-loop connection scenario.

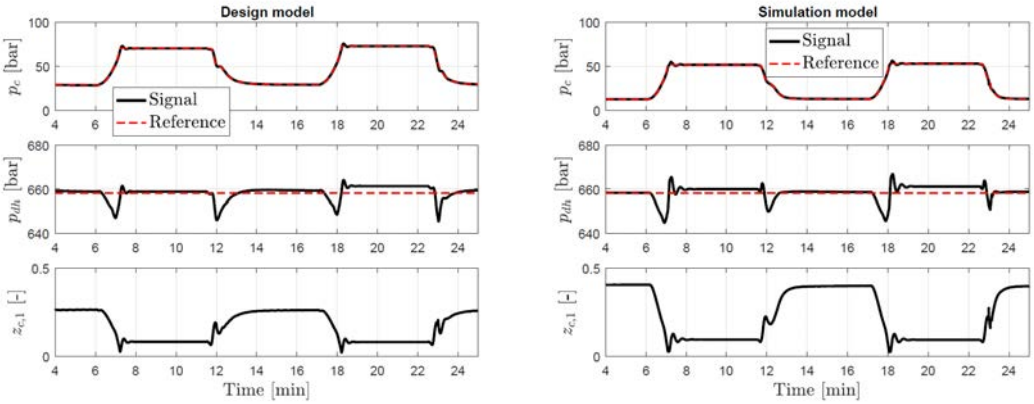

FIGURE 1.9: Closed-loop connection operation with parameter set 1. Distributed model reduces to the low order lumped model when the operations/ setpoints are changes smoothly.

while the reservoir pressure is rapidly increased by 4% at time $t = 400\,\text{s}$. Assuming that the gas kick is identified, a reference BHCP higher than the reservoir pressure is set [53]. This closed-loop simulation is shown in Figure 1.11. The results show the slow dynamics of the gas transport from the formation to the choke. The gas expansion increases the mass flow rate at the choke J_c, which drastically decreases when the gas start to exit the annulus. The void gas distribution along the wellbore is also shown. We note the effect of variable geometry on the gas distribution along the wellbore.

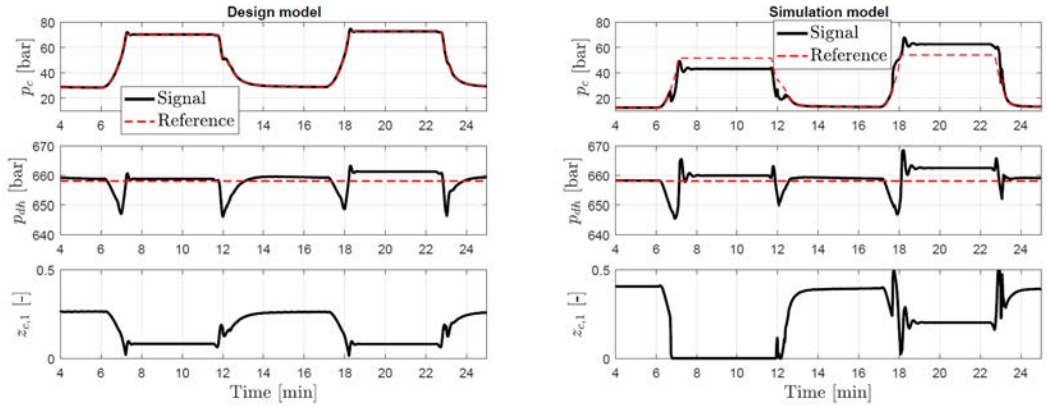

FIGURE 1.10: Closed-loop connection operation with parameter set 2. Due to rapid changes and better convergence to disturbances, faster dynamics are excited. Controller performance for the distributed model deteriorates as compared to the parameter set 1.

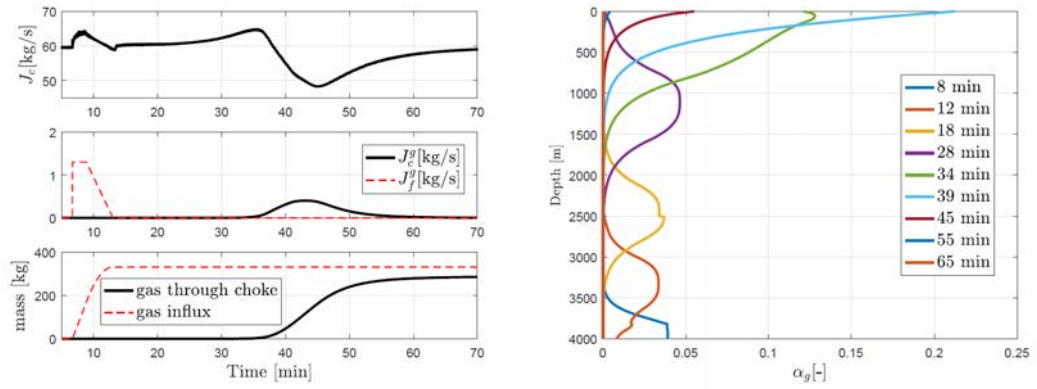

FIGURE 1.11: Simulation results of a gas influx situation. Controller is used to circulate the gas out of the annulus through the choke. *Left:* shows the behaviour of mass flow rate; first increases due to gas expansion and drastically reduces when the gas exits the choke. *Right:* shows the snapshot of the distribution of gas void fraction within the annular region during the circulation process.

Chapter 2

Reservoir models

Dans ce chapitre, nous détaillons les équations du modèle décrivant la dynamique de la pression dans le réservoir. Ce modèle s'appuie également sur des lois de conservation, s'inspire largement des travaux de [13]. Dans le cas d'un réservoir de liquide, des hypothèses simplificatrices permettent la linéarisation du modèle, ce qui n'est pas le cas des réservoirs de gaz. Un schéma numérique permettant le calcul des solutions numériques de cette équation est présenté, avec des simulations illustrant les principales caractéristiques du modèle. Nous soulignons l'importance de préserver le caractère distribué de la dynamique dans le réservoir dans le cadre de scénarios transitoires qui sont caractéristiques des situations rencontrées en forage, à l'inverse de l'ingénierie de production.

In this chapter, we describe the model reproducing the pressure dynamics inside the reservoir. The model, also based on first principles, is largely inspired from [13]. In the case of a liquid reservoir, reasonable simplifying assumptions allow the model to be linearized, contrary to the case of a gas reservoir. Again, a scheme enabling efficient computation of the numerical solution is presented, along with simulations illustrating the main features of the model. In particular, we advocate for the importance of retaining the *distributed* dynamics inside the reservoir in a transient setting such as the ones encountered in drilling, as opposed to production engineering.

2.1 Distributed model: Radial diffusion equation

We consider a porous reservoir and make the following assumptions :

A1 The reservoir is completly saturated with a single fluid.

A2 The reservoir is homogeneous in the azimuthal and vertical directions. This assumption is restrictive, particularly regarding the vertical direction : it requires the section of the wellbore in contact with the reservoir to be sufficiently short.

Applying the mass conservation law over an infinitesimal radial section (see Figure 2.1) and applying Darcy's law yields the following pressure dynamics [13]

$$\frac{1}{r}\frac{\partial}{\partial r}\left(\frac{\kappa\rho(p(t,r))}{\mu(p(t,r))}r\frac{\partial p(t,r)}{\partial r}\right) = \phi c(p(t,r))\rho(p(t,r))\frac{\partial p(t,r)}{\partial t} \tag{2.1}$$

where $p(t,r)$ is the pressure of the contained fluid, μ its viscosity, c the total compressibility (fluid and rock), κ the permeability of the rock and ϕ its porosity. For sub-surface reservoirs, the radial domain extends from the radius of wellbore (r_w), to the "infinite" extent of the reservoir (r_e) — a region not affected by the near-wellbore dynamics, i.e., $r \in [r_w, r_e]$. Assuming an instantaneous pressure equilibrium at the

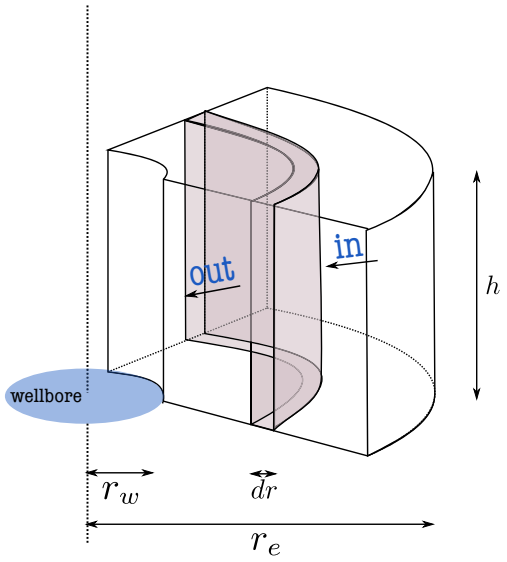

FIGURE 2.1: Schematic of the radial reservoir section. Mass conservation is applied over the highlighted infinitesimal section, with Darcy's law that gives radial diffusion equation.

near wellbore region and a zero flux set at the radial extent of the reservoir yields the following boundary conditions

$$p(t, r_w) = \text{BHCP} \tag{2.2}$$

$$\frac{\partial p}{\partial r}(t, r_e) = 0. \tag{2.3}$$

Equation (2.3) indicates that the reservoir is at rest away from the wellbore. This boundary condition should be modified in an Enhanced Oil Recovery (EOR) setting were fluids are injected from other wells to maintain a high reservoir pressure.

2.1.1 Pure liquid reservoir

It can be seen from Equation (2.1) that the equation is non linear — density, viscosity and compressibility all *a priori* depend on pressure. We make the following additional assumption that the

A3 density, viscosity and compressibility are constant.

This yields the following linear pressure dynamics

$$\frac{\partial p(t,r)}{\partial t} = \frac{a}{r}\frac{\partial}{\partial r}\left(r\frac{\partial p(t,r)}{\partial r}\right) \tag{2.4}$$

where $a = \kappa/\mu c\phi$. Applying Darcy's law [13] at the wellbore boundary of the reservoir yields the following equation defining the influx of fluid into the wellbore

$$q_{\text{inf}}(t) = \underbrace{\frac{2\pi\kappa h r}{\mu}}_{\xi}\frac{\partial p}{\partial r}(t, r_w). \tag{2.5}$$

Thus, computing the value of the influx using Equation (2.5) requires the solution of the distributed reservoir model Equation (2.1) or Equation (2.4) at each timestep.

In Section 2.2, we present approximate solutions based on various simplifying assumptions. First, we describe the model in the case of a dry gas reservoir.

2.1.2 Pure gas reservoir

Due to the the high compressibility of gas, relying on Assumption A3 would result in a highly inaccurate model for a gas reservoir. For the sake of better representation, let us write Equation (2.1) in the form

$$b(p,r)\frac{\partial p}{\partial t} - \frac{\partial}{\partial r}\left(a(p,r)\frac{\partial p}{\partial r}\right) = 0 \tag{2.6}$$

where $a(p,r)$ and $b(p,r)$ are the functions that represent different non-linear terms defined by

$$a(p,r) = r\frac{\rho(p,z(p))}{\mu(\rho(p,z(p)))} \quad , \qquad b(p,r) = \frac{r\phi}{k}c(p,z(p))\rho(p,z(p)). \tag{2.7}$$

We now detail how these terms are modeled as a function of pressure, relying on models from the literature.

Density : the z factor

For the conditions encountered in a gas reservoir, the ideal-gas law does not hold because the volume of the constituent molecules and their intermolecular forces strongly affect the volumetric behaviour of the gas [81]. Such deviation from the ideal gas behaviour is expressed as a factor z, i.e. we assume that the following EOS holds

$$p = z\rho R_g T \tag{2.8}$$

where R_g is the specific gas constant and T is the temperature. Cubic EOS accurately predict the volumetric behaviour of gas and mixtures in pressure / temperature conditions typically encountered in reservoirs [81]. They define z as the only physically meaningful root[1] of the following polynomial

$$z^3 + A_2 z^2 + A_1 z + A_0 = 0 \tag{2.9}$$

where the constants A_0, A_1 and A_2 are functions of pressure, temperature and phase composition. Several modifications were proposed since the seminal work — Van der Wall's cubic EOS, of which the modification by Peng-Robinson gives

$$A_0 = -(AB - B^2 - B^3) \tag{2.10}$$
$$A_1 = (A - 3B^2 - 2B) \tag{2.11}$$
$$A_2 = -(1 - B) \tag{2.12}$$

[1] One or three real roots may exist, where the smallest root is typically chosen for liquids and the largest root is chosen for vapours [81].

with the EOS constants defined as

$$A = \Omega_a^0 \frac{p_r}{T_r^2}\alpha(T_r), \qquad \alpha = \left(1 + m\left(1 - \sqrt{T_r}\right)\right)^2 \tag{2.13}$$

$$B = \Omega_b^0 \frac{p_r}{T_r} \quad , \qquad m = 0.37464 + 1.54226\omega - 0.26992\omega^2 \tag{2.14}$$

where $\Omega_a^0 = 0.45724$ and $\Omega_b^0 = 0.07780$. The reduced pressure and reduced temperature are given by $p_r = p/p_c$ and $T_r = T/T_c$. Here p_c and T_c are critical pressure and temperature respectively. In what follows, we add the following assumption that the

A4 the temperature T inside the reservoir is constant.

This yields the following expression for density as a function of pressure only

$$\rho(p, z(p)) = \frac{p}{z(p)R_g T} \quad . \tag{2.15}$$

Viscosity

One of the sensitive physical property of gas with respect to pressure is viscosity. In the petroleum industry, viscosity of crude oil is typically modeled using the Lee-Gonzalez correlation that reads [81]

$$\mu(\rho(p, z(p)) = A_1 \exp\left(A_2 \rho(p, z(p))^{A_3}\right) \tag{2.16}$$

where the parameters are defined as

$$A_1 = \frac{(9.379 + 0.01607M_g)T^{1.5}}{209.2 + 19.26M_g + T} \times 10^{-4} \tag{2.17}$$

$$A_2 = 3.448 + (986.4/T) + 0.01009M_g \tag{2.18}$$

$$A_3 = 2.447 - 0.2224A_2 \quad . \tag{2.19}$$

Here M_g represents the molecular weight of the gas.

Compressibility

The compressibility of a fluid is defined as

$$c(p) = \frac{1}{p} - \frac{1}{V}\left(\frac{\partial V}{\partial p}\right)_T \tag{2.20}$$

which, using Equation (2.15), Equation (2.20) takes the following form

$$c(p, z(p)) = \frac{1}{p} - \frac{1}{z}\left(\frac{\partial z}{\partial p}\right)_T \quad . \tag{2.21}$$

2.2 Approximate solutions for liquid influx

In this section, we investigate various way to compute an approximate solution to the PDE (2.4) along with boundary conditions (2.2),(2.3). The main objective is to provide dynamical relations between the influx q_{res} and the BHCP that can be used

in appropriate contexts. In Section 2.2.1, we recall simple explicit relations typically used in the context of production. In Section 2.2.2, we derive Green's function to derive a semi-analytical solution in the form of an infinite sum.

2.2.1 Approximate solutions from production engineering

Using simplifying assumptions regarding the flow conditions, analytical expressions to calculate the influx of liquid can be derived. They are inspired from production engineering where the situations of long and sustained flow of reservoir fluids are studied [13]. These lead to the so-called quasi-steady-state solution and constant terminal rate solution.

Quasi-steady-state solution. A first approximate solution can be obtained by assuming that the outflow from the reservoir is constant, meaning $\dot{q}_{res} = 0$. Denoting q_{res}^{qss} the corresponding reservoir flow, this leads to the following relation between the value of the pressure at the wellbore boundary $p(t, r_w)$, at the radial extent, i.e., p_e and the flow

$$q_{res}^{qss} = -\frac{2\pi\kappa h}{\mu} \frac{(p(t, r_w) - p_e)}{(\ln(r_e/r_w) - 1/2)} \quad . \tag{2.22}$$

Although valid only for stabilized flow conditions, this relation, referred to as the Productivity Index (PI) relation, is sometimes used in a transient setting [82] or averaged over time [83].

Constant terminal rate solution (CTRS). Another approximate solution is obtained by assuming that the radial extent of the reservoir is infinitely far away and the pressure is constant there, i.e., p_e, giving [13]

$$\lim_{r \to +\infty} p(t, r) = p_e \tag{2.23}$$

and that the flow rate q_{res} is suddenly changed from zero to a constant value. This yields the following relation between flow rate and pressure

$$q_{\text{ctr}}(t) = -\frac{4\pi\kappa h\,(p(t, r_w) - p_e)}{\mu \left(\log \frac{4\kappa t}{\gamma\phi\mu c r_w^2} + 2S\right)} \tag{2.24}$$

where S is the skin factor — related to the additional pressure drop within the near wellbore reservoir section due to prolonged production (alongwith sand production) or decrease in the pressure drop in case of well stimulation operations. This relation[2] (2.24) is the most widely used for reservoir characterization [37], [39], [49].

A test case to compare the different influx models is set to assert the need of distributed reservoir pressure dynamics and influx using Darcy's equation. Here, as an illustrative example, we create sinusoidal oscillations for BHCP[3] with a mean of pressure at the reservoir extent. Influx from the reservoir for such a scenario is shown in Figure 2.2. The result from the distributed model was obtained using a highly refined gridding routine (especially in the near-wellbore region, details

[2] valid for $x < 0.01$, when the logarithmic function in the denominator is expressed in the form : $-\log(\gamma x)$, see [13]. The expression is therefore a poor approximation only for a short amount of time (around 1 second). This can, however, lead to over- or under-estimate a small amount of the influx, which is a motivation for considering a distributed model.

[3] BHCP(t) $= 1.85e7 + 1e5 \sin(10t/T_n)$, where $T_n =$ Run time$/dt$.

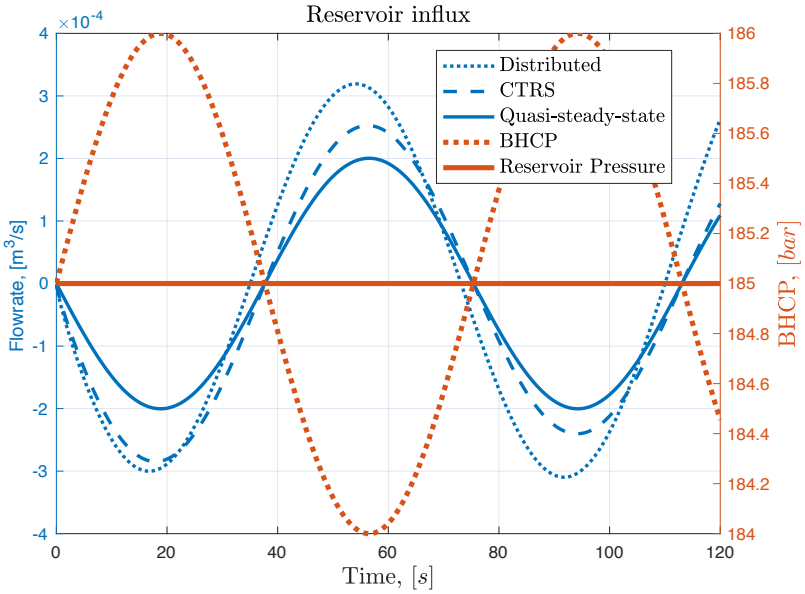

FIGURE 2.2: Response of different influx models for a test case of BHCP oscillations. The plots in red represent the sinusoidal pressure oscillations of BHCP (dashed) with respect to the reservoir pressure (solid). This represents the BHCP fluctuations due to pressure wave reflection in an event of choke set point change. The plots in blue represent the respective response for influx from various reservoir models considered.

in Section 2.3.1). The simulations show that the approximate solutions (CTRS and quasi-steady state solution) under-estimate the influx, in a transient setting. This is important because of the following reasoning. Fluctuations in the BHCP are highly likely, e.g. due to pressure wave propagations during choke set-point changes (as illustrated in Section 1.2.2). The situation where a given influx scenario turns into a well control situation is highly dependent on the cumulative volume of the influx flowing in from the reservoir [2], which, therefore, should not be under-estimated ; that will effectively increase the chance of an influx event that could normally be handled dynamically[4] in the MPD setting, to a well control situation due to the late reactions. Such instances jeopardize the safety of personnel and equipment. Thus, we argue that the distributed model is required to estimate the influx flow rates while drilling, where we are interested in the time period of *at-most a few hours* during which the transient behaviour of the reservoir dominates.

2.2.2 Solution based on Green's function

In this section, we derive a general solution to (2.4) relying on the computation of Green's function. First, we make the following change of variables

$$\varphi(t,r) = p(t,r) - \mathrm{BHCP}(t). \tag{2.25}$$

This yields the following dynamics

$$\frac{\partial \varphi(t,r)}{\partial t} = \frac{a}{r}\frac{\partial}{\partial r}\left(r\frac{\partial \varphi(t,r)}{\partial r}\right) - \frac{\partial \mathrm{BHCP}(t)}{\partial t} \tag{2.26}$$

[4] without closing the BOP — leading to NPT — to circulate out the kick.

with the initial and the boundary conditions over the domain of interest $r \in [r_w, r_e]$ are given by

$$\varphi(0,r) = \varphi_0 \tag{2.27}$$
$$\varphi(t,r_w) = 0 \tag{2.28}$$
$$\frac{\partial \varphi(t,r_e)}{\partial r} = 0. \tag{2.29}$$

Notice that BHCP_t now appears as a source term in Equation (2.26). We follow the classical procedure, consisting of solving the homogeneous radial diffusivity equation with mixed boundary conditions (2.28),(2.29), and use the corresponding Green's function to derive the general solution. Denote ϕ the solution to the homogeneous equation, obtained by taking $\mathrm{BHCP}(t) \equiv 0$ in (2.26). We look for a particular solution by applying the separation of variables method, i.e., of the form

$$\phi(t,r) = f(r)g(t). \tag{2.30}$$

The functions f and g must satisfy, respectively[5]

$$rf''(r) + f'(r) + \frac{\lambda}{a} rf(r) = 0 \tag{2.31}$$

and

$$g'(t) = -\lambda g(t), \qquad g(0) = 1 \tag{2.32}$$

for some $\lambda \in \mathbb{R}$. There is only a discrete number of possible λ corresponding to a family of solutions

$$f_n(r) = Y_0(\omega_n r_w)J_0(\omega_n r) - J_0(\omega_n r_w)Y_0(\omega_n r), \qquad g_n(t) = e^{-\lambda_n t} \tag{2.33}$$

with

$$\lambda_n = \epsilon^2 \omega_n^2 \tag{2.34}$$

where the ω_n, $n \in \mathbb{N}^*$ are zeros of the following Bessel equation

$$-Y_0(\omega_n r_w)J_1(\omega_n r_e) + J_0(\omega_n r_w)Y_1(\omega_n r_e) = 0 \tag{2.35}$$

and Y_i, J_i, $i = 0, 1$ are the Bessel functions of the first and second kind, respectively. The f_n form Riesz basis of $\mathcal{L}^2$, but not a Hilbert basis. It possesses, however, a bi-orthonormal basis $(\psi_n)_{n\in\mathbb{N}^*}$ defined as

$$\psi_n = \frac{f_n r}{A_n} \quad , \qquad A_n = \frac{1}{2}\left(r_e^2 f_n^2(\omega_n r_e) - r_w^2 \frac{f_n'(\omega_n r_w)^2}{\omega_n^2} \right) \tag{2.36}$$

which yields the following expression of the homogeneous solution

$$\phi(t,r) = \sum_{n=1}^{\infty} a_n f_n(r) g_n(t) \tag{2.37}$$

[5] *notation :* for a function f, the first and second derivatives are denoted as f' and f'' respectively.

where the coefficients a_n are determined from the initial condition as follows :

$$a_n = \int_{r_w}^{r_e} \phi_0(r)\psi_n(r)dr \tag{2.38}$$

where $\phi_0 = p_i - \text{BHCP}_0$. Defining the following Green's function

$$G(r,\xi,t) = \sum_{n=1}^{\infty} \psi_n(\xi) f_n(r) g_n(t) \tag{2.39}$$

it is now possible to represent the general solution in terms of the scalar product as

$$\phi(t,r) = \int_{r_w}^{r_e} G(r,\xi,t)\phi_0(\xi)d\xi. \tag{2.40}$$

Now that the general solution for the homogenous diffusivity equation is derived, we now treat the source term. The general solution may now be represented as

$$\begin{aligned}\varphi(t,r) = &\int_{r_w}^{r_e} \varphi_0(\xi)G(r,\xi,t) - \text{BHCP}(t)\int_{r_w}^{r_e} G(r,\xi,0)d\xi \\ &+ \text{BHCP}(0)\int_{r_w}^{r_e} G(r,\xi,t)d\xi + \int_0^t \text{BHCP}(\tau)\int_{r_w}^{r_e} G_t(r,\xi,t-\tau)d\xi d\tau.\end{aligned} \tag{2.41}$$

An approximate solution can thus be computed by truncating the series (2.39). As will appear in Section 2.3, this representation is useful in the context of a continuous influx, but cannot be used to model kicks, due to the occurence of a Gibbs phenomenon. In the next section, we detail how the reservoir dynamics can be numerically solved.

2.3 Numerical simulations

2.3.1 Numerical method

In this section, we present a numerical scheme to solve equations of the form

$$b(p,r)\frac{\partial p}{\partial t} - \frac{\partial}{\partial r}\left(a(p,r)\frac{\partial p}{\partial r}\right) = 0. \tag{2.42}$$

The scheme is the so-called θ–scheme as described in [84]. We detail here the specific computations needed to implement the scheme for the liquid and gas reservoir models of Sections 2.1.1 and 2.1.2. Consider a (possibly irregular) grid

$$r_w = r_1 < \cdots < r_N = r_e \tag{2.43}$$

and denote $p_i^n = p(r_i, n\Delta t)$. Denote the operator $A_h = -\frac{\partial}{\partial r}\left(a(p,r)\frac{\partial p}{\partial r}\right)$ and an intermediate variable

$$U_i^n = \theta p_i^{n+1} + (1-\theta)p_i^n \tag{2.44}$$

that is a function of the values of the state at the current and future timesteps n and $n+1$ respectively. The variable θ is a design parameter that sets the implicitness

of the scheme: $\theta = 0$ being fully explicit and $\theta = 1$ being fully implicit[6]. Using a forward Euler discretization scheme over time on (2.42) yields

$$\frac{b(U_i^n, r_i)}{\Delta t}\left(p_i^{n+1} - p_i^n\right) + A_h(U_i^n) = 0. \tag{2.45}$$

The approximation of the operator A_h is chosen as follows [84]

$$A_h(U_i^n) = -\frac{1}{(r_{i+1/2} - r_{i-1/2})}\left(a(U_{i+1/2}^n, r_{i+1/2})\left(\frac{U_{i+1}^n - U_i^n}{r_{i+1} - r_i}\right) - a(U_{i-1/2}^n, r_{i-1/2})\left(\frac{U_i^n - U_{i-1}^n}{r_i - r_{i-1}}\right)\right). \tag{2.46}$$

The operator defined in Equation (2.46) is a function of the variables at the centres of the cells and at the interfaces. Refer to the stencil in the Figure 2.3. The general rep-

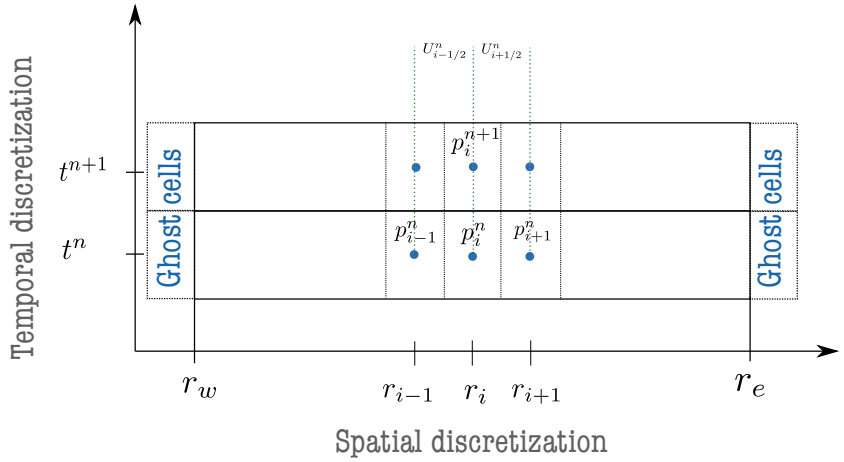

FIGURE 2.3: Stencil for the numerical scheme described to solve the diffusion equations. Provides a degree of freedom to choose the implicitness of the numerical scheme.

resentation of the intermediate variable at the cell centre is given by Equation (2.44) and the same at the interface reads

$$U_{i+1/2}^n = \frac{\theta}{2}\left(p_i^{n+1} + p_{i+1}^{n+1}\right) + \frac{(1-\theta)}{2}\left(p_i^n + p_{i+1}^n\right). \tag{2.47}$$

At the boundaries, simple extrapolation is performed, which yields

$$U_0^{n+1} = \text{BHCP}, \qquad U_{N+1}^{n+1} - U_N^{n+1} = 0. \tag{2.48}$$

Let us now define the variables

$$\alpha_1 = \frac{1}{(r_{i+1/2} - r_{i-1/2})}\frac{1}{(r_{i+1} - r_i)} \tag{2.49}$$

$$\alpha_2 = \frac{1}{(r_{i+1/2} - r_{i-1/2})}\frac{1}{(r_i - r_{i-1})} \tag{2.50}$$

[6] the special case of $\theta = 0.5$ is referred to as the Crank-Nicolson method.

that allows us to represent the equation to be solved at each time step in a compact form that reads, for $i = 1, ..., N$

$$F := \frac{b(U_i^n, r_i)}{\Delta t}\left(p_i^{n+1} - p_i^n\right) - \alpha_1 a(U_{i+1/2}^n, r_{i+1/2})\left(U_{i+1}^n - U_i^n\right) + \alpha_2 a(U_{i-1/2}^n, r_{i-1/2})\left(U_i^n - U_{i-1}^n\right) = 0. \quad (2.51)$$

We solve Equation (2.51) at each time step n to find the future solution at the timestep $n+1$. In other words, we find the zero of the defined function F with the knowledge of solution at previous timesteps. To do so, we use Newton's algorithm. We denote J_F the Jacobian matrix of F with respect to the solution at the new time step U^{n+1}. To improve the accuracy and to decrease the computational burden of this numerical scheme, we now derive the analytical Jacobian of F. Due to the dependency on 3 spatial locations: $i-1, i$ and $i+1$ for the operator at i, the Jacobians have a tri-diagonal structure and the respective derivatives can be calculated as follows:

$$\frac{\partial F}{\partial p_{i-1}^{n+1}} = -\theta\alpha_2 a(U_{i-1/2}^n, r_{i-1/2}) + \frac{\theta}{2}\alpha_2\left(U_i^n - U_{i-1}^n\right)\frac{\partial a}{\partial p_{i-1}^{n+1}}(U_{i-1/2}^n, r_{i-1/2}) \quad (2.52)$$

$$\frac{\partial F}{\partial p_{i+1}^{n+1}} = -\theta\alpha_1 a(U_{i+1/2}^n, r_{i+1/2}) - \frac{\theta}{2}\alpha_1\left(U_{i+1}^n - U_i^n\right)\frac{\partial a}{\partial p_{i+1}^{n+1}}(U_{i+1/2}^n, r_{i+1/2}) \quad (2.53)$$

$$\begin{aligned}\frac{\partial F}{\partial p_i^{n+1}} = \frac{b(U_i^n, r_i)}{\Delta t} + \frac{\theta}{\Delta t}\left(p_i^{n+1} - p_i^n\right)\frac{\partial b}{\partial p_i^{n+1}}(U_i^n, r_i) + \theta\alpha_1 a(U_{i+1/2}^n, r_{i+1/2}) \\ - \frac{\theta}{2}\alpha_1\left(U_{i+1}^n - U_i^n\right)\frac{\partial a}{\partial p_i^{n+1}}(U_{i+1/2}^n, r_{i+1/2}) + \theta\alpha_2 a(U_{i-1/2}^n, r_{i-1/2}) \\ + \frac{\theta}{2}\alpha_2\left(U_i^n - U_{i-1}^n\right)\frac{\partial a}{\partial p_i^{n+1}}(U_{i-1/2}^n, r_{i-1/2}). \quad (2.54)\end{aligned}$$

Equations (2.52)–(2.54) are the expressions of the Jacobian for the general radial diffusion equation (2.42). We now detail the specific computations for the gas and liquid reservoir models under consideration.

Real gas

Due to the highly pressure dependent properties of real gas, utilizing the $\theta-$ scheme requires an elaborate description of various derivatives, specially for the Jacobian matrix. Other cases — ideal gas and liquid — will only be specific cases of real gas scenario assuming pressure independencies for certain physical properties. First, recalling from Equation (2.7) that

$$a(p, r) = r\frac{\rho(p, z(p))}{\mu(\rho(p, z(p)))} \quad , \qquad b(p, r) = \frac{r\phi}{k}c(p, z(p))\rho(p, z(p)).$$

Applying chain rule it is simple to verify that

$$\frac{\partial a(p,r)}{\partial p} = r\frac{\mu(\rho(p,z(p)))\left(\frac{\partial \rho}{\partial p}+\frac{\partial \rho}{\partial z}\frac{\partial z}{\partial p}\right)-\rho(p,z(p))\left(\frac{\partial \mu}{\partial \rho}\left(\frac{\partial \rho}{\partial p}+\frac{\partial \rho}{\partial z}\frac{\partial z}{\partial p}\right)\right)}{\mu^2(\rho(p,z(p)))} \tag{2.55}$$

$$\frac{\partial b(p,r)}{\partial p} = \frac{r\phi}{k}\left(c(p,z(p))\left(\frac{\partial \rho}{\partial p}+\frac{\partial \rho}{\partial z}\frac{\partial z}{\partial p}\right)+\rho(p,z(p))\left(\frac{\partial c}{\partial p}+\frac{\partial c}{\partial z}\frac{\partial z}{\partial p}\right)\right). \tag{2.56}$$

We now define the derivatives of the functions defining the gas properties : $z-$factor, density, viscosity and compressibility.

$z-$factor

Using Equations (2.9) to (2.14) and by representing the EOS constants as linear function of pressure $A = ap$ and $B = bp$ for $a = \frac{\Omega_a^0 \alpha(T_r)}{p_c T_r^2}$ and $b = \frac{\Omega_b^0}{p_c T_r}$ one can write the cubic EOS as

$$z^3 - (1-bp)z^2 + (ap - 3b^2p^2 - 2bp)z - (abp^2 - b^2p^2 - b^3p^3) = 0. \tag{2.57}$$

Writing Equation (2.57) in a compact form reads

$$h(z,p) = 0. \tag{2.58}$$

Using the implicit function theorem, one can establish that

$$\frac{\partial h}{\partial p} + \frac{\partial h}{\partial z}\frac{\partial z}{\partial p} = 0 \tag{2.59}$$

$$g(z,p) := \frac{\partial z}{\partial p} = -\frac{\partial h/\partial p}{\partial h/\partial z}. \tag{2.60}$$

Now, from Equation (2.57) it is straightforward to compute the following:

$$h_1(z,p) := \frac{\partial h}{\partial z} = 3z^2 - 2(1-bp)z - 3b^2p^2 + (a-2b)p \tag{2.61}$$

$$h_2(z,p) := \frac{\partial h}{\partial p} = 3b^3p^2 + (2b^2 - 2ab - 6b^2z)p + bz^2 + (a-2b)z \tag{2.62}$$

$$g(z,p) = -\frac{h_2(z,p)}{h_1(z,p)} \tag{2.63}$$

$$\frac{\partial^2 z}{\partial p^2} = \frac{\partial g(z,p)}{\partial p} = -\frac{h_1(\partial h_2/\partial p) - h_2(\partial h_1/\partial p)}{h_1^2} \tag{2.64}$$

$$\frac{\partial^2 z}{\partial z \partial p} = \frac{\partial g(z,p)}{\partial z} = -\frac{h_1(\partial h_2/\partial z) - h_2(\partial h_1/\partial z)}{h_1^2} \tag{2.65}$$

with

$$\frac{\partial h_1}{\partial z} = 6z - 2(1 - bp) \tag{2.66}$$
$$\frac{\partial h_1}{\partial p} = -6b^2 p + (a - 2b + 2bz) \tag{2.67}$$
$$\frac{\partial h_2}{\partial z} = 2bz + (a - 2b - 6b^2 p) \tag{2.68}$$
$$\frac{\partial h_2}{\partial p} = 6b^3 p + (2b^2 - 2ab - 6b^2 z). \tag{2.69}$$

Density

In the case of real gas, the required derivatives for the density function given by Equation (2.15) are

$$\frac{\partial \rho}{\partial p} = \frac{M_g}{zRT} \quad , \qquad \frac{\partial \rho}{\partial z} = -\frac{pM_g}{z^2 RT} \quad . \tag{2.70}$$

Viscosity

From Equation (2.16), the only additional term require to fully define the following derivative

$$\frac{\partial \mu}{\partial p} = \frac{\partial \mu}{\partial \rho}\left(\frac{\partial \rho}{\partial p} + \frac{\partial \rho}{\partial z}\frac{\partial z}{\partial p}\right) \tag{2.71}$$

is

$$\frac{\partial \mu}{\partial \rho} = A_1 A_2 A_3 \rho^{A_3 - 1} \exp(A_2 \rho^{A_3}). \tag{2.72}$$

Compressibility

Finally the two partial derivatives for the compressibility function in Equation (2.21) with respect to p and z read

$$\frac{\partial c}{\partial p} = -\frac{1}{p^2} + \frac{1}{z^2(p)}\left(\frac{\partial z(p)}{\partial p}\right)^2 - \frac{1}{z(p)}\frac{\partial^2 z(p)}{\partial p^2} \tag{2.73}$$
$$\frac{\partial c}{\partial z} = \frac{1}{z^2(p)}\frac{\partial z(p)}{\partial p} - \frac{1}{z(p)}\frac{\partial z(p)}{\partial z \partial p} \quad . \tag{2.74}$$

Ideal gas

Studying ideal gas behavior corresponds to the scenario where $z = 1$. This case of constant z that is independent of pressure simplifies the definition of functions

$$a(p, r) = r\frac{\rho(p)}{\mu(\rho(p))} \quad , \qquad b(p, r) = \frac{r\phi}{k} c(p)\rho(p) \quad . \tag{2.75}$$

We obtain the following derivatives by applying the chain rule

$$\frac{\partial a(p,r)}{\partial p} = r\frac{\mu(\rho(p))\left(\frac{\partial \rho}{\partial p}\right) - \rho(p)\left(\frac{\partial \mu}{\partial \rho}\left(\frac{\partial \rho}{\partial p}\right)\right)}{\mu^2(\rho(p))} \tag{2.76}$$

$$\frac{\partial b(p,r)}{\partial p} = \frac{r\phi}{k}\left(c(p)\frac{\partial \rho}{\partial p} + \rho(p)\frac{\partial c}{\partial p}\right). \tag{2.77}$$

While all the required derivatives are previously defined, a different definition is required for one specific property : compressibility. The function that defines the compressibility of an ideal gas and its derivative with respect to pressure read

$$c(p) = \frac{1}{p} \quad , \qquad \frac{\partial c(p)}{\partial p} = -\frac{1}{p^2} \quad . \tag{2.78}$$

Liquid

Non-linear.

Unlike the physical properties of gas, for the application in consideration — drilling through a fully saturated single phase liquid reservoir — an important physical property that is dependent on pressure is density. Should we consider a non-linear form of solving the liquid reservoir dynamics, then using Equation (1.4) we get the functions

$$a(p,r) = \frac{r}{\mu}\left(\rho_0 + \frac{p-p_0}{C_l^2}\right), \qquad b(p,r) = \frac{r\phi}{k}c\left(\rho_0 + \frac{p-p_0}{C_l^2}\right). \tag{2.79}$$

Respective derivatives of the functions with pressure for the Jacobians are

$$\frac{\partial a(p,r)}{\partial p} = \frac{r}{\mu C_l^2} \quad , \qquad \frac{\partial b(p,r)}{\partial r} = \frac{r\phi c}{\kappa C_l^2} \quad . \tag{2.80}$$

Linear.

Nevertheless, as mentioned in Section 2.1.1, in case of single phase liquid completely saturating the reservoir pore, it is assumed that the density of the reservoir fluid do not significantly vary from the equilibrium profile. This removes any pressure dependency of the physical property of the liquid and translates to constant functions

$$a(p,r) = r\frac{\rho}{\mu} \quad , \qquad b(p,r) = \frac{r\phi}{k}c\rho \quad . \tag{2.81}$$

2.3.2 Simulation case studies

In this section we present some numerical case studies to understand the reservoir pressure dynamics. First, we consider a liquid reservoir and study different numerical methods presented in this section to solve the diffusion equation. Figure 2.4 shows the reservoir pressure profile along the radial domain. Here, we introduce a step change to the BHCP to create a drawdown. The MATLAB solver `pdepe`, with a $10,000$ grid elements (GE) is considered as the real solution for comparison purposes. It can be noted the solution obtained by the Green's function does not capture well the pressure dynamics. As we increase the number of modes, 50 in this case, a Gibbs phenomenon occurs. The situation does not improve even while considering

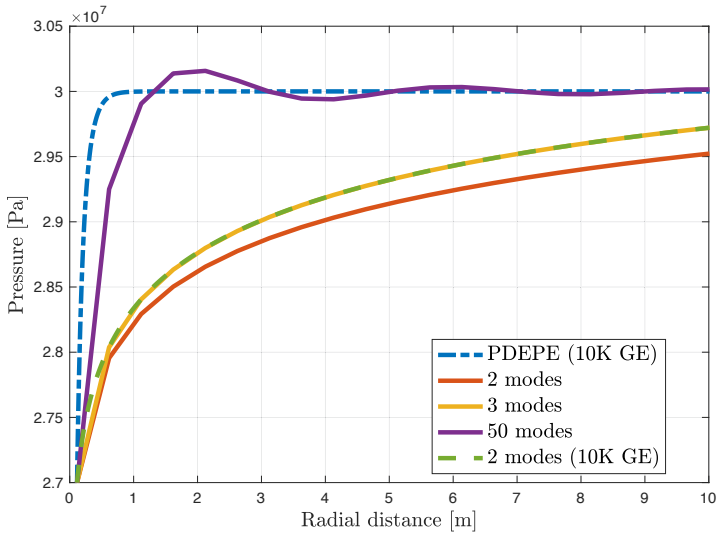

FIGURE 2.4: Comparison of reservoir pressure profile obtained by numerical and analytical Green's solutions. Solution obtained using a finer gridding in PDEPE function in MATLAB is taken as a reference solution.

a finer grid (10,000 GE) for the Green's solution. Thus, we use $\theta-$ scheme in this manuscript to solve the reservoir pressure dynamics.

Liquid Influx. We now present a situation of a case when the BHCP drops below the reservoir pore pressure, creating a drawdown and leading to a liquid influx. In presented scenario, the BHCP reduces due to a decrease in mud pump flow rate J_p, at a constant choke opening Z_c, for instance, during a pump failure on a drilling rig. Other operations like connections may lead to an influx (refer to Section 1.2.2 for variations in the BHCP). The distributed dynamics described in Section 2.1 for a liquid reservoir is used in the simulation and Figure 2.5 shows the resulting liquid influx into the wellbore. The parameter used as same as in Table 2.1.

Gas reservoir. We present a simulation that relies solely on the gas reservoir. The parameters considered for this simulation are summarized in Table 2.1. Figure 2.6 shows a comparison of the gas influx obtained by two models : distributed model using real-gas EOS and a linearized reservoir model (2.81). The simulation is set for a deep gas reservoir with a pore pressure of 420 bar and a high temperature of $\approx$ 150 °C. Effects on gas EOS properties at such reservoir conditions are prominent. However, it is shown that the linearized model for a gas reservoir provides an influx estimate similar to the distributed model. This is important because, the observers discussed in Part II, design using linearized reservoir models may be used for gas reservoirs as well—need further investigation on mapping the EOS properties for different reservoir conditions and the observer performances.

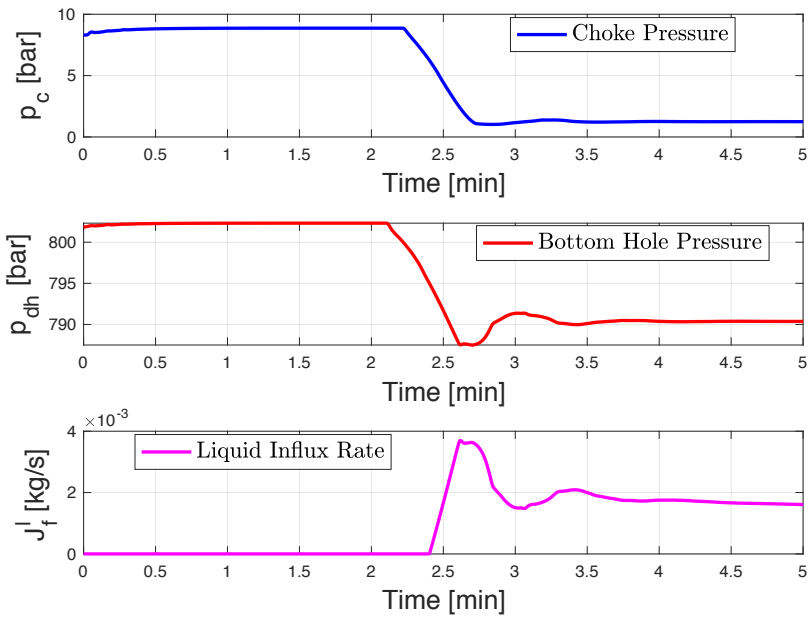

FIGURE 2.5: Simulation of a liquid influx scenario using a distributed wellbore and reservoir model. Mud pump flow is ramped down while maintaining a constant choke opening.

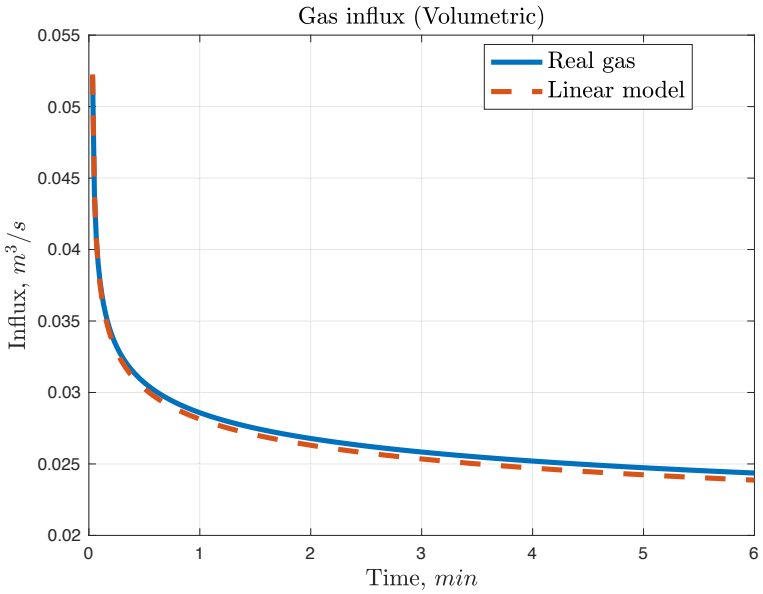

FIGURE 2.6: Comparison of gas influx obtained from two different settings of the distributed reservoir model: considering real gas behaviour and linearized gas behaviour.

TABLE 2.1: The simulation parameter values for distributed reservoir models. Gas parameters considered here are for Methane.

Parameter	**Symbol**	**Value**	**Unit**
Critical pressure	p_c	667.8	bar
Critical temperature	T_c	343	R
Molecular weight	M_g	16.04	$\mathrm{g\,mol\,mol^{-1}}$
Universal gas constant	R_g	669.94	[-]
EOS constant	Ω_a	0.45724	[-]
EOS constant	Ω_b	0.07780	[-]
Wellbore radius	r_w	0.0762	m
Reservoir extent	r_e	100	m
Reservoir thickness	h	5	m
Total compressibility of reservoir	C	8.7e-10	$\mathrm{Pa^{-1}}$
Porosity	ϕ	0.35	[-]
permeability	κ	5e-13	$\mathrm{m^2}$
Reservoir temperature	T	300	$^\circ$ F
Numerical implicitness	θ	0.95	[-]

Part II

Observer Designs

Introduction: general approach for observer design

Dans cette partie, nous présentons plusieurs observateurs qui estiment le débit de fluides depuis le réservoir vers le puits ainsi que, dans certains cas, le profil de pression dans le réservoir.

In this part, we present several observers estimating the influx of fluids from the reservoir into the wellbore, as well as, in certain cases, the pressure distribution in the reservoir.

The backstepping approach

We rely on the so-called *backstepping* approach to design observers able to estimate state variables in real-time from measurements. This method, which comes from nonlinear control design [85], has been extended to infinite-dimensional systems such as the ones studied in this manuscript, and relies on the following steps,

1. choose a generic form for the observer: in our case, the "Luenberger-like" form which consists in a copy of the plant plus output error injection terms, with gains to be determined ;
2. design a so-called "target system" with desirable stability properties. The target system represents the desired behavior of the observer error system after the gains have been designed. Typically, the target system is constructed from the original system by removing terms that potentially create instability and, sometimes, adding term that improve convergence speed ;
3. find an invertible transformation that maps the solution of the observer error system to the solutions of the target system, such that the stability of the target system implies that of the observer error system ;
4. typically, the expression of the observer gains appears as a necessary and sufficient condition for the transformation to exist.

We now illustrate this approach on a classical example from [86], which will serve as the basis for several designs in the coming sections.

Example 2.3.1. *[86] Consider the following diffusion equation*

$$\varphi_t(t,x) = \varphi_{xx}(t,x) \tag{2.82}$$
$$\varphi_x(t,0) = \xi\varphi(t,0) \tag{2.83}$$
$$\varphi_x(t,1) = 0 \tag{2.84}$$

defined on the time and spatial domains $t > 0,\ x \in [0,1]$, *along with the following measurement*

$$y(t) = \varphi(t,0). \tag{2.85}$$

The following observer

$$\hat{\varphi}_t(t,x) = \hat{\varphi}_{xx}(t,x) + l(x)\left(y - \hat{\varphi}(t,0)\right) \tag{2.86}$$
$$\hat{\varphi}_x(t,0) = \xi\hat{\varphi}(t,0) \tag{2.87}$$
$$\hat{\varphi}_x(t,1) = 0 \tag{2.88}$$

yields the following error dynamics for $\tilde{\varphi} = \varphi - \hat{\varphi}$

$$\tilde{\varphi}_t(t,x) = \tilde{\varphi}_{xx}(t,x) - l(x)\tilde{\varphi}(t,0) \tag{2.89}$$
$$\tilde{\varphi}_x(t,0) = \xi\tilde{\varphi}(t,0) \tag{2.90}$$
$$\tilde{\varphi}_x(t,1) = 0. \tag{2.91}$$

To design an observer gain $l(x)$ *such that* $\tilde{\varphi} \to 0$, *we look for an invertible transformation of the form*

$$\tilde{\varphi}(t,x) = \tilde{\psi}(t,x) - \int_0^x K(x,y)\tilde{\psi}(t,y)dy \tag{2.92}$$

that maps (2.89)–(2.91) *to the following target system*

$$\tilde{\psi}_t(t,x) = \tilde{\psi}_{xx}(t,x) - c\tilde{\psi}(t,x) \tag{2.93}$$
$$\tilde{\psi}_x(t,0) = \bar{\xi}\tilde{\psi}(t,0) \tag{2.94}$$
$$\tilde{\psi}_x(t,1) = 0 \tag{2.95}$$

where $\bar{\xi}$ *has yet to be determined. Equation* (2.92) *is a Volterra integral equation [87], [88] and* K, *defined on the triangular domain*

$$\mathcal{T} = \left\{(x,y) \in \mathbb{R}^2 \ :\ 0 \le y \le x \le 1\right\} \tag{2.96}$$

is referred to as the kernel, and has yet to be determined. Differentiating (2.92) *with respect to time and space, using* (2.93)–(2.95) *and plugging the result into* (2.89)–(2.91) *yields the following set of conditions on* K

$$K_{xx}(x,y) = K_{yy}(x,y) - cK(x,y) \tag{2.97}$$
$$2\frac{d}{dx}K(x,x) = c \tag{2.98}$$
$$K_x(x,1) = 0 \tag{2.99}$$
$$K(1,1) = 0 \tag{2.100}$$

with the abusive notation $\frac{d}{dx}K(x,x) = K_x(x,x) + K_y(x,x)$. *The observer gain* $l(x)$ *and the parameter* $\bar{\xi}$ *are given by*

$$l(x) = K_y(x,0) - \bar{\xi} \tag{2.101}$$
$$\bar{\xi} = \xi + K(0,0). \tag{2.102}$$

Notice that (2.98) and (2.100) can be solved to yield $K(0,0) = -\frac{c}{2}$ *which yields*

$$l(x) = K_y(x,0) - \xi + \frac{c}{2} \tag{2.103}$$

$$\bar{\xi} = \xi - \frac{c}{2}. \tag{2.104}$$

One can show [86] that (2.97)–(2.100) has a unique solution in $\mathcal{L}^\infty(\mathcal{T})$*. The design is summarized in the following Lemma.*

Lemma 2.3.1

Assume that the following condition is satisfied

$$c < 2\xi \tag{2.105}$$

and the gain $l(\cdot)$ *is chosen according to (2.103) and* $\bar{\xi}$ *according to (2.104). Then there exist* $C,\ \lambda > 0$ *such that the trajectories of the error system (2.89)–(2.91) starting from an initial condition* $\tilde{\varphi}_0 \in \mathcal{L}^2([0,1])$ *satisfy*

$$\|\tilde{\varphi}(t,\cdot)\|_{\mathcal{L}^2} \leq C \|\tilde{\varphi}_0\|_{\mathcal{L}^2} e^{-\lambda t}. \tag{2.106}$$

Proof : The proof relies on the following Lyapunov function

$$V(t) = \frac{1}{2}\int_0^1 \tilde{\psi}(t,x)^2 dx. \tag{2.107}$$

One can easily show that

$$\dot{V}(t) = -\bar{\xi}\tilde{\psi}(t,0)^2 - \int_0^1 \tilde{\psi}_x(t,x)^2 - c\int_0^1 \tilde{\psi}(t,x)^2 dx. \tag{2.108}$$

Since $\bar{\xi} > 0$ thanks to (2.105), one has

$$\dot{V}(t) \leq -cV(t) \tag{2.109}$$

which yields

$$\|\tilde{\psi}(t,\cdot)\|_{\mathcal{L}^2} \leq \|\tilde{\psi}_0\|_{\mathcal{L}^2} e^{-\frac{c}{2}t}. \tag{2.110}$$

Besides, there exists an inverse kernel $L \in \mathcal{L}^\infty(\mathcal{T})$ such that

$$\tilde{\psi}(t,x) = \tilde{\varphi}(t,x) - \int_0^x L(x,y)\tilde{\varphi}(t,y)dy \tag{2.111}$$

and one can show [89] that

$$\|\tilde{\varphi}(t,\cdot)\|_{L^2} \leq \left(1 + \|K\|_{\mathcal{L}^\infty(\mathcal{T})}\right) \|\tilde{\psi}(t,\cdot)\|_{\mathcal{L}^2} \tag{2.112}$$

$$\|\tilde{\psi}(t,\cdot)\|_{L^2} \leq \left(1 + \|L\|_{\mathcal{L}^\infty(\mathcal{T})}\right) \|\tilde{\varphi}(t,\cdot)\|_{\mathcal{L}^2} \tag{2.113}$$

which concludes the proof with $\lambda = \frac{c}{2}$ and $C = \left(1 + \|K\|_{\mathcal{L}^\infty(\mathcal{T})}\right)\left(1 + \|L\|_{\mathcal{L}^\infty(\mathcal{T})}\right)$. ■

This example oftens serves as the canonical system for backstepping applied to PDE control and observer design. In the next chapter, we apply the same methodology to design observers for coupled reservoir / wellbore models based on the ones presented in Part I. In Chapter 3, we design an observer for a distributed model of the wellbore coupled with the approximate CTRS solution as the influx model. This

leads us to extend results from the literature [54] on time-varying backstepping observer designs to hetero-directional hyperbolic PDEs. In Chapter 4, it is the wellbore model that we approximate by a finite-dimensional system, while keeping the full distributed wellbore dynamics. This leads to an interesting result on the observability of parabolic PDEs when the measurement is "filtered" by the finite-dimensional wellbore dynamics. Finally, in Chapter 5, we study the full (linear) distributed wellbore and reservoir dynamics, and design observers for two application scenarios: with and without bottomhole pressure sensors.

Notations. We use the following notation to denote the system of equations : $\mathbf{\Sigma}$ denotes the plant dynamics, $\widehat{\mathbf{\Sigma}}$ the observer dynamics and $\widetilde{\mathbf{\Sigma}}$ the error dynamics. By definition, the estimates of the observer $\widehat{\mathbf{\Sigma}}$ asymptotically converges to the actual states $\mathbf{\Sigma}$ as $t \to \infty$, if the error defined by $\widetilde{\mathbf{\Sigma}} = \mathbf{\Sigma} - \widehat{\mathbf{\Sigma}}$ asymptotically converges to zero as $t \to \infty$. The error dynamics is then mapped on to a target system $\mathbf{\Sigma_T}$, whose exponential stability can be guaranteed. This is achieved using standard backstepping approach [86]. Also, consider the functions $f(x, y, z)$ and $g(x)$, then the following notations are used :

$$
\begin{aligned}
f_x(x, y, z) &= \frac{\partial}{\partial x} f(x, y, z) \\
f_y(x, y, z) &= \frac{\partial}{\partial y} f(x, y, z) \\
f_z(x, y, z) &= \frac{\partial}{\partial z} f(x, y, z) \\
g'(x) &= \frac{d}{dx} g(x).
\end{aligned}
$$

We now present the different observer designs.

Chapter 3

Observer for hyperbolic PDE with time dependent reflection coefficient

Dans ce chapitre, nous synthétisons un observateur qui estime les états distribués dans le puits en présence d'un influx de liquide modélisé par le modèle CTRS (2.24). Nous réécrivons d'abord les équations dans une forme qui permet la synthèse de l'observateur, sur la base d'hypothèses simplificatrices [9], [54].

In this chapter, we design an observer that estimates the states of the distributed wellbore dynamics in the presence of a liquid influx modelled by the CTRS (2.24). We first rewrite the system dynamics in a way that is amenable to observer design, making some simplifying assumptions [9], [54].

3.1 Coupled reservoir - wellbore dynamics

During drilling operations, the reservoir section is open to the annular region of the wellbore. In general, the drillstring is equipped with non-return valves (NRVs)[1]. This allows us to know to the dynamics within the drillstring with higher degree of certainty. Thus, in what follows we assume that the

A1 fluid flowing from the bit into the annulus $q_{bit}(t)$ is known.

Besides, we assume that the flow from the reservoir is given by the CTRS (2.24), which we recall here for readability purposes

$$q_{res}(q_1, q_2, t) = -\frac{4\pi\kappa h\left(\mathrm{BHCP}(t) - p_e\right)}{\mu\left(\log\frac{4\kappa t}{\gamma\phi\mu c r_w^2} + 2S\right)} \tag{3.1}$$

where the BHCP is expressed as follows as a function of the conservative variables

$$\mathrm{BHCP}(t) = (q_1(t,0) - \rho_0)C_l^2 + p_0. \tag{3.2}$$

Writing the mass balance equation over the open section of the wellbore yields

$$\frac{q_2(t,0)}{q_1(t,0)} = \frac{q_{\mathrm{bit}}(t) + q_{\mathrm{res}}(t)}{A} \tag{3.3}$$

where A is the area of the open section of the wellbore.

[1] drill bit can be considered as NRV due to the very high pressure head for flow directions opposite to the conventional drilling fluid path.

3.1.1 Equilibrium profile

Let $t_0 > 0$ be fixed, as well as a constant circulating flow rate $\bar{q}_{bit}$ and a fixed value of the choke opening $\bar{Z}_c$. We define the equilibrium profile of interest as the steady-state solution to (1.28) along with the topside boundary condition (1.25) and the CTRS solution taken at time t_0, i.e. the functions $q_1(x)$, $q_2(x)$ are solutions of the following system of equations :

$$\frac{d\bar{q}_2(x)}{dx} = 0 \tag{3.4}$$

$$C_l^2 \frac{d\bar{q}_1(x)}{dx} = -\bar{q}_1(x) g \cos\theta - F(\bar{q}_1(x), \bar{q}_2(x)) \tag{3.5}$$

$$A\frac{\bar{q}_2(L)}{\bar{q}_1(L)} = K_c \bar{Z}_c \sqrt{\frac{2}{\bar{q}_1(L)}\left(\bar{q}_1(L)C_l^2 - \rho_0 C_l^2 + p_0 - p_{ds}\right)} \tag{3.6}$$

$$A\frac{\bar{q}_2(0)}{\bar{q}_1(0)} = \bar{q}_{\text{bit}} + q_{\text{res}}(\bar{q}_1(0), \bar{q}_2(0), t_0). \tag{3.7}$$

The function F is the frictional pressure loss in the source terms (1.30). The time instant t_0 can be seen as a degree of freedom in the design of the observer. Obviously, it must be chosen such that the actual profiles do not deviate much from the corresponding equilibrium profile, as the subsequent analysis consists in linearizing around the equilibrium profile.

3.1.2 Variable change: Riemann invariants

We now linearize system (1.28) around the equilibrium profile $\bar{q} = (\bar{q}_1(x), \bar{q}_2(x))^\top$. Denoting $\delta q = (\delta q_1, \delta q_2)^\top = q - \bar{q}$, this yields

$$\frac{\partial \delta q}{\partial t} + \mathcal{A}\frac{\partial \delta q}{\partial x} = \mathcal{S}(\delta q_1, \delta q_2). \tag{3.8}$$

In Equation (3.8), $\mathcal{A}$ is diagonalizable. More precisely, one has $\mathcal{A}R = R\Lambda$, with

$$\Lambda = \begin{bmatrix} C_l & 0 \\ 0 & -C_l \end{bmatrix}, \qquad R^{-1} = \frac{1}{2}\begin{bmatrix} C_l & 1 \\ -C_l & 1 \end{bmatrix}. \tag{3.9}$$

We consider the variable change in the form of Riemann invariants that reads

$$\begin{bmatrix} \mathrm{u}(t,x) \\ \mathrm{v}(t,x) \end{bmatrix} = \frac{1}{2}\begin{bmatrix} C_l \delta q_1 + \delta q_2 \\ -C_l \delta q_1 + \delta q_2 \end{bmatrix}. \tag{3.10}$$

Now, left multiplying Equation (3.8) with R^{-1} results in a set of linear hyperbolic PDEs of the form :

$$\mathrm{u}_t(t,x) + C_l \mathrm{u}_x(t,x) = \sigma^{++}(x)\mathrm{u}(t,x) + \sigma^{+-}(x)\mathrm{v}(t,x) \tag{3.11a}$$

$$\mathrm{v}_t(t,x) - C_l \mathrm{v}_x(t,x) = \sigma^{-+}(x)\mathrm{u}(t,x) + \sigma^{--}(x)\mathrm{v}(t,x). \tag{3.11b}$$

In this setting, variables u and v represent pressure waves that propagate in opposite directions. The $\sigma-$ terms denote their in-domain coupling, mainly due to friction. We consider here the simplified (laminar) momentum source term (1.32). Then the

$\sigma-$ terms take the form :

$$\sigma^{++}(x) = \sigma^{-+}(x) = -\frac{1}{2}\left(\frac{32\mu}{\rho_0 D_h^2} + \frac{g}{C_l}\right) \tag{3.12a}$$

$$\sigma^{+-}(x) = \sigma^{--}(x) = -\frac{1}{2}\left(\frac{32\mu}{\rho_0 D_h^2} - \frac{g}{C_l}\right). \tag{3.12b}$$

Besides, setting $\alpha_g \equiv 0$ in (1.25), linearizing around an operating point $\bar{Z}_c$ and expressing it in Riemann coordinates yields

$$\mathrm{v}(t,1) = \Theta \mathrm{u}(t,1). \tag{3.13a}$$

The reflection coefficient Θ depends on the considered operating point as follows :

$$\Theta = \left(\frac{C_l \bar{h}_2 + \bar{h}_1}{C_l \bar{h}_2 - \bar{h}_1}\right) \tag{3.13b}$$

$$\bar{h}_1 = \left.\frac{\partial h}{\partial q_1}\right|_{(\bar{q}_1, \bar{q}_2)} \tag{3.13c}$$

$$\bar{h}_2 = \left.\frac{\partial h}{\partial q_2}\right|_{(\bar{q}_1, \bar{q}_2)}. \tag{3.13d}$$

Particular attention in the design will be made, however, to ensure that the proposed observer works for a large range of operating points, i.e. that it is robust to changes in Θ. Finally, linearizing Equation (3.3) with q_{res} given by (3.1) around the equilibrium yields, in Riemann coordinates

$$\mathrm{u}(t,0) = g(t)\mathrm{v}(t,0), \qquad g(t) = \left(\frac{\bar{q}_1(0)\eta(t) + A}{\bar{q}_1(0)\eta(t) - A}\right) \tag{3.14}$$

with

$$\eta(t) = -\frac{4\pi\kappa h}{\mu\left(\log\frac{4\kappa t}{\gamma\phi\mu c r_w^2} + 2S\right)}. \tag{3.15}$$

3.1.3 Summary of the model and estimation problem

The purpose of the next sections is to design an observer for systems $\boldsymbol{\Sigma}$ of the form

$$\mathrm{v}(t,1) = \Theta \mathrm{u}(t,1) \tag{3.16}$$

$$\mathrm{u}_t(t,x) + C_l \mathrm{u}_x(t,x) = \sigma^{++}(x)\mathrm{u}(t,x) + \sigma^{+-}(x)\mathrm{v}(t,x) \tag{3.17}$$

$$\mathrm{v}_t(t,x) - C_l \mathrm{u}_x(t,x) = \sigma^{-+}(x)\mathrm{u}(t,x) + \sigma^{--}(x)\mathrm{v}(t,x) \tag{3.18}$$

$$\mathrm{u}(t,0) = g(t)\mathrm{v}(t,0) \tag{3.19}$$

relying on a measurement

$$y(t) = c_1 \mathrm{u}(t,1) + c_2 \mathrm{v}(t,1). \tag{3.20}$$

Typically, in the context of drilling, (3.20) is the expression of the topside pressure, linearized around its equilbrium value.

3.2 Observer design

The proposed observer is an exact copy of Equations (3.16) to (3.19) plus output error injection terms, and direct injection of the measurement at the topside boundary,

$$\hat{v}(t,1) = \Theta\hat{u}(t,1) - \frac{\Theta}{c_1+c_2\Theta}\left(y(t) - (c_1\hat{u}(t,1) + c_2\hat{v}(t,1))\right) \tag{3.21}$$

$$\begin{aligned}\hat{u}_t(t,x) + C_l\hat{u}_x(t,x) &= \sigma^{++}(x)\hat{u}(t,x) + \sigma^{+-}(x)\hat{v}(t,x)\\ &\quad + P_u(t,x)(y(t) - (c_1\hat{u}(t,1) + c_2\hat{v}(t,1)))\end{aligned} \tag{3.22}$$

$$\begin{aligned}\hat{v}_t(t,x) - C_l\hat{u}_x(t,x) &= \sigma^{-+}(x)\hat{u}(t,x) + \sigma^{--}(x)\hat{v}(t,x)\\ &\quad + P_v(t,x)(y(t) - (c_1\hat{u}(t,1) + c_2\hat{v}(t,1)))\end{aligned} \tag{3.23}$$

$$\hat{u}(t,0) = g(t)\hat{v}(t,0). \tag{3.24}$$

Time dependent coefficient $g(t)$ requires observer gains $P_u(t,x)$ and $P_v(t,x)$ that are function of time. The estimation error is obtained as a solution to the following system $\widetilde{\Sigma}$

$$\tilde{v}(t,1) = 0 \tag{3.25}$$

$$\begin{aligned}\tilde{u}_t(t,x) + C_l\tilde{u}_x(t,x) &= \sigma^{++}(x)\tilde{u}(t,x) + \sigma^{+-}(x)\tilde{v}(t,x)\\ &\quad - P_u(t,x)(c_1\tilde{u}(t,1) + c_2\tilde{v}(t,1))\end{aligned} \tag{3.26}$$

$$\begin{aligned}\tilde{v}_t(t,x) - C_l\tilde{u}_x(t,x) &= \sigma^{-+}(x)\tilde{u}(t,x) + \sigma^{--}(x)\tilde{v}(t,x)\\ &\quad - P_v(t,x)(c_1\tilde{u}(t,1) + c_2\tilde{v}(t,1))\end{aligned} \tag{3.27}$$

$$\tilde{u}(t,0) = g(t)\tilde{v}(t,0). \tag{3.28}$$

To design the observer gains, we rely on a variable change, that maps (3.25)–(3.28) to the following target system $\mathbf{\Sigma_T}$

$$\beta(t,1) = 0 \tag{3.29}$$

$$\alpha_t(t,x) + C_l\alpha_x(t,x) = \sigma^{++}(x)\alpha(t,x) \tag{3.30}$$

$$\beta_t(t,x) - C_l\beta_x(t,x) = \sigma^{--}(x)\beta(t,x) \tag{3.31}$$

$$\alpha(t,0) = g(t)\beta(t,0). \tag{3.32}$$

The system $\mathbf{\Sigma_T}$ is exponentially stable, and converges to zero in finite time. Indeed, one can see from (3.29),(3.31) that β converes to zero in time $1/C_l$, which, along with (3.32) yields $\alpha(t,0) = 0$ for $t > 1/C_l$ and, using (3.30), that $\alpha(t,\cdot) \equiv 0$ for $t > 2/C_l$. We map the variables $(\tilde{u},\tilde{v})$ to (α,β) using the following the invertible transformations

$$\tilde{u}(t,x) = \alpha(t,x) - \int_x^1 P^{uu}(x,y,t,)\alpha(t,y)dy - \int_x^1 P^{uv}(x,y,t)\beta(t,y)dy \tag{3.33}$$

$$\tilde{v}(t,x) = \beta(t,x) - \int_x^1 P^{vu}(x,y,t)\alpha(t,y)dy - \int_x^1 P^{vv}(x,y,t)\beta(t,y)dy. \tag{3.34}$$

Differentiating (3.33),(3.34) with respect to time and space, using (3.29)–(3.32) and plugging into (3.25)–(3.28) yields the following set of conditions on the kernels P^{uu},

P^{uv}, P^{vu} and P^{vv} :

$$P_t^{vu}(x,y,t) - C_l P_x^{vu}(x,y,t) + C_l P_y^{vu}(x,y,t) = (\sigma^{--}(x) - \sigma^{++}(y))P^{vu}(x,y,t) + \sigma^{-+}(x)P^{uu}(x,y,t) \quad (3.35)$$

$$P_t^{uu}(x,y,t) + C_l P_x^{uu}(x,y,t) + C_l P_y^{uu}(x,y,t) = (\sigma^{++}(x) - \sigma^{++}(y))P^{uu}(x,y,t) + \sigma^{+-}(x)P^{vu}(x,y,t) \quad (3.36)$$

$$P^{vu}(x,x,t) = -\frac{\sigma^{-+}(x)}{2C_l} \quad (3.37)$$

$$P^{uu}(0,y,t) = g(t)P^{vu}(0,y,t) \quad (3.38)$$

and

$$-P_t^{uv}(x,y,t) - C_l P_x^{uv}(x,y,t) + C_l P_y^{uv}(x,y,t) = (\sigma^{++}(x) - \sigma^{--}(y))P^{uv}(x,y,t) + \sigma^{+-}(x)P^{vv}(x,y,t) \quad (3.39)$$

$$-P_t^{vv}(x,y,t) + C_l P_x^{vv}(x,y,t) + C_l P_y^{vv}(x,y,t) = (\sigma^{--}(x) - \sigma^{--}(y))P^{vv}(x,y,t) + \sigma^{-+}(x)P^{uv}(x,y,t) \quad (3.40)$$

$$P^{uv}(x,x,t) = \frac{\sigma^{+-}(x)}{2C_l} \quad (3.41)$$

$$P^{vv}(0,y,t) = g(t)P^{uv}(0,y,t) \quad (3.42)$$

along with the following expression of the observer gains

$$\begin{bmatrix} P_u(x) \\ P_v(x) \end{bmatrix} = -(C_l/c_1)\begin{bmatrix} P^{uu}(x,1,t) \\ P^{vu}(x,1,t) \end{bmatrix}. \quad (3.43)$$

For (3.35)–(3.42) to be well-posed, either initial conditions have to be added, or the time-varying parameter $g(t)$ needs to be extended to negative times. We chose the latter solution here, as g defined by (3.14) continuously extends to $g(t) \equiv -1, \forall\, t \leq 0$, i.e., as $\lim_{t\to 0^+} \eta(t) = 0$ in Equation (3.14), $g(t) \equiv -1$. We have the following theorem.

Theorem 3.2.1

Under the assumptions

$$\sigma^{++}(x), \sigma^{--}(x), \sigma^{+-}(x), \sigma^{-+}(x) \in \mathcal{C}(\mathcal{K})$$
$$g(t) \in \mathcal{C}(\mathcal{K})$$

where $\mathcal{K} = \mathcal{T} \times \mathcal{R}$, the system equations (3.39)- (3.42) admit an unique continuous solutions on $\mathcal{K}$.

Proof : Although technical, the proof relies on classical tools : the kernel PDEs are transformed into integral equations using the method of characteristics. The method of successive approximations is then used to construct a solution to the integral equations in the form of an infinite series. The proof is a direct extension of the one presented in [55] for the time-invariant case and the one in [54] for a single time-varying kernel PDE. We prove here the well-posedness of a generic equation of the form

$$-F_t - \mu F_x + \mu F_\xi = a(x)G + b(x,\xi)F \quad (3.44)$$

$$-G_t + \mu G_x + \mu G_\xi = d(x)F + e(x,\xi)G \quad (3.45)$$

$$F(x,x,t) = f(x) \quad (3.46)$$

$$G(0,\xi,t) = g(t)F(0,\xi,t). \quad (3.47)$$

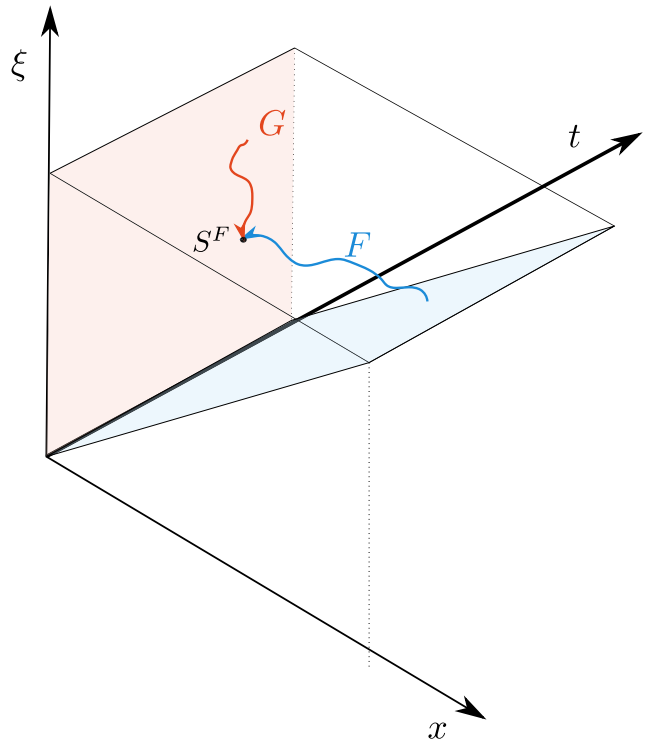

FIGURE 3.1: Characteristic curves for time dependent kernels. Kernel G hits the boundary $x = 0$ and F hits the boundary $x = \xi$.

If the Equations (3.44) to (3.47) are well-posed, then there exists an unique solution for the Equations (3.35) to (3.42). To do so, we convert the PDEs into integral equations and define characteristic curves in the (t, x)-plane along which the equations are integrated. For Equation (3.44), we define the characteristic curves (χ, ζ, τ) along which the equations can be integrated as the solutions of the following Cauchy problem :

$$\chi'(x,\xi,t;s) = -\mu \qquad \zeta'(x,\xi,t;s) = \mu \qquad \tau'(x,\xi,t;s) = -1 \tag{3.48}$$

$$\chi(x,\xi,t;s^F) = x \qquad \zeta(x,\xi,t;s^F) = \xi \qquad \tau(x,\xi,t;s^F) = t \tag{3.49}$$

form which it is easy to establish additional relations that read

$$\chi^0(x,\xi,t) := \chi(x,\xi,t;0) = x + \mu s^F(x,\xi,t) \tag{3.50}$$

$$\zeta^0(x,\xi,t) := \zeta(x,\xi,t;0) = \xi - \mu s^F(x,\xi,t) \tag{3.51}$$

$$\tau^0(x,\xi,t) := \tau(x,\xi,t;0) = t + s^F(x,\xi,t) \tag{3.52}$$

for $\forall s \in [0, s^F(x,\xi)]$ and each $(\chi, \zeta, \tau) \in \Theta$ where Θ is the $\mathbb{R}^{3\times3}$ space on which the Kernals have an unique continuous solution. Following the schematic of the characteristic curves in Figure 3.1, when solving the curves (ξ, χ, τ) one hits the boundary

where $x = \xi$. This provides the following condition:

$$\chi(x,\xi,t;0) = \zeta(x,\xi,t;0) \tag{3.53}$$
$$x + \mu s^F(x,\xi,t) = \xi - \mu s^F(x,\xi,t) \tag{3.54}$$
$$s^F(x,\xi,t) = \frac{\xi - x}{2\mu} \tag{3.55}$$

and one can further solve for

$$\chi(x,\xi,t;0) = \frac{x+\xi}{2} \quad \zeta(x,\xi,t;0) = \frac{x+\xi}{2} \quad \tau(x,\xi,t;0) = t + \left(\frac{\xi - x}{2\mu}\right). \tag{3.56}$$

Similarly for Equation (3.45), we define the characteristic curves (α,β,γ) as the solutions of the following Cauchy problem :

$$\alpha'(x,\xi,t;s) = \mu \qquad \beta'(x,\xi,t;s) = \mu \qquad \gamma'(x,\xi,t;s) = -1 \tag{3.57}$$
$$\alpha(x,\xi,t;s^G) = x \qquad \beta(x,\xi,t;s^G) = \xi \qquad \gamma(x,\xi,t;s^G) = t \tag{3.58}$$

and the slope the characteristic curve gives the following initial conditions

$$\alpha(x,\xi,t;0) = x - \mu s^G(x,\xi,t) \tag{3.59}$$
$$\beta(x,\xi,t;0) = \xi - \mu s^G(x,\xi,t) \tag{3.60}$$
$$\gamma(x,\xi,t;0) = t + s^G(x,\xi,t). \tag{3.61}$$

For this set of the characteristic curves (α,β,γ) it can be noted that the curves hit the boundary defined by $x = 0$. This means, at $x = 0$, $\alpha(x,\xi,t;0) = 0$ and thus $s^G(x,\xi) = x/\mu$. Further conditions on the curve read

$$\alpha(x,\xi,t;0) = 0 \qquad \beta(x,\xi,t;0) = \xi - x \qquad \tau(x,\xi,t;0) = t + x/\mu \tag{3.62}$$
$$\alpha^0(x,\xi,t) = 0 \qquad \beta^0(x,\xi,t) = \xi - x \qquad \tau^0(x,\xi,t) = t + x/\mu \tag{3.63}$$

for $\forall s \in [0, s^F(x,\xi)]$. To show the existence of a solution for Equations (3.44) to (3.45), one must convert them into integral form and provide an upper bound within the integral limits. First, we integrate Equation (3.44) along the characteristic curve (χ,ζ,τ) for the limit set by $s \in [0, s^F(x,\xi,t)]$ that yields

$$\begin{aligned}\int_0^{s^F(x,\xi,t)} &\frac{d}{ds}F(\chi(s),\zeta(s),\tau(s)) \\ &= \int_0^{s^F(x,\xi,t)} (a(\chi(x,\xi,t;s))G(\chi(x,\xi,t;s),\zeta(x,\xi,t;s),\tau(x,\xi,t;s)) \\ &+ b(\chi(x,\xi,t;s),\zeta(x,\xi,t;s))\ F(\chi(x,\xi,t;s),\zeta(x,\xi,t;s),\tau(x,\xi,t;s)))\,ds\end{aligned} \tag{3.64}$$

and further we can write

$$\begin{aligned}F(x,\xi,t) &= F(\chi^0,\zeta^0,\tau^0) \\ &+ \int_0^{s^F(x,\xi,t)} (a(\chi(x,\xi,t;s))G(\chi(x,\xi,t;s),\zeta(x,\xi,t;s),\tau(x,\xi,t;s)) \\ &+ b(\chi(x,\xi,t;s),\zeta(x,\xi,t;s))F(\chi(x,\xi,t;s),\zeta(x,\xi,t;s),\tau(x,\xi,t;s)))ds.\end{aligned} \tag{3.65}$$

Using the boundary condition given by Equation (3.46) we denote

$$\begin{aligned} F(x,\xi,t) &= f(\chi^0(x,\xi,t)) \\ &+ \int_0^{s^F(x,\xi,t)} (a(\chi(x,\xi,t;s))G(\chi(x,\xi,t;s),\zeta(x,\xi,t;s),\tau(x,\xi,t;s)) \\ &+ b(\chi(x,\xi,t;s),\zeta(x,\xi,t;s))F(\chi(x,\xi,t;s),\zeta(x,\xi,t;s),\tau(x,\xi,t;s)))ds. \end{aligned} \tag{3.66}$$

Similarly, integrating Equation (3.45) along the characteristic curve (α,β,γ) for the limits $s \in [0, s^G(x,\xi,t)]$ yields

$$\begin{aligned} G(x,\xi,t) &= G(\alpha^0,\beta^0,\gamma^0) \\ &+ \int_0^{s^G(x,\xi,t)} (d(\alpha(x,\xi,t;s))F(\alpha(x,\xi,t;s),\beta(x,\xi,t;s),\gamma(x,\xi,t;s)) \\ &+ e(\alpha(x,\xi,t;s),\beta(x,\xi,t;s))G(\alpha(x,\xi,t;s),\beta(x,\xi,t;s),\gamma(x,\xi,t;s)))ds. \end{aligned} \tag{3.67}$$

We may now use the boundary condition given by Equation (3.47) to write

$$\begin{aligned} G(x,\xi,t) &= g(\gamma^0(x,\xi,t))F(0,\beta^0(x,\xi,t),\gamma^0(x,\xi,t)) \\ &+ \int_0^{s^G(x,\xi,t)} (d(\alpha(x,\xi,t;s))F(\alpha(x,\xi,t;s),\beta(x,\xi,t;s),\gamma(x,\xi,t;s)) \\ &+ e(\alpha(x,\xi,t;s),\beta(x,\xi,t;s))G(\alpha(x,\xi,t;s),\beta(x,\xi,t;s),\gamma(x,\xi,t;s)))ds. \end{aligned} \tag{3.68}$$

Using Equation (3.66) to define $F(0,\beta^0(x,\xi,t),\gamma^0(x,\xi,t))$ in Equation (3.68) will yields

$$\begin{aligned} G(x,\xi,t) &= g(\gamma^0(x,\xi,t)) \Big(f(\chi^0(0,\beta^0,\gamma^0)) + \\ &\int_0^{s^F(0,\beta^0,\gamma^0)} (a(\chi(0,\beta^0,\gamma^0;s))G(\chi(0,\beta^0,\gamma^0;s),\zeta(0,\beta^0,\gamma^0;s),\tau(0,\beta^0,\gamma^0;s)) \\ &+ b(\chi(0,\beta^0,\gamma^0;s),\zeta(0,\beta^0,\gamma^0;s))\ F(\chi(0,\beta^0,\gamma^0;s),\zeta(0,\beta^0,\gamma^0;s),\tau(0,\beta^0,\gamma^0;s)))ds \Big) \\ &+ \int_0^{s^G(x,\xi,t)} (d(\alpha(x,\xi,t;s))F(\alpha(x,\xi,t;s),\beta(x,\xi,t;s),\gamma(x,\xi,t;s)) \\ &+ e(\alpha(x,\xi,t;s),\beta(x,\xi,t;s))G(\alpha(x,\xi,t;s),\beta(x,\xi,t;s),\gamma(x,\xi,t;s)))ds. \end{aligned} \tag{3.69}$$

Let us define some intermediate variables that read

$$\varphi(x,\xi,t) = f(\chi^0(x,\xi,t)) \tag{3.70}$$

$$\psi(x,\xi,t) = g(\gamma^0(x,\xi,t))f(\chi^0(0,\beta^0,\gamma^0)) \tag{3.71}$$

and denote

$$\mathbf{H} = \begin{bmatrix} F & G \end{bmatrix}^T \tag{3.72}$$

$$\boldsymbol{\phi}(x,\xi,t) = \begin{bmatrix} \varphi(x,\xi,t) & \psi(x,\xi,t) \end{bmatrix}^T. \tag{3.73}$$

We define the functionals on $\mathbf{H}$ as the following :

$$\begin{aligned} \Phi[\mathbf{H}](x,\xi,t) = \int_0^{s^F(x,\xi,t)} &[a(\chi(x,\xi,t;s))G(\chi(x,\xi,t;s),\zeta(x,\xi,t;s),\tau(x,\xi,t;s)) \\ &+ b(\chi(x,\xi,t;s),\zeta(x,\xi,t;s))F(\chi(x,\xi,t;s),\zeta(x,\xi,t;s),\tau(x,\xi,t;s))]ds \end{aligned} \tag{3.74}$$

$$\begin{aligned}\Psi[\mathbf{H}](x,\xi,t) = g(\gamma^0(x,\xi,t))\int_0^{s^F(0,\beta^0,\gamma^0)}[a(\chi(0,\beta^0,\gamma^0;s))\times \\ G(\chi(0,\beta^0,\gamma^0;s),\zeta(0,\beta^0,\gamma^0;s),\tau(0,\beta^0,\gamma^0;s)) \\ + b(\chi(0,\beta^0,\gamma^0;s),\zeta(0,\beta^0,\gamma^0;s))F(\chi(0,\beta^0,\gamma^0;s),\zeta(0,\beta^0,\gamma^0;s),\tau(0,\beta^0,\gamma^0;s))]ds \\ + \int_0^{s^G(x,\xi,t)}[d(\alpha(x,\xi,t;s))F(\alpha(x,\xi,t;s),\beta(x,\xi,t;s),\gamma(x,\xi,t;s)) \\ + e(\alpha(x,\xi,t;s),\beta(x,\xi,t;s))G(\alpha(x,\xi,t;s),\beta(x,\xi,t;s),\gamma(x,\xi,t;s))]ds. \quad (3.75)\end{aligned}$$

We now use the method of successive approximation to prove the existence of solution for the kernels. This is done by defining a sequence that reads

$$\mathbf{H}^0(x,\xi,t) = 0 \quad (3.76)$$

$$\mathbf{H}^m(x,\xi,t) = \boldsymbol{\phi}(x,\xi,t) + \boldsymbol{\Phi}[\mathbf{H}^{m-1}](x,\xi,t). \quad (3.77)$$

To find an upper bound for the sequence, let us consider the following change of variable, $\eta = \zeta(x,\xi,t;s)$. we then have

$$d\eta = \frac{d\zeta}{ds}ds = \mu\ ds. \quad (3.78)$$

Then,

$$\int_0^{s^F(x,\xi,t)}\zeta^m(x,\xi,t;s)ds = \int_{\zeta^0}^{\xi}\frac{\eta^m}{\mu}d\eta \le M_\mu\int_0^{\xi}\eta^m d\eta = M_\mu\frac{\xi^{m+1}}{m+1}. \quad (3.79)$$

Similarly, using a variable change $\eta = \beta(x,\xi,t;s)$, it can be shown that

$$\int_0^{s^F(x,\xi,t)}\beta^m(x,\xi,t;s)ds \le M_\mu\frac{\xi^{m+1}}{m+1} \quad (3.80)$$

where $M_\mu = \max(1, 1/\mu)$. Under the assumption

$$|\Delta F(x,\xi,t;s)| \le M^m\frac{\xi^m}{m!} \quad (3.81)$$

$$|\Delta G(x,\xi,t;s)| \le M^m\frac{\xi^m}{m!} \quad (3.82)$$

where

$$M = (\bar{g}(\bar{a}+\bar{b}) + \bar{d} + \bar{e})M_\mu \quad (3.83)$$

$$\bar{a} = \max(a(\chi(x,\xi,t;s))) \quad (3.84)$$

$$\bar{b} = \max(b(\chi(x,\xi,t;s))). \quad (3.85)$$

We can derive the upper bound for the functionals as

$$|\Phi[\Delta\mathbf{H}]| \le (\bar{a}+\bar{b})\frac{M^m}{m!}\int_0^{s^F}\zeta^m(x,\xi,t;s)ds \quad (3.86)$$

$$\le M^{m+1}\frac{\xi^{m+1}}{(m+1)!} \quad (3.87)$$

and

$$|\Psi[\Delta\mathbf{H}](x,\xi,t)| \leq \bar{g}(\bar{a}+\bar{b}) \int_0^{s_0^F} \frac{M^m \zeta^m(0,\beta^0,\gamma^0;s)}{m!} \tag{3.88}$$

$$+ \int_0^{s^G} (\bar{d}+\bar{e}) \frac{M^m \beta^m(x,\xi,t;s)}{m!} \tag{3.89}$$

$$\leq (\bar{g}(\bar{a}+\bar{b})+\bar{d}+\bar{e}) \frac{M^m}{m!} \frac{\xi^{m+1}}{m+1} \tag{3.90}$$

$$\leq M^{m+1} \frac{\xi^{m+1}}{m+1} \tag{3.91}$$

which concludes the proof. ■

It is now established that there exists an unique solution for the kernels of the form given by Equations (3.44) to (3.47). While this translates to the form of hyperbolic equations required to solve for P^{uv} and P^{vv} given by Equations (3.39) to (3.42), a similar approach can be taken to show the existence of an unique solution for Equations (3.35) to (3.38). The observer gains $P_u(t,x)$ and $P_v(t,x)$ can now be obtained by numerically solving Equations (3.35) to (3.42).

Chapter 4

Observer design for a coupled ODE and parabolic PDE system

Dans ce chapitre, nous construisons un observateur et des conditions d'observabilité pour un système couplé : la dynamique dans le puits est décrite par une Equation Différentielle Ordinaire (EDO) d'ordre trois, alors que la dynamique dans le réservoir est décrite par une Equations aux Dérivées Partielles (EDP). Après avoir présenté un observateur générique, nous détaillons le cas particulier du modèle couplé puits-réservoir.

In this chapter, we construct an observer and derive observability conditions for a coupled system : wellbore dynamics described by 3-dimensional ODE system and reservoir dynamics by an infinite dimensional PDE. At first, we present the generic design. Then, the desired coupling of the wellbore-reservoir models will be shown as a specific case of the following design.

4.1 Problem statement

The system $\mathbf{\Sigma}$ is a linear time-invariant n-dimensional ODE system coupled with a parabolic PDE given by the radial-diffusion equation, defined as

$$\frac{dx}{dt}(t) = Ax(t) + Bu(t,a) \tag{4.1}$$

$$y(t) = Hx(t) \tag{4.2}$$

$$u_t(t,r) = \frac{\epsilon}{r^{m-1}}\left(r^{m-1}u_r(t,r)\right)_r \tag{4.3}$$

with $A \in \mathbb{R}^{n\times n}$, $B \in \mathbb{R}^{n\times 1}$, $H \in \mathbb{R}^{1\times n}$, for $t \in (0,T]$ and initial conditions $x_0 \in \mathbb{R}^n$ and for $r \in (a,b)$, $t \in (0,T]$, with diffusion coefficient $\epsilon > 0$ and some integer parameter $m > 0$, related to the geometry of the underling physical problem. Boundary conditions are

$$u_r(t,a) = \beta u(t,a) + Dx(t) \tag{4.4}$$

$$u_r(t,b) = 0 \tag{4.5}$$

with $\beta > 0$, and initial conditions $u_0 \in C(a,b)$. The system is understood as a dynamic system with combined state $x \in C\left([0,T];\mathbb{R}^n\right)$, $u \in C\left([0,T];\mathcal{L}^2(a,b)\right)$, and output $y \in C\left([0,T];\mathbb{R}\right)$. The estimation objective is to compute an estimate $\widehat{x}$, $\widehat{u}$ from measurements $y(t) \in \mathbb{R}$ with exponential convergence in the sense of a norm. The proposed observer is a copy of Equations (4.1) to (4.5) with output error feedback : Luenberger-like observer. Estimate of the states are solution to the system denoted

by $\widehat{\mathbf{\Sigma}}$ that reads

$$\frac{d\widehat{x}}{dt}(t) = A\widehat{x}(t) + B\widehat{u}(t,a) + L\left(y(t) - \widehat{y}(t)\right) \tag{4.6}$$
$$\widehat{y}(t) = H\widehat{x}(t) \tag{4.7}$$
$$\widehat{u}_t(t,r) = \frac{\epsilon}{r^{m-1}}\left(r^{m-1}\widehat{u}_r(t,r)\right)_r + l_{n+1}(r)\left(y(t) - \widehat{y}(t)\right) \tag{4.8}$$
$$\widehat{u}_r(t,a) = \beta\widehat{u}(t,a) + D\widehat{x}(t) + l_{n+2}\left(y(t) - \widehat{y}(t)\right) \tag{4.9}$$
$$\widehat{u}_r(t,b) = l_{n+3}\left(y(t) - \widehat{y}(t)\right) \tag{4.10}$$

for $t \in (0,T]$, $r \in (a,b)$, initial conditions $\widehat{x}_0 \in \mathbb{R}^n$, $\widehat{u}_0 \in \mathcal{L}^2(0,1)$ and the boundary conditions are given by Equations (4.10) to (4.9).

For an observer gain $L = [l_1, l_2, \cdots, l_n]$, $l_{n+1} \in \mathcal{L}^2(a,b)$, $l_{n+2} \in \mathbb{R}$, and $l_{n+3} \in \mathbb{R}$, the estimation error is defined as the difference between the state and the observer state, that is, $\widetilde{*} := * - \widehat{*}$. The estimation error $\widetilde{x}$, $\widetilde{u}$ is a solution of the estimation error system denoted by $\widetilde{\mathbf{\Sigma}}$ that reads

$$\frac{d\widetilde{x}}{dt}(t) = A\widetilde{x}(t) + B\widetilde{u}(t,a) - LH\widetilde{x}(t) \tag{4.11}$$
$$\widetilde{y}(t) = H\widetilde{x}(t) \tag{4.12}$$
$$\widetilde{u}_t(t,r) = \frac{\epsilon}{r^{m-1}}\left(r^{m-1}\widetilde{u}_r(t,r)\right)_r - l_{n+1}(r)H\widetilde{x}(t) \tag{4.13}$$
$$\widetilde{u}_r(t,a) = \beta\widetilde{u}(t,a) + D\widetilde{x}(t) - l_{n+2}H\widetilde{x}(t) \tag{4.14}$$
$$\widetilde{u}_r(t,b) = -l_{n+3}H\widetilde{x}(t). \tag{4.15}$$

Exponential convergence of the estimate $\widehat{x}$, $\widehat{u}$ to the state x, u is equivalent to the exponential stability of zero solution of the estimation error system. The main result, in Theorem 4.3.1, provides a way to compute observer gains L, l_{n+1}, l_{n+2}, and l_{n+3}, to guarantee exponential stability of the estimation error system. Before the statement of the main result, an additional observability condition is required. We now make the following assumptions.

A1 The finite dimensional subsystem given by Equations (4.1) to (4.2) is observable, that is, $\text{rank}(\mathcal{O}) = n$, with $\mathcal{O} = \begin{bmatrix} H & HA & \cdots & HA^{n-1} \end{bmatrix}^T$. This assumption guarantees the existence of a linear and invertible transformation $T_{\mathcal{O}} : \mathbb{R}^n \mapsto \mathbb{R}^n$ that maps the system defined by Equations (4.1) to (4.2) to the observer canonical form, [90]. The transformation $T_{\mathcal{O}}$ is an invertible matrix, satisfying

$$T_{\mathcal{O}}A_{\mathcal{O}} = AT_{\mathcal{O}}, \quad T_{\mathcal{O}}B_{\mathcal{O}} = B, \quad H_{\mathcal{O}} = HT_{\mathcal{O}}, \tag{4.16}$$

where $A_{\mathcal{O}}$, $B_{\mathcal{O}}$, $H_{\mathcal{O}}$ are in observer canonical form, that is

$$A_{\mathcal{O}} = \begin{bmatrix} a_1 & 1 & 0 & \cdots & 0 \\ a_2 & 0 & 1 & \cdots & 0 \\ \vdots & \vdots & \vdots & \ddots & \vdots \\ a_{n-1} & 0 & 0 & \cdots & 1 \\ a_n & 0 & 0 & \cdots & 0 \end{bmatrix}, B_{\mathcal{O}} = \begin{bmatrix} b_1 \\ b_2 \\ \vdots \\ b_n \end{bmatrix}, \tag{4.17}$$
$$H_{\mathcal{O}} = \begin{bmatrix} 1 & 0 & \cdots & 0 \end{bmatrix}. \tag{4.18}$$

A2 *Observability of the coupled System.* None of the eigenvalues $\lambda_k \in \mathbb{R}$, $k \in \mathbb{N}$ of the radial Laplacian operator with Neumann boundary conditions, that is

$$\begin{cases} \epsilon \dfrac{d}{dr}\left(r^{m-1}\dfrac{d}{dr}\phi(r)\right) = -\lambda_k r^{m-1}\phi(r) \\ \phi_n'(a) = 0 \\ \phi_n'(b) = 0 \end{cases} \tag{4.19}$$

are, simultaneously, solutions to the polynomial equation $D(\lambda_k) = 0$, with

$$D(\xi) = b_n + b_{n-1}\xi + b_{n-2}\xi^2 + \cdots + b_2\xi^{n-2} + b_1\xi^{n-1} \tag{4.20}$$

and at least one b_i, $i \in \{1, 2, \cdots, n\}$ is different from zero. This assumption is required so that the PDE states are observable through the ODE states. We describe briefly the methodology followed to define obsever gains that guarantee the stability of the estimation error system.

4.2 Methodology

Following the backstepping method for PDEs [86], we seek a pair of transformations $T_{\mathcal{O}} : \mathbb{R}^n \to \mathbb{R}^n$ and $T_u : \mathcal{L}^2(0,1) \times \mathbb{R}^n \to \mathcal{L}^2(0,1)$, that map the states $\widetilde{x}, \widetilde{u}$ satisfying Equations (4.11) to (4.15), to states $\widetilde{z}, w$ satisfying the target system

$$\frac{d\widetilde{z}}{dt}(t) = F\widetilde{z}(t) + B_{\mathcal{O}} w(t,a) \tag{4.21}$$

with initial condition $\widetilde{z}_0 = T_{\mathcal{O}}^{-1}\widetilde{x}_0$ and $F \in \mathbb{R}^{n\times n}$ is in companion form, that is

$$F = \begin{bmatrix} f_1 & 1 & 0 & \cdots & 0 \\ f_2 & 0 & 1 & \cdots & 0 \\ \vdots & \vdots & \vdots & \ddots & \vdots \\ f_{n-1} & 0 & 0 & \cdots & 1 \\ f_n & 0 & 0 & \cdots & 0 \end{bmatrix} \tag{4.22}$$

and

$$w_t(t,r) = \frac{\epsilon}{r^{m-1}}\left(r^{m-1}w_r(t,r)\right)_r - \sigma w(t,r) \tag{4.23}$$

for $r \in (a,b)$, $t \in (0,T]$, and boundary conditions

$$w_r(t,a) = (\beta - \frac{\sigma}{2\epsilon}(b-a))w(t,a) \tag{4.24}$$

$$w_r(t,b) = 0 \tag{4.25}$$

with initial conditions $w_0 \in C(a,b)$, satisfying $\widetilde{u}_0 = T_w(w_0, z_0)$. The finite-dimensional transformation $T_{\mathcal{O}}$ is defined by Equations (4.16) to (4.17), while T_u is the sum of a second-kind Volterra integral transformation acting on w and a linear spatially-varying transformation acting on z, that is

$$\widetilde{x}(t) = T_{\mathcal{O}}\widetilde{z}(t) \tag{4.26}$$

$$\widetilde{u}(t,r) = w(t,r) - \int_a^r K(r,s)w(s,t)ds + (\gamma(r) - \gamma(a))\,\widetilde{z}(t). \tag{4.27}$$

Substitution of Equations (4.26) to (4.27) in the error Equations (4.11) to (4.15) and target systems results in a hyperbolic equation and boundary condition for the kernel K and a differential-algebraic system of equation and boundary condition for γ. Thus, existence of a transformation T_u in the form of Equation (4.27) is guaranteed by the existence of a solution to the hyperbolic PDE and DAE systems, which is addressed in Lemma 4.3.1 and Lemma 4.3.2. Invertibility is given by invertibility of $T_{\mathcal{O}}$, the triangular structure of the pair given by Equations (4.29) to (4.30) and the fact that the part of the operator T_u acting on w is a second-kind Volterra integral. To ensure stability of the target system, the eigenvalues of F are selected with negative real part and σ is chosen positive, satisfying

$$\sigma \leq \frac{2\epsilon\beta}{b-a}. \tag{4.28}$$

Once the eigenvalues of F and the value of σ are chosen, there is a unique value for the observer gains L and l_n, permitted for consistency of the transformations. These are the observer gains that guarantee the convergence of the estimate to the unknown system states x and u; are presented next in Theorem 4.3.1.

4.3 Main Result

Theorem 4.3.1

Let the premises in assumptions A1 and A2 hold. Consider the estimation error system (4.11)-(4.15), and a similarity transformation $T_{\mathcal{O}} \in \mathbb{R}^{n\times n}$ that maps Equations (4.1) to (4.2) to observer canonical form in Equations (4.16) to (4.17). Let the ODE observer gain $L \in \mathbb{R}^{n\times 1}$ be chosen such that the eigenvalues μ_i, $i \in \{1,\dots,n\}$ of the companion matrix $F \in \mathbb{R}^{n\times n}$ in Equation (4.22), defined as

$$F = A_{\mathcal{O}} - L_{\mathcal{O}} H_{\mathcal{O}} \tag{4.29}$$
$$L = T_{\mathcal{O}} L_{\mathcal{O}} \tag{4.30}$$

have negative real part, and the PDE observer gains $l_{n+1} \in \mathcal{L}^2(a,b)$, $l_{n+2} \in \mathbb{R}$, and $l_{n+3} \in \mathbb{R}$ computed from

$$l_{n+1}(r) = \epsilon\gamma_1''(r) + \epsilon\frac{n-1}{r}\gamma_1'(r) - \sum_{i=1}^{n}\left(\gamma_i(r) - \gamma_i(a)\right) f_i \tag{4.31}$$

for $r \in (a,b)$, and

$$l_{n+2} = \gamma_1'(a) - d_1, \qquad l_{n+3} = \gamma_1'(b) \tag{4.32}$$

where $\gamma_i(r)$, $i \in \{1,\dots,n\}$, is the solution of a differential-algebraic system of equations

$$\epsilon K_s(r,a) + \epsilon\left(\beta - \frac{\sigma}{2\epsilon}(b-a) - \frac{m-1}{a}\right) K(r,a) + \sum_{i=1}^{n}\left(\gamma_i(r) - \gamma_i(a)\right) b_i = 0 \tag{4.33}$$

for $r \in (a,b)$, and

$$\begin{array}{rcl} \dfrac{\epsilon}{r^{m-1}}\dfrac{d}{dr}\left(r^{m-1}\dfrac{d}{dr}\gamma_2(r)\right) & = & \gamma_1(r)-\gamma_1(a), \\ \dfrac{\epsilon}{r^{m-1}}\dfrac{d}{dr}\left(r^{m-1}\dfrac{d}{dr}\gamma_3(r)\right) & = & \gamma_2(r)-\gamma_2(a), \\ \vdots & \vdots & \vdots \\ \dfrac{\epsilon}{r^{m-1}}\dfrac{d}{dr}\left(r^{m-1}\dfrac{d}{dr}\gamma_n(r)\right) & = & \gamma_{n-1}(r)-\gamma_{n-1}(a), \end{array} \tag{4.34}$$

for $r \in (a,b)$, with boundary conditions

$$\gamma_i'(a) = d_i, \qquad \gamma_i'(b) = 0, \tag{4.35}$$

for all $i \in \{2,\dots,n\}$, where b_i are the coefficients of $B_{\mathcal{O}}$ and d_i are the coefficients of $D_{\mathcal{O}} = DT_{\mathcal{O}}$. In Equation (4.33), $K \in \mathcal{L}^2(\mathcal{T})$ is the solution to a second-order hyperbolic equation

$$\begin{cases} \dfrac{1}{r^{m-1}}\left(r^{m-1}K_r(r,s)\right)_r - \left(s^{m-1}\left(\dfrac{K(r,s)}{s^{m-1}}\right)_s\right)_s = -\dfrac{\sigma}{\epsilon}K(r,s) \\ \text{with boundary conditions} \\ K(r,r) = \dfrac{\sigma}{2\epsilon}(r-b) \\ K_r(b,s) = 0 \end{cases} \tag{4.36}$$

with σ positive, chosen as

$$\underline{\mu} \le \sigma \le \frac{2\epsilon\beta}{b-a} \tag{4.37}$$

$$\underline{\mu} = \min_{i\in\{1,2,\dots,n\}} \{|\mu_i|\}. \tag{4.38}$$

This choice of observer gains guarantees that estimation error system is exponentially stable, that is

$$\|\widetilde{x}(t)\|_2 \le \kappa_1 \exp(-\underline{\mu}t)\left(\|\widetilde{x}_0\|_2 + \|\widetilde{u}_0\|_{\mathcal{H}^1}\right) \tag{4.39}$$

$$\|\widetilde{u}(\cdot,t)\|_{\mathcal{L}^2} \le \kappa_2 \exp(-\underline{\mu}t)\left(\|\widetilde{x}_0\|_2 + \|\widetilde{u}_0\|_{\mathcal{H}^1}\right) \tag{4.40}$$

for some positive κ_1, κ_2 .

Proof : The stability is then verified with Lyapunov-like functions

$$V_1(t) = \frac{1}{2}\int_a^b w^2(t,r)r^{m-1}dr \tag{4.41}$$

$$V_2(t) = \frac{\epsilon\theta}{2}w(t,a)^2a^{m-1} + \frac{1}{2}\int_a^b w_r^2(t,r)r^{m-1}dr \tag{4.42}$$

with

$$\theta = \beta - \frac{\sigma}{2\epsilon}(b-a) \tag{4.43}$$

which satisfies $\theta > 0$, according to the condition (4.28). The time derivatives of $V_1(t)$ and $V_2(t)$ along the trajectories of the w-system (4.23)–(4.25), satisfy

$$\frac{dV_1}{dt}(t) \leq -2V_1(t) \tag{4.44}$$
$$\frac{dV_2}{dt}(t) \leq -2\sigma V_2(t). \tag{4.45}$$

From the comparison principle

$$V_1(t) \leq \exp\left[-2\sigma t\right] V_1(0) \tag{4.46}$$
$$V_2(t) \leq \exp\left[-2\sigma t\right] V_2(0) \tag{4.47}$$

and consequently,

$$\|w(\cdot,t)\|_{\mathcal{L}^2} \leq \exp\left[-\sigma t\right] \|w_0\|_{\mathcal{L}^2} \tag{4.48}$$
$$|w(t,a)| \leq \exp\left[-\sigma t\right] \left(|w_0(a)| + k_1 \| \left(w_0\right)_r \|_{\mathcal{L}^2}\right) \tag{4.49}$$

with

$$k_1 = \frac{a^{-\frac{(m-1)}{2}}}{\sqrt{\epsilon\theta}} \tag{4.50}$$

consequently

$$|w(t,a)| \leq k_2 \exp\left[-\sigma t\right] \|w_0\|_{\mathcal{H}^1} \tag{4.51}$$

with $k_2 = \max\{1, k_1\}$. The observer gain $L = [l_1, l_2, \ldots, l_n]^T$ is chosen via pole placement. That is, given a set of n complex-valued numbers $\{\mu_1, \mu_2, \ldots, \mu_n\}$ with negative real parts, it is always possible to find L such that the eigenvalues of $F = A - LH$, are exactly $\{\mu_1, \mu_2, \ldots, \mu_n\}$. From the variation of constants formula

$$\widetilde{z}(t) = \exp[Ft]\widetilde{z}_0 + \int_0^t \exp[F(t-\tau)]Bw(a,\tau)d\tau. \tag{4.52}$$

Then, there exists $k_3 > 0$, such that the norm of the state $\widetilde{x}(t)$ is bounded as follows

$$\|\widetilde{z}(t)\|_2 \leq k_3 \exp[-\underline{\mu}t]|\widetilde{z}_0|_2 + k_3\|B\|_2 \int_0^t \exp[-\underline{\mu}(t-\tau)]|w(a,\tau)|d\tau \tag{4.53}$$

with $\underline{\mu} = \min_{i\in\{1,2,\ldots,n\}}\{|\mu_i|\}$. From (4.28), it follows that $\sigma > \underline{\mu} > 0$, and therefore

$$\|\widetilde{z}(t)\|_2 \leq k_3 \exp[-\underline{\mu}t]\widetilde{z}_0 + \frac{k_2k_3}{\sigma - \underline{\mu}} \exp[-\underline{\mu}t]\|B\|_2 \|w_0\|_{H_1}. \tag{4.54}$$

The inequalities (4.48), (4.51) and (4.54) imply that the zero solution of the target system (4.21),(4.23)–(4.25) is stable, with exponential bounds

$$\|w(\cdot,t)\|_{\mathcal{L}^2} \leq \exp\left[-\sigma t\right] \|w_0\|_{\mathcal{L}^2} \tag{4.55}$$
$$|\widetilde{z}(t)|_2 \leq k_3 \exp[-\underline{\mu}t]|\widetilde{z}_0|_2 + k_4 \exp[-\underline{\mu}t] \|w_0\|_{H_1} \tag{4.56}$$

with

$$k_4 = \frac{k_2k_3}{\sigma - \underline{\mu}}\|B\|_2. \tag{4.57}$$

Finally, since the transformation $T_{\mathcal{O}}$ and the second-kind Volterra integral part of T_u are bounded and invertible, [90] and [87] together with the fact that (4.26)-(4.27) has

a triangular structure, imply the existence there exists positive κ_1, κ_2, such that

$$\|\widetilde{x}(t)\|_2 \leq \kappa_1 \exp(-\underline{\mu} t) \left(\|\widetilde{x}_0\|_2 + \|\widetilde{u}_0\|_{\mathcal{H}^1}\right)$$
$$\|\widetilde{u}(\cdot, t)\|_{\mathcal{L}^2} \leq \kappa_2 \exp(-\underline{\mu} t) \left(\|\widetilde{x}_0\|_2 + \|\widetilde{u}_0\|_{\mathcal{H}^1}\right).$$

■

The well-posedness of the DAE (4.34) and the hyperbolic PDE (4.36) are studied in next two lemmas.

Lemma 4.3.1

There is a unique $\mathcal{L}^2(\mathcal{T})$ solution to the hyperbolic equation (4.36).

Proof : A solution to hyperbolic system can be found following the procedure described in [91] for kernel equations required for stabilization of diffusion equations in spherical domain, or the procedure described in [92], for kernel equations required for stabilization of diffusion equations with spatially-variable diffusion coefficients. ■

Lemma 4.3.2

The system of differential algebraic equations (DAE), (4.34) with boundary conditions (4.35) and by the algebraic equation (4.33), has a unique solution $\gamma_i(r) \in \mathcal{L}^2(0,1)$, $i \in \{1, \ldots, n\}$.

Proof : Define

$$\overline{\gamma}_i(r) = \gamma_i(r) - \gamma_i(a) \tag{4.58}$$

for $i \in \{1, 2, \ldots, n\}$. Consider the regular Sturm-Liouville [93] problem

$$\begin{cases} \epsilon \dfrac{d}{dr}\left(r^{m-1} \dfrac{d}{dr}\phi_k(r)\right) = -\lambda_k \phi_k(r) r^{m-1} \\ \text{for } r \in (a,b), \text{ with boundary conditions} \\ \phi_k'(a) = 0 \\ \phi_k'(b) = 0 \end{cases} \tag{4.59}$$

for $r \in (a,b)$, with $k \in \mathbb{N}$. The solution to (4.59) is available as an analytic expression [94]

$$\phi_k(r) = c_k \left(r^{-v} J_v(\mu_k r) - r^{-v} \frac{J_{v+1}(\mu_k a)}{Y_{v+1}(\mu_k a)} Y_v(\mu_k r)\right) \tag{4.60}$$

with $v = \frac{m}{2} - 1$. The values $\mu_k \in \mathbb{R}$, $k \in \mathbb{N}$ are the solutions to the equation

$$P_{v+1}(\mu_k a, \mu_k b) = 0 \tag{4.61}$$

where P_v is the difference of cross-products of first and second-kind Bessel functions [95]

$$P_v(x,y) = J_v(x) Y_v(y) - J_v(y) Y_v(x). \tag{4.62}$$

The eigenvalues λ_k, $k \in \mathbb{N}$ of the Sturm-Liouville problem (4.59) are

$$\lambda_k = \epsilon \mu_k^2. \tag{4.63}$$

Coefficients $c_k, k \in \mathbb{N}$ are chosen for normalization. The set of functions $\phi_k, k \in \mathbb{N}$ form a basis in the Hilbert space $\mathcal{L}^2_m = \mathcal{L}^2\left([a,b], r^{m-1}dr\right)$. Consider a series representation of the functions $\overline{\gamma}_i$, $i \in \{1, 2, \cdots, n\}$ in terms of the basis $\phi_k \in \mathcal{C}^\infty(a,b)$,

that is

$$\overline{\gamma}_i(r) = \sum_{k=0}^{\infty} p_{i,k}\phi_k(r). \tag{4.64}$$

One can verify that

$$\sum_{i=1}^{n} p_{i,k} = -z_k \tag{4.65}$$

with

$$z_k = -\int_a^b \left(\epsilon K_s(r,a) + \epsilon\left(\beta - \frac{\sigma}{2\epsilon}(b-a) - \frac{m-1}{a}\right)K(r,a)\right) \times \phi_k(r) r^{m-1} dr \tag{4.66}$$

and

$$\lambda_k p_m + p_{i-1,k} = -\epsilon a^{m-1} d_i \phi_k(a). \tag{4.67}$$

For each $k \in \mathbb{N}$, the $n-1$ algebraic equations (4.67) together with the equation (4.65) result in a n-dimensional algebraic system that one needs to solve in order to compute $\{q_{1,k}, q_{2,k}, \cdots, q_{n,k}\}$. In other words, the coefficients in the series (4.64) should satisfy an infinite sequence of n-dimensional linear systems

$$\begin{bmatrix} \lambda_k & 1 & \cdots & 0 & 0 \\ 0 & \lambda_k & \cdots & 0 & 0 \\ \vdots & \vdots & \ddots & \vdots & \vdots \\ 0 & 0 & \cdots & \lambda_k & 1 \\ b_n & b_{n-1} & \cdots & b_2 & b_1 \end{bmatrix} \begin{bmatrix} p_{n,k} \\ p_{n-1,k} \\ \vdots \\ p_{2,k} \\ p_{1,k} \end{bmatrix} = \begin{bmatrix} \beta_k d_n \\ \beta_k d_{n-1} \\ \vdots \\ \beta_k d_2 \\ z_k \end{bmatrix} \tag{4.68}$$

where $\beta_k = -\epsilon a^{m-1}\phi_k(a)$. Note that the generalized Fourier coefficients define a function uniquely in the space of definition, that is $\mathcal{L}^2\left([a,b], r^{m-1}dr\right)$, for that reason, a unique solution of the algebraic system in the is a necessary and sufficient condition for the existence of a solution. Define

$$D(\xi) = \det\left(\begin{bmatrix} \xi & 1 & 0 & \cdots & 0 & 0 \\ 0 & \xi & 1 & \cdots & 0 & 0 \\ 0 & 0 & \xi & \cdots & 0 & 0 \\ \vdots & \vdots & \vdots & \ddots & \vdots & \vdots \\ 0 & 0 & 0 & \cdots & \xi & 1 \\ b_n & b_{n-1} & b_{n-2} & \cdots & b_2 & b_1 \end{bmatrix}\right) \tag{4.69}$$

$$= b_n + b_{n-1}\xi + b_{n-2}\xi^2 + \cdots + b_2\xi^{n-2} + b_1\xi^{n-1}. \tag{4.70}$$

The sequence of linear systems (4.68) has a unique solution $q_{i,k}$, with $i \in \{1, 2, \ldots, n\}$, $k \in \mathbb{N}$, if and only if $D(\lambda_k) \neq 0$, for all $k \in \mathbb{N}$. This condition is related to the observability of the coupled system, since it defines a cancellation between the spectral values of the PDE and zeros of the ODE. This condition appears in Assumption 2. ■

4.4 Numerical case study

4.4.1 Coupled model

The finite-dimensional part of the following model is an adaptation from [36] and we present the following modification to isolate the drillstring and the annular regions into two separate control volumes. A particular treatment of the boundary condition

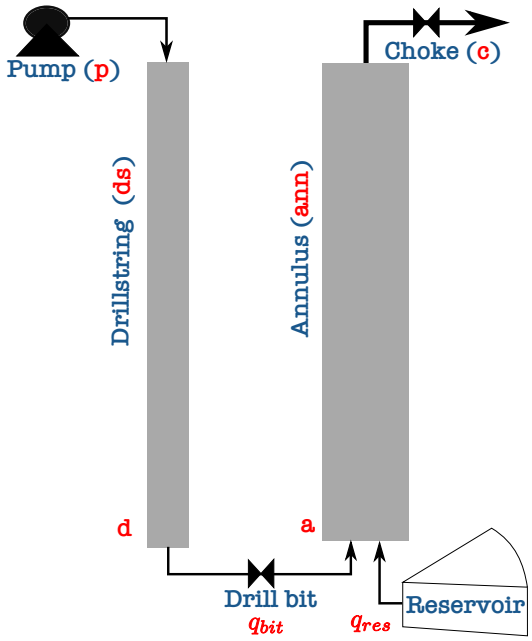

FIGURE 4.1: Schematic representation of the fluid flow through two control volumes of finite dimensional subsystem : drillstring and annulus separated by the drill bit. This adaption from [36] allows the influx model to be coupled in the annulus. Letters in red denotes the location of the corresponding states.

is presented to account for the liquid influx while the reservoir PDE is described in Chapter 2. The model derives from the first principles and the mass conservation equations for the control volumes drillstring ds and annulus ann, as shown in the Figure 4.1, reads

$$\left(\frac{V_{ds}}{\beta_{ds}}\right)\frac{dp_p(t)}{dt} = q_p(t) - q_d(t) \tag{4.71}$$

$$\left(\frac{V_{ann}}{\beta_{ann}}\right)\frac{dp_c(t)}{dt} = q_a(t) - q_c(t) \tag{4.72}$$

where V is the control volume and β the bulk modulus of the liquid. We assume a constant liquid density ρ_0, same as [36]. The subscripts for the volumetric flow rate $q(t)$ denotes the corresponding location (with reference to the schematic 4.1). The fluid flow rate entering the annulus, from both the drillstring and the reservoir satisfies the continuity relation

$$q_a(t) = q_d(t) + q_{\text{res}}(t). \tag{4.73}$$

The momentum balance using the linearized frictional pressure loss[1] function (1.32), for the drillstring control volume, for a wellbore of depth h_L reads

$$M_{ds}\frac{dq_d(t)}{dt} = p_p(t) - p_d(t) - F_{ds}(q_d(t)) + \rho_0 g h_L. \tag{4.74}$$

Representing the pressure at the bottom of the drillstring $p_d(t)$ as a sum of pressure losses in the annulus and across the drill bit gives

$$M_{ds}\frac{dq_d(t)}{dt} = p_p(t) - p_c(t) - F_{ann}(q_d(t) + q_{res}(t)) - F_{ds}(q_d(t)) - \Delta p_{bit}(t) \tag{4.75}$$

where the pressure loss across the bit is given by

$$\Delta p_{bit}(t) = \frac{\rho_0}{2c_d^2 A_n^2} q_d^2(t). \tag{4.76}$$

We consider here the influx $q_{\text{res}}(t) = \xi p_r(t, r_w)$ given by the distributed reservoir pressure model (2.1). To preserve the structure of the observer design, we denote the states of the finite dimensional subsystem as the perturbed[2] dynamics of (4.71), (4.72) and (4.75) around the steady state values for the choke opening $\bar{Z}_c$, e.g. $\delta p_c = p_c - \bar{p}_c$. We can then write

$$x(t) = [\delta p_c(t), \quad \delta p_p(t), \quad \delta q_d(t)]^\top. \tag{4.77}$$

Defining the variable change $\varphi(t,r) = p(t,r) - \bar{p}(t,r)$, the PDE subsystem that governs the dynamics of the reservoir pressure profile is given by $\varphi(t,r)$ for $r \in [r_w, r_e]$. The model takes the following form

$$\frac{dx(t)}{dt} = Ax(t) + B\varphi(t, r_w) \tag{4.78}$$
$$y(t) = Hx(t) \tag{4.79}$$
$$\varphi_t(t,r) = \frac{a}{r}(r\varphi_r(t,r))_r \tag{4.80}$$
$$\varphi_r(t, r_w) = \beta\varphi(t, r_w) + Dx(t) \tag{4.81}$$
$$\varphi_r(t, r_e) = 0 \tag{4.82}$$

where

$$A = \begin{bmatrix} a_0 & 0 & 0 \\ 0 & 0 & a_1 \\ 0 & a_2 & a_3 \end{bmatrix}, \qquad B = \begin{bmatrix} b_0 \\ 0 \\ b_1 \end{bmatrix}, \tag{4.83}$$
$$D = \begin{bmatrix} d_0 & 0 & d_1 \end{bmatrix}. \tag{4.84}$$

Definition of the matrix elements and the intermediate variables are given in Table 4.1 and the physical parameters are given in Table 4.2. Two measurements are typically available on drilling facilities, namely pump and choke pressure, which

[1] assuming a constant area for each control volume, the Equation (1.32) is valid and the area corresponds to the subscripts, e.g. for $F_{ds}(q)$ we use the area of drillstring to calculate velocity corresponding to the flowrate q.

[2] setting $\alpha_g \equiv 0$ in the choke equation (1.25) and linearizing around the steady state operating point $\bar{Z}_c$ will linearize (4.72). Equivalently (4.76) can be linearized around $\bar{q}_d$.

yields

$$H = \begin{bmatrix} 1 & 0 & 0 \\ 0 & 1 & 0 \end{bmatrix}. \tag{4.85}$$

These two measurements are required to make the pair (A, H) observable. Thus, the design of Section 4.2 has to be slightly adapted to account for multiple outputs. They pose no difficulty using a block observer canonical form (see Appendix C), since the presence of multiple outputs only adds degrees of freedom to estimate the state of the scalar PDE.

4.4.2 Simulations

A test case, where the opening of the choke valve is increased suddenly, is considered here to illustrate the results. This leads to reduction of the pressure at the bottom of the wellbore and thus result in an influx from the reservoir. Figure 4.2 shows the comparison between the influx from the plant, the influx estimated by the an observer, with multiple tunings. A comparison with the *open-loop* simulation has appeared in [56].

Although the stability of the dynamics ensures that the latter provides an asymptotic estimate of the influx, it is desirable to speed up the convergence thanks to an observer. Indeed, the time-scale of the reservoir dynamics is much slower than that of the wellbore dynamics [57]. We include normally random noise to the measurement signal and use a static time-step Linear Quadratic Regulator to design the observer gains. It can be observed from the Figure 4.2 that the desired performance is a trade-off between noise amplification, undesirable over-shoots and convergence speed.

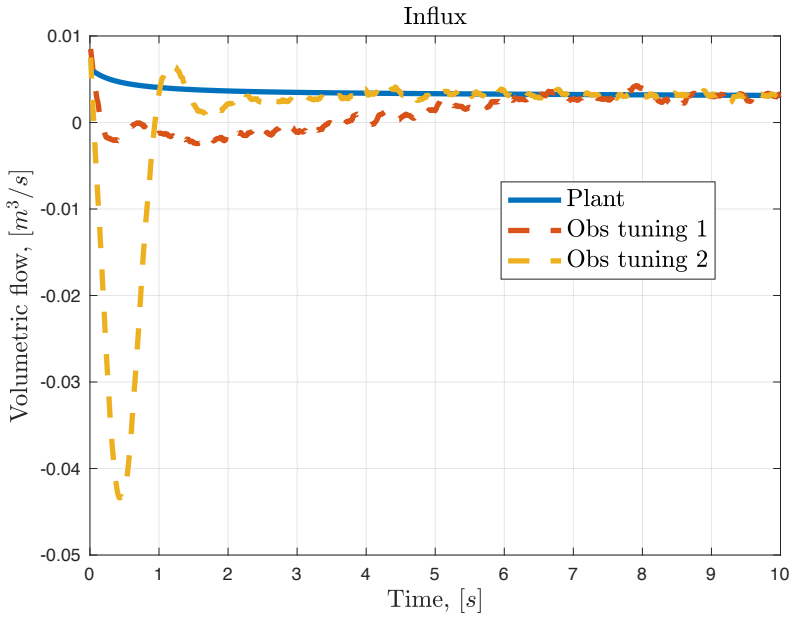

FIGURE 4.2: Observer performance to estimate the influx into the wellbore. Different tuning exhibits the trade-off between handling noise, overshoots and convergence rate.

TABLE 4.1: Definition of matrix elements and intermediate variables.

Element	Definition	Element	Definition
a_0	$-\frac{\beta_{ann}}{V_{ann}}\left(\frac{A_a D_a^2}{32\mu h_L}+\frac{K_c \bar{Z}_c}{\sqrt{2\rho_0(\bar{p}_c-p_0)}}\right)$	a_1	$-\frac{\beta_{ds}}{V_{ds}}$
a_3	$-\frac{32\mu h_L}{M_{ds}A_d D_d^2}+\frac{\rho_0 \bar{q}_d}{M_{ds}c_d^2 A_n^2}$	a_2	$\frac{1}{M_{ds}}$
b_0	$\frac{\beta_{ann}}{V_{ann}}\left(\frac{A_a D_a^2}{32\mu h_L}\right)$	b_1	$-\frac{1}{M_{ds}}$
d_0	$-\frac{A_a D_a^2}{32\mu\xi h_L}$	d_1	$-\frac{1}{\xi}$
M_{ds}	$\frac{\rho_0 h_L}{A_d}$	β	$-\frac{d_0}{\xi}$

TABLE 4.2: Definition and simulation values of wellbore and fluid parameters.

Parameter	Symbol	Value	Unit
Bulk modulus	$\beta_{ann,ds}$	6.896e+08	Pa
Annulus diameter	D_a	0.1809	m
Drillstring diameter	D_d	0.1143	m
Depth of the well	h_L	2000	m
Thickness of reservoir	h	2	m
Mud viscosity	μ	40e-2	Pa s
Choke constant	K_c	0.0029	[-]
Steady state choke opening	$\bar{Z}_c$	0.8	[-]
Bit nozzle constant	c_d	0.8	[-]
Bit nozzle area	A_n	7.459e-4	m^2
Reference pressure	p_o	1e5	Pa
Reference density	ρ_o	780	$kg\,m^{-3}$
Permeability	κ	5e-12	m^2
Porosity	ϕ	0.2	[-]
Total compressibility (reservoir)	c	2.32e-9	Pa^{-1}

Chapter 5

Observer design for a coupled hyperbolic and parabolic PDE system

Dans ce chapitre, nous synthétisons un observateur pour un système dont les dynamiques du réservoir et du puits sont distribuées, et prennent la forme d'équations parabolique (2.1) et hyperbolique (1.28), respectivement. Nous envisageons deux scénarios. Dans le premier, des capteurs sont pression sont positionnés à la fois en surface et au fonds du puits. L'observateur qui en résulte découle naturellement de résultats de la littérature. Nous présentons ensuite la principale contribution de ce chapitre : un observateur pour le cas où seule la mesure de surface est disponible. Cette synthèse repose sur une nouvelle transformation de backstepping, dont un des noyaux vérifie, de manière remarquable, une équation de diffusion sur un domaine carré. Le caractère bien-posé des équations du noyau est démontré en combinant la méthode des approximations successives avec la fonction de Green.

In this chapter, we describe the observer design for the coupled system that contains distributed dynamics for wellbore and reservoir given by the set of hyperbolic PDEs (1.28) and parabolic PDE (2.1) respectively. We investigate two potential scenarios. In the first one, mesurement of both the topside annulus pressure and BHCP are available. The observer design then relies on existing results from the literature. We then present the main contribution of this chapter : an observer design for the case where only the topside measurement is available. It relies on a novel backstepping transformation, where some of the kernels satisfy hyperbolic PDEs on triangular domains, while one kernel satisfies a diffusion equation on a square domain. The well-posedness of this system is assessed combining successive approximations and Green's functions.

5.1 Observer design

In this section we consider the influx $q_{\text{res}}(t) = \xi p_r(t, r_w)$ given by the distributed reservoir pressure model (2.1). Defining the variable change $\varphi(t,r) = p(t,r) - \bar{p}(t,r)$ and using the Equations (2.2), (3.3) and (3.10) gives[1]

$$\varphi_r(t, r_w) = -\frac{\delta q_{bit}(t)}{\xi} + \underbrace{\frac{2A}{\xi\bar{\rho}}}_{\theta} \mathrm{v}(t,0) + \underbrace{\frac{A}{\xi\bar{\rho}C_l}}_{\gamma} \varphi(t, r_w). \tag{5.1}$$

[1] $\bar{p}(t,r)$ is the steady state reservoir pressure profile

Now the coupled system takes the form

$$\mathrm{v}(t,1) = \Theta \mathrm{u}(t,1) \tag{5.2}$$
$$\mathrm{u}_t(t,x) + C_l \mathrm{u}_x(t,x) = \sigma^{++}(x)\mathrm{u}(t,x) + \sigma^{+-}(x)\mathrm{v}(t,x) \tag{5.3}$$
$$\mathrm{v}_t(t,x) - C_l \mathrm{u}_x(t,x) = \sigma^{-+}(x)\mathrm{u}(t,x) + \sigma^{--}(x)\mathrm{v}(t,x) \tag{5.4}$$
$$\mathrm{u}(t,0) = \frac{\varphi(t,r_w)}{C_l} + \mathrm{v}(t,0) \tag{5.5}$$
$$\varphi_r(t,r_w) = -\frac{\delta q_{bit}}{\xi} + \theta \mathrm{v}(t,0) + \gamma \varphi(t,r_w) \tag{5.6}$$
$$\varphi_t(t,r) = a\varphi_{rr}(t,r) + \lambda(r)\varphi_r(t,r) \tag{5.7}$$
$$\varphi_r(t,r_e) = 0. \tag{5.8}$$

Equation (5.7) represents the linearized radial diffusion equation with $\lambda(r) = a/r$. The structure of the bi-directional coupling can be explained as follows : the downward travelling pressure wave 'v' influences the flux out of the reservoir and reflects into the upward travelling pressure wave 'u'. This interconnection has a feedback structure that potentially generates instability. It is the case, e.g. when the pressure in the wellbore is significantly decreased by an influx of gas from the reservoir, since a larger pressure differential increases the flux. However, for the case considered here of a liquid influx, instability is unlikely as the density of the oil from the reservoir is very close to that of the drilling mud.

We now present two different ways of designing an observer to estimate the reservoir influx depending on the availability of downhole measurements.

5.2 Design with two measurements

In this section, we assume that choke pressure and BHCP measurements are available to estimate the influx from the reservoir. More precisely, we assume that we measure

$$y_c(t) = c_1 \mathrm{u}(t,1) + c_2 \mathrm{v}(t,1) \rightarrow \text{a measure of } p_c(t) \tag{5.9}$$
$$y_b(t) = \varphi(t,r_w) \rightarrow \text{a measure of BHCP}(t). \tag{5.10}$$

Equation (5.10) is valid under the following assumption[2] :

A1 The boundary shared between the wellbore and the reservoir is at mechanical equilibrium during the period of study.

[2]measurement is not equal only during the prolonged exposure of the reservoir to the wellbore during drilling, resulting in the formation of mud cake. Even in case of an additional pressure drop, i.e., skin factor $S \neq 0$, observer design would be similar should the skin factor not affect the observability of the system.

5.2.1 Wellbore observer

Measuring the BHCP allows one to decouple the reservoir and wellbore dynamics and design two separate observers. More precisely, the wellbore dynamics read

$$\mathrm{v}(t,1) = \Theta \mathrm{u}(t,1) \tag{5.11}$$
$$\mathrm{u}_t(t,x) + C_l \mathrm{u}_x(t,x) = \sigma^{++}(x)\mathrm{u}(t,x) + \sigma^{+-}(x)\mathrm{v}(t,x) \tag{5.12}$$
$$\mathrm{v}_t(t,x) - C_l \mathrm{u}_x(t,x) = \sigma^{-+}(x)\mathrm{u}(t,x) + \sigma^{--}(x)\mathrm{v}(t,x) \tag{5.13}$$
$$\mathrm{u}(t,0) = \frac{\varphi(t,r_w)}{C_l} + \mathrm{v}(t,0). \tag{5.14}$$

A Luenburger-like observer is proposed as an exact copy of the plant with output error injection terms, and the BHCP is directly injected at the boundary $x = 0$, as follows

$$\widehat{\mathrm{v}}(t,1) = \Theta \widehat{\mathrm{u}}(t,1) + \epsilon \left(y_c(t) - (c_1 \widehat{\mathrm{u}}(t,1) + c_2 \widehat{\mathrm{v}}(t,1))\right) \tag{5.15}$$
$$\begin{aligned}\widehat{\mathrm{u}}_t(t,x) + C_l \widehat{\mathrm{u}}_x(t,x) = {} & \sigma^{++}(x)\widehat{\mathrm{u}}(t,x) + \sigma^{+-}(x)\widehat{\mathrm{v}}(t,x) \\ & + P^{+}(x)(y_c(t) - (c_1 \widehat{\mathrm{u}}(t,1) + c_2 \widehat{\mathrm{v}}(t,1)))\end{aligned} \tag{5.16}$$
$$\begin{aligned}\widehat{\mathrm{v}}_t(t,x) - C_l \widehat{\mathrm{v}}_x(t,x) = {} & \sigma^{-+}(x)\widehat{\mathrm{u}}(t,x) + \sigma^{--}(x)\widehat{\mathrm{v}}(t,x) \\ & + P^{-}(x)(y_c(t) - (c_1 \widehat{\mathrm{u}}(t,1) + c_2 \widehat{\mathrm{v}}(t,1)))\end{aligned} \tag{5.17}$$
$$\widehat{\mathrm{u}}(t,0) = \frac{y_b(t)}{C_l} + \widehat{\mathrm{v}}(t,0). \tag{5.18}$$

Defining the error coordinates as $\widetilde{*} := * - \widehat{*}$ yields

$$\widetilde{\mathrm{v}}(t,1) = \bar{\Theta} \widetilde{\mathrm{u}}(t,1) \tag{5.19}$$
$$\begin{aligned}\widetilde{\mathrm{u}}_t(t,x) + C_l \widetilde{\mathrm{u}}_x(t,x) = {} & \sigma^{++}(x)\widetilde{\mathrm{u}}(t,x) + \sigma^{+-}(x)\widetilde{\mathrm{v}}(t,x) \\ & - P^{+}(x)\left(c_1 \widetilde{\mathrm{u}}(t,1) + c_2 \widetilde{\mathrm{v}}(t,1)\right)\end{aligned} \tag{5.20}$$
$$\begin{aligned}\widetilde{\mathrm{v}}_t(t,x) - C_l \widetilde{\mathrm{v}}_x(t,x) = {} & \sigma^{-+}(x)\widetilde{\mathrm{u}}(t,x) + \sigma^{--}(x)\widetilde{\mathrm{v}}(t,x) \\ & - P^{-}(x)\left(c_1 \widetilde{\mathrm{u}}(t,1) + c_2 \widetilde{\mathrm{v}}(t,1)\right)\end{aligned} \tag{5.21}$$
$$\widetilde{\mathrm{u}}(t,0) = \widetilde{\mathrm{v}}(t,0). \tag{5.22}$$

The effective reflection coefficient $\bar{\Theta}$ is a function of the linearization points of the choke equation that reads

$$\bar{\Theta} = \left(\frac{\Theta - \epsilon c_1}{1 + \epsilon c_2}\right). \tag{5.23}$$

The design parameter ϵ provides a freedom to choose the influence of measurements and the observed states — higher ϵ amplifies measurement noise. It is possible to change the value of ϵ according to the choke opening to maintain a constant effective reflection coefficient $\bar{\Theta}$ throughout the operation, but a time-dependent coefficient induces additional dynamics that may lead to instability. Importantly, a necessary and sufficient condition for the stability of the system $\widetilde{\Sigma}$ is that $\bar{\Theta}$ satisfy

$$-1 < \bar{\Theta} < 1. \tag{5.24}$$

Rather, it is possible to map the value of $\bar{\Theta}$ throughout the operating range and chose a constant epsilon that ensures that Equation (5.24) is satisfied for all values of Z_c.

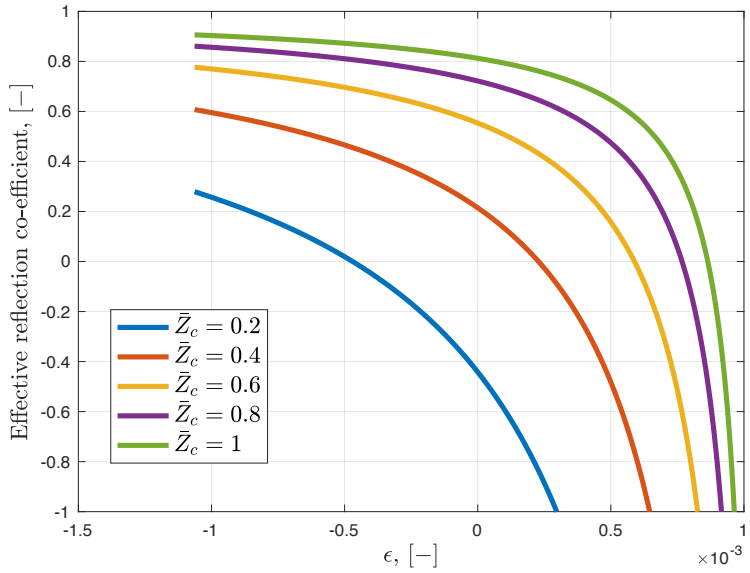

FIGURE 5.1: Mapping of effective reflection coefficient $\bar{\Theta}$ to a range of choke opening. Rapidly converging observer is obtained as $\bar{\Theta} \to 0$.

This point is illustrated in Figure 5.1. Setting $\bar{\Theta}$ close to zero yields a rapidly converging observer. The observer gains $P^+(x)$ and $P^-(x)$ are found by using standard backstepping approach [86] This is done by mapping the error system on to a target system whose stability can be guaranteed. We choose the target system $\mathbf{\Sigma_T}$ that reads

$$\beta(t,1) = \bar{\Theta}\alpha(t,1) \tag{5.25}$$
$$\alpha_t(t,x) + C_l\alpha_x(t,x) = \sigma^{++}(x)\alpha(t,x) \tag{5.26}$$
$$\beta_t(t,x) - C_l\beta_x(t,x) = \sigma^{--}(x)\beta(t,x) \tag{5.27}$$
$$\alpha(t,0) = \beta(t,0). \tag{5.28}$$

The mapping is achieved using invertible transformations that are functions of Volterra integrals. We choose the following change of variables

$$\tilde{u}(t,x) = \alpha(t,x) - \int_x^1 P^{uu}(x,\xi)\alpha(\xi,t)d\xi - \int_x^1 P^{uv}(x,\xi)\beta(\xi,t)d\xi \tag{5.29}$$
$$\tilde{v}(t,x) = \beta(t,x) - \int_x^1 P^{vu}(x,\xi)\alpha(\xi,t)d\xi - \int_x^1 P^{vv}(x,\xi)\beta(\xi,t)d\xi \tag{5.30}$$

The observer gains $P^+(x)$ and $P^-(x)$ satisfy

$$P^+(x) = \frac{\bar{\Theta}C_lP^{uv}(x,1) - C_lP^{uu}(x,1)}{c_1 + \bar{\Theta}c_2} \tag{5.31}$$
$$P^-(x) = \frac{\bar{\Theta}C_lP^{vv}(x,1) - C_lP^{vu}(x,1)}{c_1 + \bar{\Theta}c_2}. \tag{5.32}$$

where P^{uu}, P^{uv}, P^{vu} and P^{vv} are the backstepping Kernels that satisfy a set of hyperbolic PDEs given by

$$-C_l P^{uu}_{\xi}(x,\xi) + C_l P^{uu}_{x}(x,\xi) + \left(\sigma^{++}(x) - \sigma^{++}(\xi)\right) P^{uu}(x,\xi) + \sigma^{+-}(x) P^{vu}(x,\xi) = 0 \tag{5.33}$$

$$-C_l P^{vu}_{\xi}(x,\xi) - C_l P^{vu}_{x}(x,\xi) + \left(\sigma^{--}(x) - \sigma^{++}(\xi)\right) P^{vu}(x,\xi) + \sigma^{-+}(x) P^{uu}(x,\xi) = 0 \tag{5.34}$$

$$C_l P^{uv}_{\xi}(x,\xi) - C_l P^{uv}_{x}(x,\xi) + \left(\sigma^{++}(x) - \sigma^{--}(\xi)\right) P^{uv}(x,\xi) + \sigma^{+-}(x) P^{vv}(x,\xi) = 0 \tag{5.35}$$

$$C_l P^{vv}_{\xi}(x,\xi) + C_l P^{vv}_{x}(x,\xi) + \left(\sigma^{--}(x) - \sigma^{--}(\xi)\right) P^{vv}(x,\xi) + \sigma^{-+}(x) P^{uv}(x,\xi) = 0 \tag{5.36}$$

satisfying the following boundary conditions that read

$$P^{uv}(x,x) = \frac{\sigma^{+-}(x)}{2C_l} \quad , \qquad P^{vu}(x,x) = -\frac{\sigma^{-+}(x)}{2C_l} \quad . \tag{5.37}$$

Lemma 5.2.1

Under the condition (5.24) and the observer gains defined in Equations (5.31) and (5.32), the error system (5.19)–(5.22) converges to zero [96].

5.2.2 Reservoir observer

As a second step, we consider a subsystem that governs the reservoir dynamics only, that reads

$$\varphi_r(t,r_w) = -\frac{\delta q_{bit}}{\xi} + \theta \mathrm{v}(t,0) + \gamma \varphi(t,r_w) \tag{5.38}$$

$$\varphi_t(t,r) = a\varphi_{rr}(t,r) + \lambda(r)\varphi_r(t,r) \tag{5.39}$$

$$\varphi_r(t,r_e) = 0. \tag{5.40}$$

Again, we propose an Luenberger-like observer that contains the exact copy of the plant with output error injection terms, that take the form

$$\widehat{\varphi}_r(t,r_w) = -\frac{\delta q_{bit}}{\xi} + \theta \widehat{\mathrm{v}}(t,0) + \gamma \widehat{\varphi}(t,r_w) + l_1(y_r(t) - \widehat{\varphi}(t,r_w)) \tag{5.41}$$

$$\widehat{\varphi}_t(t,r) = a\widehat{\varphi}_{rr}(t,r) + \lambda(r)\widehat{\varphi}_r(t,r) + l(r)(y_r(t) - \widehat{\varphi}(t,r_w)) \tag{5.42}$$

$$\widehat{\varphi}_r(t,r_e) = 0. \tag{5.43}$$

Now, the error system reads

$$\widetilde{\varphi}_r(t,r_w) = (\gamma - l_1)\widetilde{\varphi}(t,r_w) + \theta \widetilde{\mathrm{v}}(t,0) \tag{5.44}$$

$$\widetilde{\varphi}_r(t,r) = a\widetilde{\varphi}_{rr}(t,r) + \lambda(r)\widetilde{\varphi}_r(t,r) - l(r)\widetilde{\varphi}(t,r_w) \tag{5.45}$$

$$\widetilde{\varphi}_r(t,r_e) = 0. \tag{5.46}$$

We note from Lemma (5.2.1) that the term $\widetilde{\mathrm{v}}(t,0)$ acts as a vanishing disturbance to (5.44)–(5.46). We first study the unperturbed dynamics and design $l(r)$ such that they are exponentially stable. We do so by mapping them to the following stable

target system

$$\psi_t(t,r) = a\psi_{rr}(t,r) + \lambda(r)\psi_r(t,r) - C\psi(t,r) \tag{5.47}$$
$$\psi_r(t,r_w) = K\psi(t,r_w) \tag{5.48}$$
$$\psi_r(t,r_e) = 0. \tag{5.49}$$

Here, C and K are the design parameters that provide a trade-off between convergence rate and robustness to uncertainties. Again, we consider the change of variable as a function of invertible Volterra integral transformation given by

$$\varphi(t,r) = \psi(t,r) - \int_{r_w}^{r} L(r,y)\psi(y,t)dy. \tag{5.50}$$

Through standard backstepping approach, it can be seen that the observer gains l_1 and $l(r)$ satisfy

$$\gamma + L(r_w,r_w) - K - l_1 = 0 \tag{5.51}$$
$$-aL_y(r,r_w) + (aK + \lambda(r_w))L(r,r_w) + l(r) = 0 \tag{5.52}$$

and the Kernel $L(r,y)$ is a solution of a parabolic equation that reads

$$a\left(L_{rr}(r,y) - L_{yy}(r,y)\right) + \lambda(r)L_r(r,y) + \lambda(y)L_y(r,y) + \left(C + \lambda'(y)\right)L(r,y) = 0 \tag{5.53}$$
$$2a\frac{d}{dr}L(r,r) - C = 0 \tag{5.54}$$
$$L(r_e,r_e) = 0 \tag{5.55}$$
$$L_r(r_e,y) = 0. \tag{5.56}$$

Stability of the combined observer

Modifying the backstepping transformations such that the entire wellbore-reservoir state is mapped to a stable target system induces nonlinear, nonlocal relations between the backstepping kernels, which severely complicates the proof of their well-posedness. The simulations in section 5.2.3 shows that the considered coupled system is stable. However, to theoretically guarantee the exponential stability, slight modifications in the topside measurement is considered. Details are in Section 5.3.

5.2.3 Numerical simulations

We consider various industry relevant scenarios to study the performance and robustness of this combined observer design. Table 5.1 summarizes the simulation parameters.

Drilling into a high pressure pocket. During drilling, it is common to encounter pockets of hydrocarbons with higher pressure than anticipated. Drilling into such zones will lead to an influx. We present here a case where a section with known reservoir pressure is drilled using MPD and a high pressure pocket is encountered at 5 s. The pressure within the pocket is considered to be 50% higher than that of the anticipated. As depicted on Figure 5.2, the observer successfully estimates the influx, while no influx is detected in the absence of an observer (i.e. in open loop). The near wellbore reservoir pressure distribution is also estimated by the observer as

TABLE 5.1: Wellbore parameters used for the simulation of industry relevant scenarios.

Parameter	Symbol	Value	Unit
Flow rate at bit	q_{bit}	0.03	$m^3\,s^{-1}$
Length of the wellbore	L	2000	m
Choke constant	K_c	2.85e-03	[-]
Steady state choke opening	$\bar{Z}_c$	0.95	[-]
Velocity of sound	C_l	940.30	$m\,s^{-1}$
Reference pressure	p_0	1e+05	Pa
Reference density	ρ_0	780	$kg\,m^{-3}$

shown on Figure 5.3. Interestingly, the reservoir pressure is poorly estimated away from the wellbore but this does not affect the influx estimation.

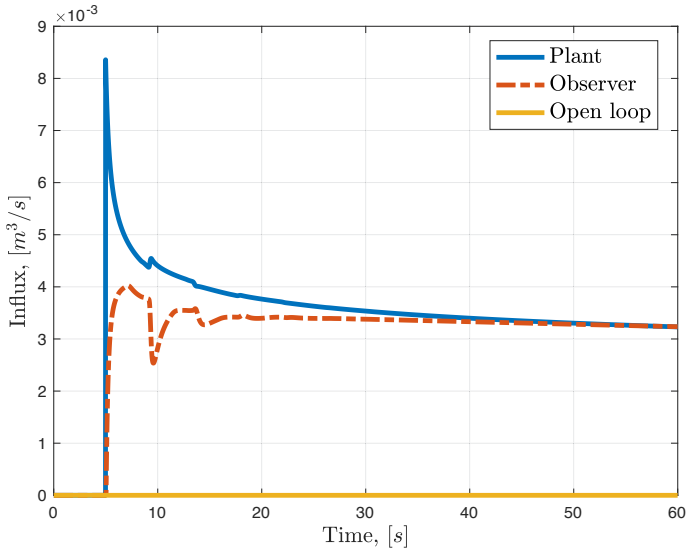

FIGURE 5.2: Influx estimation by the observer in comparison to the plant measurement and in the absence of an observer for the scenario of drilling into a high pressure pocket.

In presence of transients. During MPD operation, there are instances when the choke opening is varied rapidly in order to maintain the required BHCP. We present the case here with an over estimation of the reservoir and wellbore parameters to emulate the uncertainty of these parameters in practice, inclusive of transients introduced by the choke variations. The perturbation of wellbore states from the steady state profile, reservoir pressure and permeability are assumed to be overestimated by 10% each and Z_c varied from 0.8 to 0.4 in 1 s. Despite the uncertainty in the reservoir and wellbore parameters, the observer successfully estimates the influx and the near wellbore reservoir pressure distribution as depicted in Figures 5.4 and 5.5 respectively.

Rather, changing the form of measurement used to design the observer leads to a well-posed observer design for the coupled wellbore-reservoir dynamics. The design is detailed in the following section.

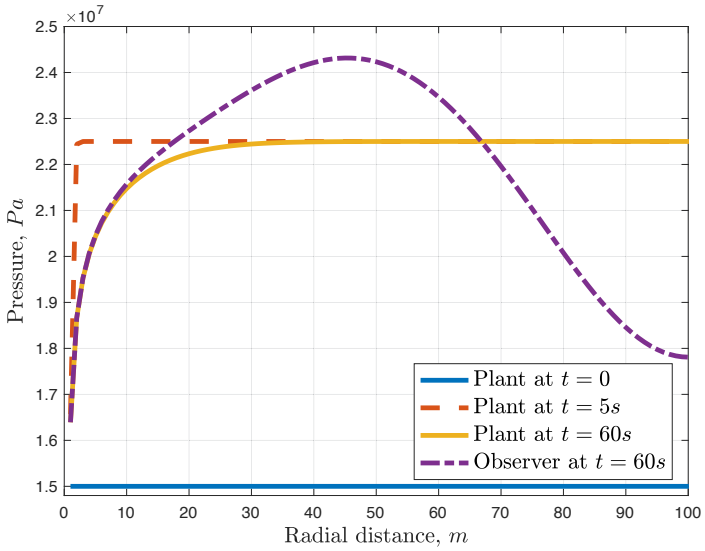

FIGURE 5.3: Time snapshots of distributed pressure profile within the reservoir obtained from plant in comparison to that of the estimation by the observer for the scenario of drilling into a high pressure pocket.

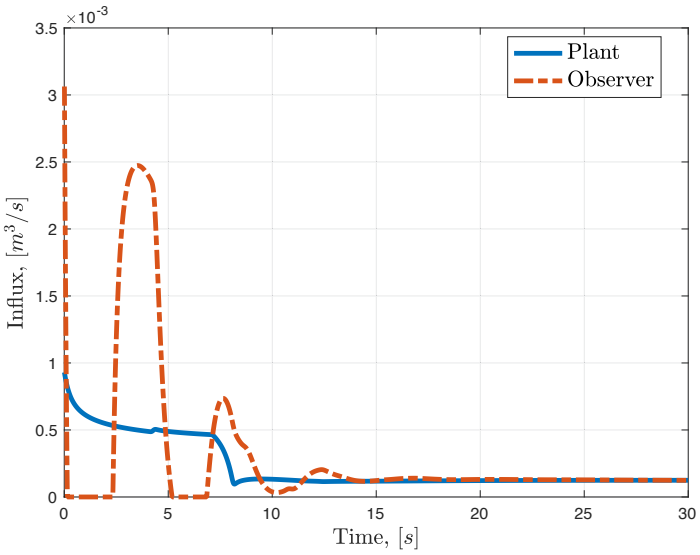

FIGURE 5.4: Influx estimation by the observer in comparison to the plant measurement for the case of pressure transients due to rapid choke opening variations.

5.3 Topside sensing

We now propose an observer design that relies on topside measurement only. Again, we propose a Luenburger-like observer that is an exact copy of the plant $\mathbf{\Sigma}$ with output error injection terms. For readability purposes, we assume that the measurement[3] is

$$y(t) = \mathrm{u}(t, 1). \tag{5.57}$$

[3]this assumption is not restrictive as for a different measurement $y_c = c_1 u(1,t) + c_2 v(1,t)$ rewrites $y_c = (c_1 + c_2\Theta)\, u(1,t)$ and the design is unchanged up to a constant factor.

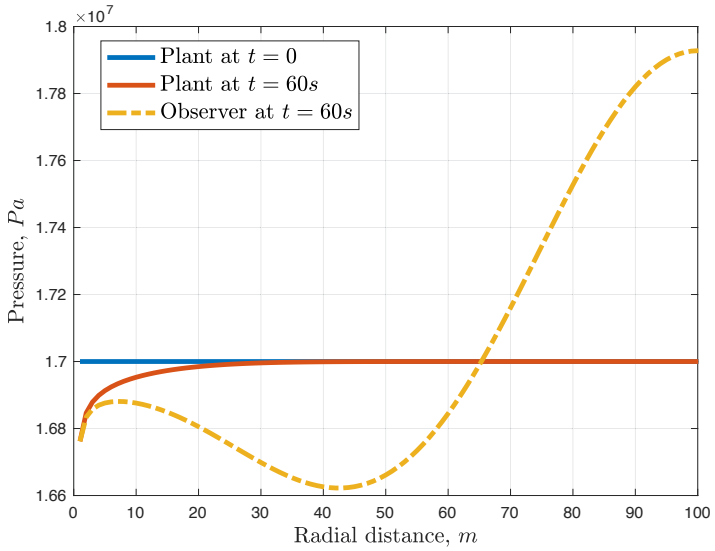

FIGURE 5.5: Time snapshots of distributed pressure profile within the reservoir obtained from plant in comparison to that of the estimation by the observer for the case of pressure transients due to rapid choke opening variations.

The state estimates are solution of the observer system $\widehat{\Sigma}$ that reads

$$\widehat{\mathrm{v}}(t,1) = \Theta \mathrm{u}(t,1) \tag{5.58}$$

$$\widehat{\mathrm{u}}_t(t,x) + C_l \widehat{\mathrm{u}}_x(t,x) = \sigma^{++}(x)\widehat{\mathrm{u}}(t,x) + \sigma^{+-}(x)\widehat{\mathrm{v}}(t,x) + p_u(x)(y(t) - \widehat{\mathrm{u}}(t,1)) \tag{5.59}$$

$$\widehat{\mathrm{v}}_t(t,x) - C_l \widehat{\mathrm{v}}_x(t,x) = \sigma^{-+}(x)\widehat{\mathrm{u}}(t,x) + \sigma^{--}(x)\widehat{\mathrm{v}}(t,x) + p_v(x)(y(t) - \widehat{\mathrm{u}}(t,1)) \tag{5.60}$$

$$\widehat{\mathrm{u}}(t,0) = \widehat{\mathrm{v}}(t,0) + \frac{\widehat{\varphi}(t,r_w)}{C_l} \tag{5.61}$$

$$\widehat{\varphi}_r(t,r_w) = -\frac{\delta q_b}{\xi} + \theta \widehat{\mathrm{v}}(t,0) + \gamma \widehat{\varphi}(t,r_w) \tag{5.62}$$

$$\widehat{\varphi}_t(t,r) = a\widehat{\varphi}_{rr}(t,r) + \lambda(r)\widehat{\varphi}_r(t,r) + p(x)(y(t) - \widehat{\mathrm{u}}(t,1)) \tag{5.63}$$

$$\widehat{\varphi}_r(t,r_e) = -d_0. \tag{5.64}$$

The observer gains $p_u(x), p_v(x)$ and $p(x)$ are yet to be defined. The objective is to find these observer gains such the solution to the error system converges exponentially to zero, ie., the estimated states converge to the real value exponentially over time. State error is the difference between the real and estimated values of the system states. They are represented as a solution to the error system $\widetilde{\Sigma}$ that reads

$$\widetilde{\mathrm{v}}(t,1) = 0 \tag{5.65}$$

$$\widetilde{\mathrm{u}}_t(t,x) + C_l \widetilde{\mathrm{u}}_x(t,x) = \sigma^{++}(x)\widetilde{\mathrm{u}}(t,x) + \sigma^{+-}(x)\widetilde{\mathrm{v}}(t,x) - p_u(x)\widetilde{\mathrm{u}}(t,1) \tag{5.66}$$

$$\widetilde{\mathrm{v}}_t(t,x) - C_l \widetilde{\mathrm{v}}_x(t,x) = \sigma^{-+}(x)\widetilde{\mathrm{u}}(t,x) + \sigma^{--}(x)\widetilde{\mathrm{v}}(t,x) - p_v(x)\widetilde{\mathrm{u}}(t,1) \tag{5.67}$$

$$\widetilde{\mathrm{u}}(t,0) = \widetilde{\mathrm{v}}(t,0) + \frac{\widetilde{\varphi}(t,r_w)}{C_l} \tag{5.68}$$

$$\widetilde{\varphi}_r(t,r_w) = \gamma \widetilde{\varphi}(t,r_w) + \theta \widetilde{\mathrm{v}}(t,0) \tag{5.69}$$

$$\widetilde{\varphi}_t(t,r) = a\widetilde{\varphi}_{rr}(t,r) + \lambda(r)\widetilde{\varphi}_r(t,r) - p(x)\widetilde{\mathrm{u}}(t,1) \tag{5.70}$$

$$\widetilde{\varphi}_r(t,r_e) = d_0. \tag{5.71}$$

We now want to map the error system $\widetilde{\Sigma}$ onto a stable target system. We choose a system such that the in-domain coupling terms of the wellbore dynamics are removed. This allows the stability to be guaranteed. Denoted by $\mathbf{\Sigma_T}$, the target system reads

$$\widetilde{\beta}(t,1) = 0 \tag{5.72}$$

$$\widetilde{\alpha}_t(t,x) + C_l\widetilde{\alpha}_x(t,x) = \sigma^{++}(x)\widetilde{\alpha}(t,x) + \sigma^{+-}(x)\widetilde{\beta}(t,x) + \int_x^1 g_\alpha(x,y)\widetilde{\beta}(t,y)dy \tag{5.73}$$

$$\widetilde{\beta}_t(t,x) - C_l\widetilde{\beta}_x(t,x) = \sigma^{--}(x)\widetilde{\beta}(t,x) + \int_x^1 g_\beta(x,y)\widetilde{\beta}(t,y)dy \tag{5.74}$$

$$\widetilde{\alpha}(t,0) = \widetilde{\beta}(t,0) + \frac{\widetilde{\psi}(t,r_w)}{C_l} \tag{5.75}$$

$$\widetilde{\psi}_r(t,r_w) = \bar{\gamma}\widetilde{\psi}(t,r_w) + \theta\widetilde{\beta}(t,0) \tag{5.76}$$

$$\begin{aligned}\widetilde{\psi}_t(t,r) = a\widetilde{\psi}_{rr}(t,r) + \lambda(r)\widetilde{\psi}_r(t,r) - c\widetilde{\psi}(t,r) + h(r)\widetilde{\beta}(t,0)\\ + \int_0^1 l(r,x)\widetilde{\beta}(t,x)dx\end{aligned} \tag{5.77}$$

$$\widetilde{\psi}_r(t,r_e) = 0 \tag{5.78}$$

where h,l, g_α, g_β are yet to be designed. The stability properties of the target system are assessed in the following Lemma.

Lemma 5.3.1

Consider (5.72)–(5.78) with initial conditions $(\alpha_0, \beta_0, \psi_0)$ in $\mathcal{L}^2([0,1]) \times \mathcal{L}^2([0,1]) \times \mathcal{L}^2([r_w, r_e])$. There exists C, λ such that the solutions satisfy

$$\|(\alpha(t,\cdot), \beta(t,\cdot), \psi(t,\cdot))\| \leq C\,\|(\alpha_0, \beta_0, \psi_0)\|\, e^{-\lambda t} \tag{5.79}$$

provided that $c > 0$ and $\bar{\gamma} > 0$.

Proof : Notice that β converges to zero in finite time. Therefore, for $t > 1/C_l$, ψ satisfies

$$\widetilde{\psi}_r(t,r_w) = \bar{\gamma}\psi(t,r_w) \tag{5.80}$$

$$\widetilde{\psi}_t(t,r) = a\widetilde{\psi}_{rr}(t,r) + \lambda(r)\widetilde{\psi}_r(t,r) - c\widetilde{\psi}(t,r) \tag{5.81}$$

$$\widetilde{\psi}_r(t,r_e) = 0 \tag{5.82}$$

which is exponentially stable as proved in Chapter 4. Finally, α satisfies a simple transport equation with vanishing input, and thus also exponentially converges to zero. ■

5.3.1 Backstepping transformation

Kernel equations

We now seek a variable change as the following set of Volterra equations

$$\widetilde{u}(t,x) = \widetilde{\alpha}(t,x) - \int_x^1 K^u(x,y)\widetilde{\alpha}(t,y)dy \tag{5.83}$$

$$\widetilde{v}(t,x) = \widetilde{\beta}(t,x) - \int_x^1 K^v(x,y)\widetilde{\alpha}(t,y)dy \tag{5.84}$$

$$\widetilde{\varphi}(t,r) = \widetilde{\psi}(t,r) - \int_{r_w}^r L(r,s)\widetilde{\psi}(t,s)ds - \int_0^1 M(r,y)\widetilde{\alpha}(t,y)dy. \tag{5.85}$$

Remark 5. *Notice that the transformation (5.83)–(5.85) does not feature integral terms depending on β in the right-hand-side. As will appear, this is not only sufficient for observer design but actually necessary, as adding such terms would result in ill-posed kernel equations.*

Differentiating with respect to time and space and plugging into the error and target systems yields the following set of observer gains

$$p_u(x) = -C_l K^u(x,1) \tag{5.86}$$
$$p_v(x) = -C_l K^v(x,1) \tag{5.87}$$
$$p(x) = -C_l M(r,1) \tag{5.88}$$

while the kernels satisfy the following set of equations

$$aL_{rr}(r,s) = aL_{ss}(r,s) - L_s(r,s)\lambda(s) - (\lambda'(s)+c)L(r,s) - \lambda(r)L_r(r,s) \tag{5.89}$$
$$\frac{d}{dr}L(r,r) = \frac{c}{2a} \tag{5.90}$$
$$L(r_e,r_e) = 0 \tag{5.91}$$
$$L_r(r_e,s) = 0 \tag{5.92}$$

on the one hand, and

$$C_l K^u_y(x,y) + C_l K^u_x(x,y) = \left(\sigma^{++}(x) - \sigma^{++}(y)\right) K^u(x,y) + \sigma^{+-}(x)K^v(x,y) \tag{5.93}$$
$$-C_l K^v_x(x,y) + C_l K^v_y(x,y) = \left(\sigma^{--}(x) - \sigma^{++}(y)\right) K^v(x,y) + \sigma^{-+}(x)K^u(x,y) \tag{5.94}$$
$$2C_l K^v(x,x) = -\sigma^{-+}(x) \tag{5.95}$$
$$C_l K^u(0,y) = C_l K^v(0,y) + M(r_w,y) \tag{5.96}$$

with the following diffusion equation and boundary conditions

$$C_l M_y(r,y) = aM_{rr}(r,y) + \lambda(r)M_r(r,y) - \sigma^{++}(y)M(r,y) \tag{5.97}$$
$$M_r(r_w,y) = \gamma M(r_w,y) + \theta K^v(0,y) \tag{5.98}$$
$$M_r(r_e,y) = 0 \tag{5.99}$$
$$M(r,0) = \left(a\bar{\gamma} + \lambda(r_w)\right) L(r,r_w) - aL_r(r,r_w) \tag{5.100}$$

on the other hand. Finally, h, g_α, g_β and $\bar{\gamma}$ are given by

$$h(r) = C_l M(r,0) - \theta a L(r,r_w) + \int_{r_w}^{r} L(r,s)h(s)ds \tag{5.101}$$
$$g_\alpha(x,y) = \sigma^{+-}(y) + \int_x^y K^u(x,s)g_\alpha(s,y)ds \tag{5.102}$$
$$g_\beta(x,y) = \sigma^{+-}(y) + \int_x^s K^v(x,s)g_\alpha(s,y)ds \tag{5.103}$$
$$l(r,y) = \sigma^{+-}(y)M(r,y) + \int_x^y M(r,s)g_\alpha(s,y)ds + \int_{r_w}^{r} L(r,s)l(s,y) \tag{5.104}$$
$$\bar{\gamma} = \gamma + L(r_w,r_w). \tag{5.105}$$

Remark 6. *The structure of these kernel equations is rather novel, in particular, equations (5.97)–(5.100) which are parabolic kernel PDEs on a square domain. They appear*

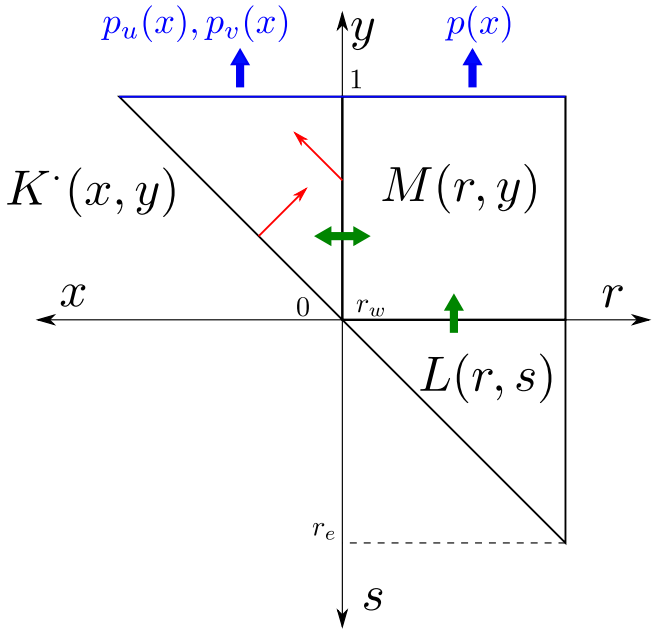

FIGURE 5.6: Schematic representation of the kernel equations. The green arrows represent coupling at the boundaries. The red arrows represent the characteristic lines over which to integrate Equations (5.93)–(5.96). The black boundaries of the domain all correspond to boundary conditions for the kernels. Finally, the blue boundaries and arrows denote the "output" of these equations, i.e., the observer gains. The Equations are solved "from bottom to top" on this diagram.

due to the coupling between a parabolic and a hyperbolic PDE in the observer error equations. Interestingly, adding terms in β in the backstepping transformation as suggested in Remark 5 would yield a similar kernel equation but with an opposite sign in front of the M_y term, i.e. an ill-posed parabolic operator with infinitely many unstable eigenvalues.

Well-posedness of the kernel equations

The structure of the kernel equations is as described on Figure 5.6. Notice first that (5.90)–(5.92) have been widely studied, e.g. in [86] where their well-posdeness has been established. Thus, there exists a solution $L(r,s)$ for $r,s \in \mathcal{T}_r$ given by $r_w \leq s \leq r \leq r_e$. We now define G as the Green's function associated to the following mixed initial-boundary value problem

$$N_y(r,y) = \frac{a}{C_l r}\left(rN_r\right)_r(r,y) - \sigma^{++}(y)N(r,y) \tag{5.106}$$
$$N_r(r_w,y) = \xi N(r_w,y) \tag{5.107}$$
$$N_r(r_e,y) = 0 \tag{5.108}$$
$$N(r,0) = N_0(r) \tag{5.109}$$

that is the function such that

$$N(r,y) = \int_{r_w}^{r_e} G(r,s,y)N_0(s)ds. \tag{5.110}$$

The existence of such a function is a classical result of functional analysis, see e.g. [97]. Then, for some constant Γ, one can rewrite Equations (5.97)–(5.100) as

$$M(r,y) = \int_{r_w}^{r_e} T(s)G(r,s,y)ds + \Gamma \int_0^y K^v(0,\eta)G(r,r_w,y-\eta)d\eta \tag{5.111}$$

where

$$T(r) = \left(a\bar{\gamma} + \lambda(r_w)\right) L(r,r_w) - aL_r(r,r_w) \tag{5.112}$$

Plugging (5.111) into (5.93)–(5.96) yields

$$C_l K^u_y(x,y) + C_l K^u_x(x,y) = \left(\sigma^{++}(x) - \sigma^{++}(y)\right) K^u(x,y) + \sigma^{+-}(x)K^v(x,y) \tag{5.113}$$

$$-C_l K^v_x(x,y) + C_l K^v_y(x,y) = \left(\sigma^{--}(x) - \sigma^{++}(y)\right) K^v(x,y) + \sigma^{-+}(x)K^u(x,y) \tag{5.114}$$

$$2C_l K^v(x,x) = -\sigma^{-+}(x) \tag{5.115}$$

$$\begin{aligned} C_l K^u(0,y) =& C_l K^v(0,y) + \int_{r_w}^{r_e} T(s)G(r_w,s,y)ds \\ &+ \Gamma \int_0^y K^v(0,\eta)G(r_w,r_w,y-\eta)d\eta. \end{aligned} \tag{5.116}$$

Finally, Equations (5.113)–(5.116) can be solved using the methods of characteristics and successive approximations. We are now ready to state the main result of this chapter.

Theorem 5.3.1

Consider system (5.2)–(5.8) with the measurement (5.57) and the observer (5.58)–(5.64) with the gains defined by (5.86)–(5.88). Then the estimates exponentially converge in $\mathcal{L}^2([0,1])^2 \times \mathcal{L}^2([r_w,r_e])$, to the true states provided the following condition is satisfied

$$c < \frac{2a\gamma}{r_e - r_w}. \tag{5.117}$$

Proof : If (5.117) is satisfied then $\bar{\gamma} > 0$, thus the target system is exponentially stable. The existence of the kernels implies that the error system and the target system have equivalent stability properties, thus the result. ■

Chapter 6

Conclusion and perspectives

Le problème étudié dans ce manuscrit est l'estimation de la pression et du débit de l'influx du réservoir en temps réel, pendant des opérations de type MPD. Nous avons étudié des influx de gaz et de liquide depuis la formation poreuse et les dynamiques mono- et diphasique qui en résultent dans le puits.

Les solutions proposées sont basées sur des modèles qui prennent en compte la nature distribuée de la dynamique, à la fois dans le réservoir et le puits. Les modèles distribués ont fait l'objet de nombreuses publications en ce qui concerne la dynamique du puits [4], [9], [72]. Une contribution originale de ce manuscrit est la conception d'un schéma numérique adpaté à deux aspects particulièrement importants en MPD: la géométrie variable des conduits, ainsi que le traitement des conditions frontières. Une mauvaise prise en compte des variations de la surface de la section du puits peut conduire à de grandes erreurs d'estimation de la pression de fonds, qui est une variable clé de ce procédé. Par ailleurs, les conditions frontières ont un rôle prédominant dans la dynamique des systèmes de MPD, ne serait-ce qu'à la frontière correspondant à la position de l'actionneur, à savoir la vanne de régulation. Des améliorations de ce modèle sont encore possible, sans porter atteinte à la structure du modèle ni à son schéma de résolution numérique. En particulier, l'implémentation d'une loi de glissement permettant la transition entre écoulement mono- et diphasique, telle que celles de [72], [98], pourrait faire l'objet de contributions futures. De manière importante, les modifications futures du modèle peuvent être rapidement transféré vers le partenaire industriel grâce à l'intégration du modèle dans le cadre de développement de Kelda Drilling Controls.

L'étude des phénomènes de diffusion transitoires dans la région du réservoir proche du puits est une contribution originale de ce manuscrit. Un modèle, basé sur de simples équations de conservation et la loi de Darcy est décrit, ainsi qu'un schéma numérique permettant d'en calculer les solutions. La comparaison avec l'état-de-l'art des modèles utilisés pour la caractérisation de réservoirs montre d'importantes différences pendant les transitoires, qui peuvent être prédominants dans les opérations de MPD. Malgré la compressibilité a priori beaucoup plus importante du gaz par rapport au liquide, les simulations numériques présentées ici ne semblent pas conclure à un comportement hautement non-linéaire dans aucun des cas. Ce point mérite d'être examiné en plus de détails, mais il est encourageant quant à l'utilisation des observateurs synthétisés dans les Chapitres 3–5, et qui se basent sur des modèles linéaires du réservoir. Les améliorations à apporter au modèle du réservoir sont de multiple nature. D'une part, il est nécessaire de prendre en compte l'hétérogénéité verticale du réservoir le long de la section ouverte du puits. Cela pourrait être accompli en considérant des tranches de réservoir comme dans [10], [39] ou une équation de diffusion à deux dimensions d'espace, comme suggéré dans [13]. D'autre part, il y a la nécessité de mettre au point un modèle couplé gaz-liquide de l'influx.

Afin d'estimer le débit entrant de liquide depuis le réservoir, et son impact sur la dynamique du puits, nous nous sommes appuyés sur des avancées récentes en synthèse d'observateurs pour les systèmes linéaires de dimension infinie et, en particulier, la méthode du backstepping. Nos contributions se reposent majoritairement sur des mesures de

surface. Nous avons considéré différentes combinaisons de modèles distribués ou agrégés, à la fois pour le réservoir et le puits.

Quand une simple relation de type CTRS est considéré avec la dynamique distribuée du puits, il en résulte un phénomène de transport dans le puits avec un coefficient frontière de réfection des ondes temps-variant. Nous avons proposé un observateur consistant en une copie du système augmentée par des termes d'injection d'erreur de sortie et des gains d'observateurs dépendant du temps. Nous montrons que la dynamique de l'erreur d'observation converge vers zéro en utilisant la méthode standard du basktepping, avec un noyau dépendant du temps.

Une autre possibilité est d'utiliser un modèle réduit pour le puits, mais de conserver la nature distribuée du réservoir. Cela mène à un résultat intéressant sur l'observabilité des systèmes couplés EDO-EDP de diffusion. En effet, l'existence d'une transformation de backstepping est équivalente, dans ce cas, à la condition d'observabilité spectrale de l'EDP à travers l'EDO : les zéros de transmission de l'EDO ne doivent pas coïncider avec les valeurs propres de l'opérateur de diffusion de l'EDP.

Enfin, quand les deux dynamiques distribuées sont retenues, nous présentons un nouvel observateur qui permet l'estimation de tous les états distribués à partir d'une seule mesure de surface. A la différence des EDO, les EDP hyperboliques couplées n'ont pas de zéros de transmission et la seule restriction de cette synthèse est la vitesse de convergence du système d'erreur. Bien que l'observateur présenté ici ne soit valable que pour deux équations hyperboliques linéaires, nous sommes convaincus qu'il pourra s'étendre, avec un nombre approprié de sorties mesurées, à un modèle d'écoulement dipahsique, c'est-à-dire à trois (ou plus) équations de transport, de manière similaire à l'extension de [96] vers [55], [99], ou de [100] vers [101]. Cette extension sera cruciale pour envisager l'estimation de dynamiques de réservoir pendant un influx de gaz, qui est de loin l'application industrielle la plus pertinente de ces recherches.

The problem under consideration in this manuscript is the estimation of the pore pressure and influx flow rate in *real-time* during MPD operations. We study both gas and liquid influxes from the formation and the resulting dynamics— single or multiphase flow— inside the wellbore.

The proposed solution relies on models taking into account the distributed nature of the dynamics, both in the reservoir and in the wellbore. Distributed models have been the topic of many contributions for dynamics inside the annulus [4], [9], [72]. An original contribution presented in this manuscript is the design of a numerical scheme handling two aspects that may have a significant impact in MPD: the variable geometry of the pipes, as well as the treatment of the boundary conditions. Failing to take into account variations in the cross-sectional area of the pipe may lead to poor estimation of BHCP, which is a crucial variable. Besides, boundary conditions have a predominant role in the dynamics of MPD systems, if only at the location of the actuator, namely the MPD choke valve. Improvements to this model can be made without modifying the structure of the model or the numerical scheme. In particular, the implementation of a slip law enabling the transition between single-phase liquid flow and two-phase flow, as in [72], [98] should be considered in future work. Importantly, modifications to the model can now be transferred to the industrial partner of the HYDRA project, thanks to the integration of the model in Kelda Drilling Control's framework.

The study of the diffusion phenomena in the near-wellbore region of the reservoir is an original contribution of this manuscript. A model, based on simple first principles and Darcy's law is described, along with an appropriate numerical scheme. The comparison with state-of-the-art models used for reservoir characterization shows

discrepancies during transients, which are likely to occur in MPD operations. Despite the much higher compressibility of gas with respect to liquid a priori, the simulations conducted for this manuscript do not exhibit highly nonlinear behavior in either case. While this point needs to be further examined, it is encouraging as the observers designed in Chapters 3–5 rely on linearized reservoir dynamics. The improvements to be made to the reservoir models are two-fold. First, their is a need to take into account the vertical inhomogeneity of the open region of the wellbore into account. This could be done by considering layers of reservoir as in [10], [39] or a two-dimensional diffusion equation as suggested in [13]. Second, a model of gas *and* liquid flow entering the wellbore should be derived.

To estimate the flow rate of liquid from the reservoir and its impact on the wellbore dynamics, we rely on recent advances in linear infinite-dimensional system observer design and, in particular, on the backstepping method. Our contributions rely solely on topside sensing. We consider various combination of distributed and simplified models for both the wellbore and the reservoir dynamics.

When a simplified CTRS relation is considered with the distributed dynamics of the wellbore, it translates in a transport phenomenon in the wellbore with a time varying reflection co-efficient. We propose an observer consisting of a copy of the system with output error injection terms and time-varying observer gains. The observer error dynamics are proved to converge to zero using a standard backstepping tool – a Volterra transformation mapping it to a stable target system, with a time-varying kernel.

Another option is to use a reduced-order model for the wellbore, but to retain the distributed nature of the reservoir pressure dynamics. This leads to an interesting result on the observability of coupled diffusion PDE-ODE systems. Indeed, the existence of a backstepping transformation is, in that case, equivalent to the spectral observability of the PDE through the ODE's dynamics: the transmission zeros of the ODE must not lie on eigenvalues of the PDE diffusion operator.

Finally, when both the distributed dynamics of the wellbore and observer are considered, we present a novel design enabling estimation of all distributed states with a single topside measurement. Contrary to ODEs, coupled hyperbolic PDEs have no transmission zeros and the only restriction in the design lies in the convergence speed of the error system. While the presented design only works for two linear hyperbolic PDEs representing the wellbore dynamics, we strongly believe that it will extend, with an appropriate number of measurements, to a model of two-phase flow, i.e. to three (or more) transport PDEs, similarly to the extension of [96] to [55], [99] or [100] to [101]. This extension will be crucial to envision estimation of reservoir dynamics during a gas kick, which is by far the most relevant industrial application.

Appendix A

Kelda software development test framework

Une partie importante du projet HYDRA a consisté à intégrer le simulateur diphasique dans l'architecture de développement logicielle de Kelda. Dans ce chapitre, nous présentons les détails de cette intégration. Nous décrivons la terminologie en développement logiciel. Kelda oriente son effort de développement sur un environnement basé sur les tests fréquents, afin d'assurer que de nouvelles fonctionnalités ne perturbent pas le produit existant.

An integral part of the HYDRA project is to integrate the simulator into the Kelda's software development test framework. In this chapter, we present the details and the efforts taken thus far towards the integration. We first introduce the terminologies in software development. Test-driven development (TDD) is a focus at Kelda to develop their products. This ensures that adding new features to the existing product does not hamper the current product.

A.1 Test automation

A.1.1 Software testing

Test automation can automate some repetitive, but necessary tasks, in a formalized testing process already in place, or perform additional testing that would be difficult to do manually. Test automation is critical for continuous delivery and continuous testing, where the software development team works in short cycles so the software can be released any time. Generally, the two types of test automation are

- Graphical user interface (GUI) testing, where the operator can test the software with the use of arrows and mouse clicks, offering an easier interface to communicate with the software functionalities,
- API driven testing, usually bypasses the user interface and uses a programming interface to the application to validate the behaviour under test.

A growing trend in software development is the use of what is called as unit tests that allow the execution to determine whether various sections of the code are acting as expected under different circumstances. Test cases describe the tests that need to be run on the program.

Test automation, mostly using unit testing, is a key feature of extreme programming and agile software development, and is known as test-driven development (TDD) or test-first development. Unit tests are written to define the functionality before the code is written and usually the program fails the tests in the beginning of the development cycle. However, these unit tests and the products evolve and

are extended as coding progresses, issues are discovered and the code is subjected to refactoring. Only when all the tests for all the demanded features pass, the code is considered complete. An assert statement is an integral part of the TDD, which is a statement that checks if a certain condition is met. If the condition of the assert statement is not met, the test is considered as a failure. To understand the test framework, the reader is introduced to certain features of the object oriented programming (OOP) in the following section.

A.2 Object oriented programming

Object-oriented programming (OOP) is a programming paradigm based on the concept of 'objects', which can contain data, in the form of fields (often known as attributes), and code, in the form of procedures (often known as methods). In OOP, computer programs are designed by making them consist of objects that interact with one another. OOP languages are diverse but are class-based, meaning objects are instances of classes, which also determine their types.

A.2.1 Class and objects

Programming languages that support OOP typically use inheritance for code reuse and extendability in the form of class and objects:

- Class is the definition of the data format of the variables, and the functions that are defined for the class variables.
- Object is an instance of a class. In other words, when an object of a class is defined, it incorporates the attributes (variables) and methods (functions) of the definition class. For example, apple and orange can be considered as objects of the class fruits.

A.2.2 Encapsulation

Data encapsulation is an important feature of OOP, in which the accessibility to the data within the class is clearly defined. This allows the data to be secured and not altered from outside the definition of the class. Three encapsulation features available in OOP are *private*, where the data can be accessed only within that class, *protected*, where the data can be accessed within that class and the subclass and *public* which provides global access to the defined variables. Subclass is a class that is one step below in hierarchy to the master class (in C++, an OOP language), which by definition inherits all the attributes and methods that are defined as *protected.* We now present the framework maintained at Kelda.

A.2.3 Kelda test framework

Since MPD operations are safety critical in nature, a robust framework to test the control system is necessary. When an MPD control system is developed there are typically three main phases of development and testing from design to field operation as illustrated in Figure A.1. First, in the design phase frequent iterations and tests based on the design models are performed.

The second phase is the verification phase. In this step, the MPD system is tested on a software platform, called as software in the loop (SIL). This phase could include tests performed in a flow loop setup, i.e., an emulated well with real hardware and

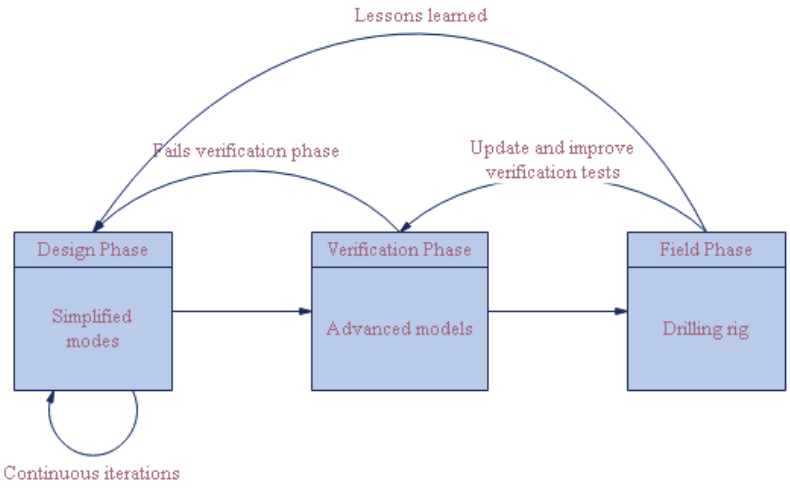

FIGURE A.1: Schematic of different test phases of software product development.

piping, which is known as hardware in the loop (HIL). In general, flow loop tests are performed prior to the first fielding of the MPD system, but not necessarily in subsequent upgrades. The advantage of the flow loop test is that the hardware and software are tested and verified together. If the MPD system fails the verification, it is necessary to go back to the design phase.

Third, if the verification phase is passed, the MPD control is ready for field operations. Prior to drilling, the MPD system is typically run through a set of site acceptance tests (SAT) in cased hole. The industrial scenarios presented in this manuscript are based on common SAT tests performed in the field. The lessons learned from the operation are used as input to the next round of the design phase and to improve and extend the test scenarios in the verification phase.

A.2.4 Unit tests: Straume®

Straume® is a hydraulics simulation software commercialized by Kelda for MPD applications. We present the test framework used for the development of Straume®. A schematic of the definition of classes and the inheritance of the properties and methods of the classes to subclasses and objects are represented in the Figure A.2. Kelda uses *Matlab.System* (a base class for system objects, available in MATLAB) to interface external models and make them available directly in Simulink. Simulink uses a feature called *code generation* that makes the simulation using the external model efficient, by compiling the code into an executable file in the C language. The test framework can be understood using the following points:

- The Simulink model and the corresponding source code (which is the MATLAB script equivalent to the Simulink block) are named *StraumeCore*. The standard syntax of this source code contains the methods (functions in class) initialize, step and reset, to define the initialization, computation for one timestep and to reset the simulation correspondingly. Fluid and well configurations are considered as the input attributes for this source code.

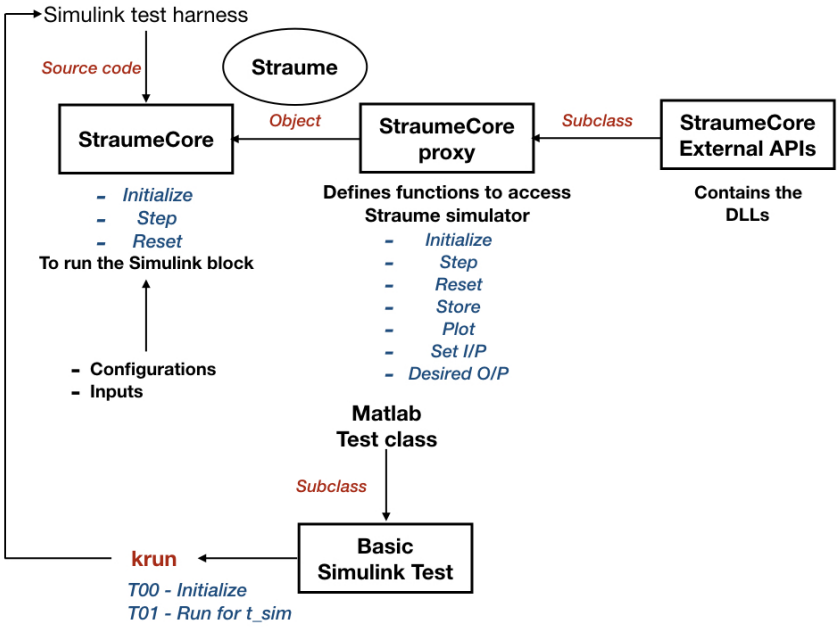

FIGURE A.2: Schematic of the test framework developed for Straume ®.

- For computational efficiency and compartmentalization of the product developement, Kelda uses dynamically loading libraries (DLLs). DLLs are precompiled executable files that can be shared between libraries of different programming languages. As the name goes, DLLs are dynamically loaded when they are called within a function. All the DLLs are defined in the class *StraumeCore External APIs*.

- The class *StraumeCore proxy* is a subclass of the class *StraumeCore External APIs*. This allows *StraumeCore proxy* to access all the DLLs and contains the methods for execution of Staume®, thus providing a clean interface to the DLLs.

- *Straume* is an object of *StraumeCore proxy* that is used within the source code *StraumeCore*. Since an object is a copy/ an instance of the class, unit tests are run using the object *Straume* to check the functionalities and execution of the features added to product, as DLLs.

- The unit tests are defined in the class *Basic Simulink Test*, which is itself a subclass of the global class *Matlab Test class* defined within MATLAB. This allows *Basic Simulink Test* to benefit from the additional features that may be defined within MATLAB.

- *krun* is the command with a particular syntax that makes it possible to filter tests before they are executed, so as to not run all the tests all the time. The unit tests are defined in the form T** [1] to create the object *Straume* and execute the corresponding test.

[1] **:=01,02,...

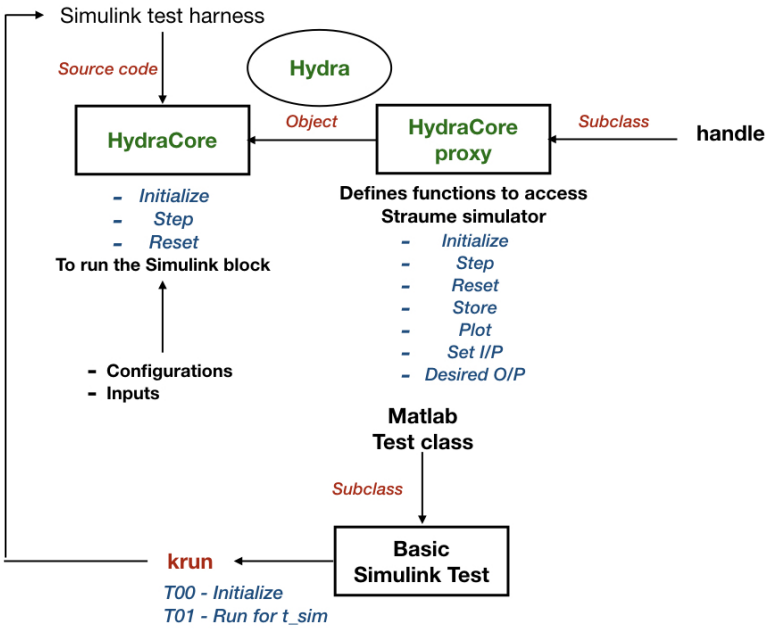

FIGURE A.3: Schematic of integrating HYDRA model into the Kelda's test framework.

A.2.5 Unit tests: HYDRA model

We now present the modifications necessary to integrate the HYDRA model into the framework. By doing so, the user can switch between the simulators Straume® and HYDRA model to test any feature that can be added to these products. Such integration also helps in testing other products such as the controller Leidar® as developed by Kelda. By defining the key performance indicators (KPIs) for the controller performance, measures to benchmark control performance can be made available to the industry. This is of particular interest in the drilling community due to the lack of such benchmarking measures for the safety critical operations. Referring to the Figure A.3, we present the following modifications

- The source code and the Simulink block are named as *HydraCore*. Computations within as defined as functions, which eliminates the need to compile the DLLs. Thus, *StraumeCore External APIs* are replaced by the global class defined in MATLAB called *handle*.
- *HydraCore proxy* contains the scripts that run the functions defined for the HYDRA model.
- An object called *Hydra* is defined as an instance of the above mentioned classes.
- Pre-defined unit tests by Kelda can now be used to check the functionalities of the HYDRA model using the object *Hydra*.

A.3 Test case

The unit test discussed in this report is to compare the performance of the simulators to the change of pump flow while maintaining a constant choke opening. The

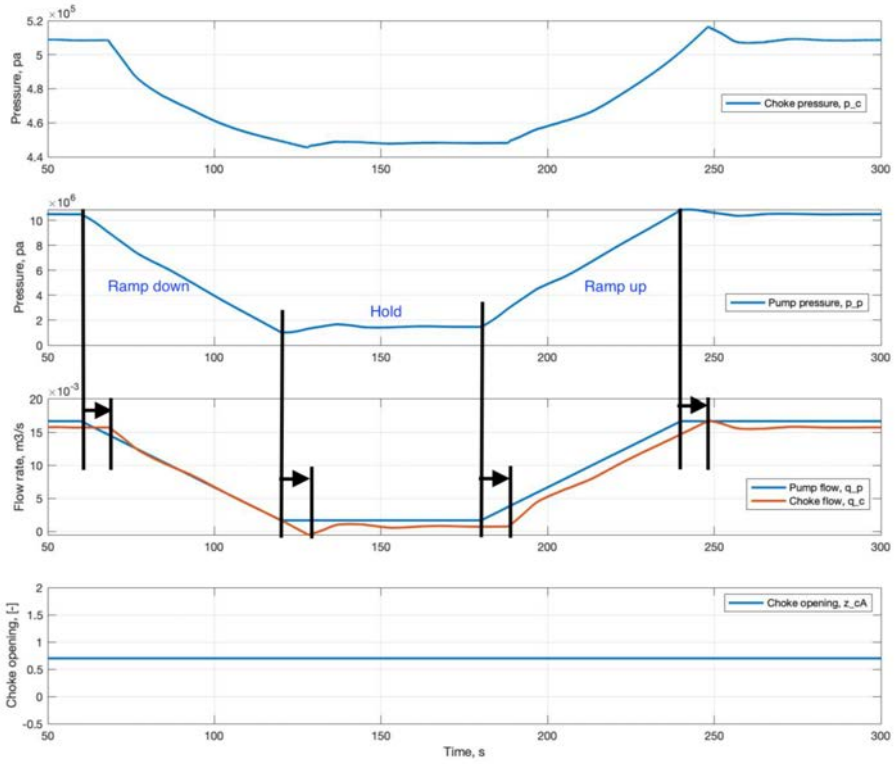

FIGURE A.4: Plot of the unit test to study the effect of flow changes in the HYDRA model.

scenario described in this unit test is similar to connections, a regular operation used to connect/ disconnect a drillpipe into/ from the drillstring.

Here, the flow from the mud pump is ramped down slowly and maintained constant for a certain period before ramping back up to the operational flow. This is done while maintaining a constant choke opening. A point to note is that the choke actuator dynamics is considered differently in both the simulators.

For a given pump flow that is ramped-down and -up, the corresponding flow at the choke is shown in Figure A.4. It can be noted that the effect at the choke, due to the flow variation at the pump is delayed by a few seconds, which is due to the consideration of distributed pressure dynamics in the simulators. The responses from both the simulators are similar for the considered unit test while the reasoning for the noticeable discrepancies are as follows.

Conclusions It can be concluded that the HYDRA model has been successfully integrated in the Kelda's test framework developed for Straume®. This will allow the operator to test controllers (Leidar®) and observers for their performances with respect to two different simulators - the commercial product Straume®, which is developed with the goal of being computationally efficient and effective for control objectives; and HYDRA model that is developed by the ESRs within the project HYDRA which considers the distributed pressure dynamics within the wellbore during multiphase fluid flows.

This integration of the HYDRA model into the test framework is considered as an upgrade to Straume® since the results from HYDRA model will provide a better

understanding of the distributed dynamics that may be lost in the bargain of computation efficiency and cost in Straume®. This fact is more pronounced in the scenarios that contain multiphase fluid flows, which is beyond the scope of this manuscript. This integration will also allow the operator to switch between these two simulator as and when required depending on the operational conditions.

Appendix B

Controller testing

Ce chapitre décrit le contrôleur qui forme la base du logiciel Leidar®. Le modèle d'écoulement du Chapitre 1 est utilisé pour tester la performance de ce contrôleur.

This chapter introduces the model-based controller that forms the basis of Leidar®. The distributed flow model that was introduced in Chapter 1 has been used to test the controller performance.

B.1 Model-based control

The commercial product Leidar® at our industrial partner Kelda is a model-based controller. Leidar®, that runs the design model [36] to estimate the BHCP has proven success in numerous field operations around the world. A basic model-based control law for the choke pressure as in [12] can be expressed as

$$q_{c,r} = \frac{V}{\beta} c_1 e + q_p, \tag{B.1}$$

where $q_{c,r}$ is the desired flow through the choke, c_1 the proportional control gain and e the pressure error given by $e = p_{sp} - p_c$, and p_{sp} the desired choke set point. The corresponding choke opening Z_c for a given flow through the choke is found by inverting the choke equation that reads

$$q_c = K_c Z_c \sqrt{\frac{2}{\rho}(p_c - p_{ds})}, \tag{B.2}$$

where K_c is the choke characteristics and p_{ds} the pressure downstream the choke valve. Using an adaptive model-based controller [12], the effective bulk modulus of the system is estimated using real-time pressure and flow measurements. This improves the performance of such controller as opposed to a non-adaptive controller.

B.2 Test Framework

As a first step towards the upgrading and testing of Leidar®, the HYDRA model was integrated into the test framework (for scenario simulations) that was developed at Kelda. This was part of the HYDRA Deliverable D4.1 As a result, the HYDRA model also provides an additional option to evaluate and verify the performance of Leidar controller and Leidar estimators. This is shown as a schematic in Figure B.1. The test framework is setup in a way that the user can choose as a *virtual rig* (that is considered as the dynamic during real-life operation by the controller) from the

simplified design model, the commercial product for multiphase fluid simulation Straume® and the academically developed HYDRA model to be used by Leidar® to track the required setpoint, e.g., for the BHCP or choke pressure.

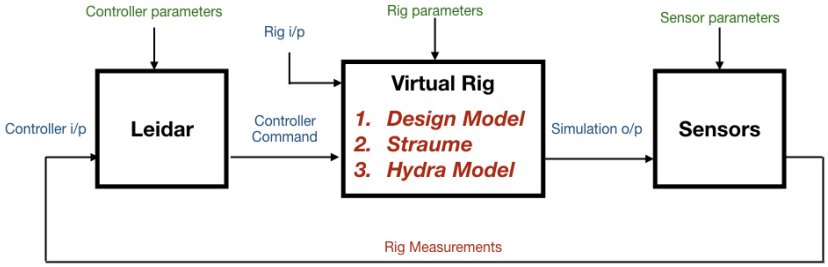

FIGURE B.1: Schematic of the framework for controller performance testing.

B.3 Result

To understand the performance of Leidar®, an user test has been set up to run the controller using the design model and the HYDRA model. Configurations for wellbore, fluid and choke shared in confidence by Kelda have been used. The operating conditions have been set for a pump flow of 1000 lpm[1] and a surface backpressure of 25 *bar* to circulate off-bottom, that is to not drill ahead but to circulate fluid along the given flow path. The controller is run to maintain the surface backpressure at the choke by varying the opening of the choke valve, to track a given reference pressure. The snapshot of the simulation result is depicted in Figure B.2.

[1] litres per minute

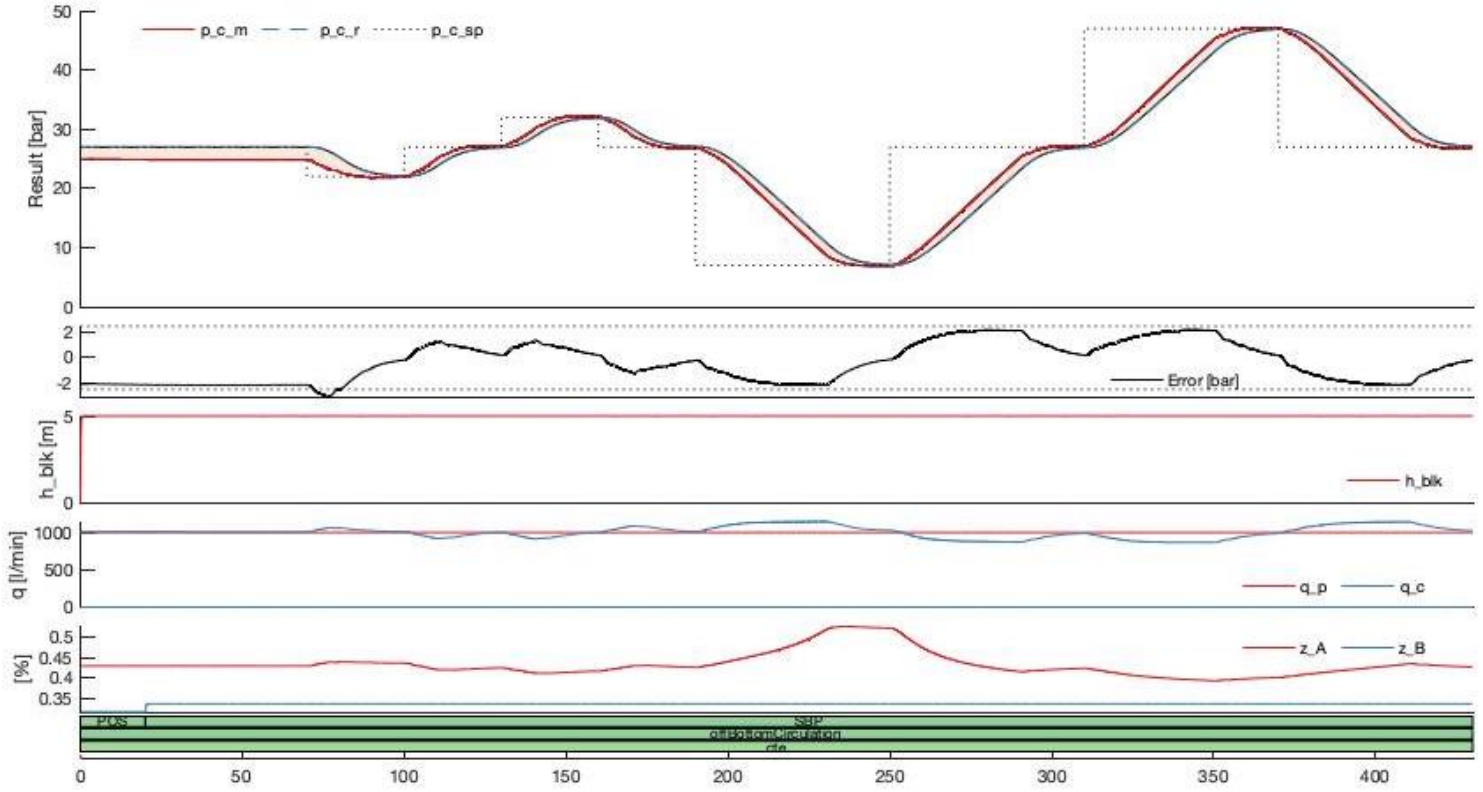

FIGURE B.2: Controller performance with HYDRA model for an user test. The subplots, in the same order of occurrence are - measured, reference and set-point pressure at the choke; error between the reference and measured choke pressure from the virtual rig; height of the travelling block in the virtual rig; flow rates at the pump and choke; % opening of the chokes A and B; the legends, POS for the position mode of the controller, followed by the user test scenario - circulating off-bottom.

It can be noted that choke pressure obtained from the HYDRA model deviates from the +/- 2 *bar* error range during the rapid ramp- ups and downs of the controller setpoint. Such occurrence can be attributed to the distributed momentum of the fluid along the wellbore. The HYDRA model reveals different closed-loop performance which confirms the need for controller testing with a distributed model such as the HYDRA model. A part of the difference arises from the absence of actuator (i.e., the choke) dynamics in the HYDRA model. A smoother tracking of the reference choke pressure in the HYDRA model can be attributed to the presence of distributed pressure dynamics throughout the flow path. In contrast, the design model uses the ODE formulation of the dynamics that assumes any effect to be seen across the flow path *immediately.* Such comparisons are also presented in [53].

Conclusions It can be concluded that the HYDRA model has been successfully integrated into the Kelda's controller test framework. This will allow the user to test Kelda's controller (Leidar®) for its performance with respect to two different simulators - simplified design model, the commercial product Straume®, which is developed with the goal of being computationally efficient and effective for control objectives; and HYDRA model that is developed by the ESRs within the project HYDRA which considers the distributed pressure dynamics within the wellbore during multi-phase fluid flows.

This integration of the HYDRA model into the controller test framework is considered as an upgrade to Leidar® test framework, and will thus be a part of future controller improvements pursued by Kelda. It is observed that the simplified model and efficient implementation of the control algorithm can be sufficient to handle different dynamics that arise in the real-life operations, that are captured in the distributed models mentioned in this manuscript. This has been tested to be true in the real-life drilling operations in various drilling rigs across the world by Kelda. The user can now have an additional simulator to run with Leidar® to test its performance. This will lead to creation of various industry standard benchmark scenarios, which is the focus of future work.

Embedding HYDRA model in the Straume® and Leidar® software packages of Kelda secures the technology transfer of the results of the HYDRA project to the company.

Appendix C

Block canonical form

We refer to the system described by Equation (4.78) and define a transformation for the states that reads

$$\widetilde{z}(t) = T_o^{-1}\widetilde{x}(t) \tag{C.1}$$

and choose a particular transformation matrix such that

$$\begin{bmatrix} \widetilde{z}_1 \\ \widetilde{z}_2 \\ \widetilde{z}_3 \end{bmatrix} = \begin{bmatrix} 1 & 0 & 0 \\ 0 & 1 & 0 \\ 0 & -a_3 & a_1 \end{bmatrix} \begin{bmatrix} \widetilde{x}_1 \\ \widetilde{x}_2 \\ \widetilde{x}_3 \end{bmatrix}. \tag{C.2}$$

Now the system (4.78) can be written as

$$\begin{bmatrix} \dot{\widetilde{z}}_1 \\ \dot{\widetilde{z}}_2 \\ \dot{\widetilde{z}}_3 \end{bmatrix} = \begin{bmatrix} a_0 & 0 & 0 \\ 0 & a_3 & 1 \\ 0 & a_1 a_2 & 0 \end{bmatrix} \begin{bmatrix} \widetilde{z}_1 \\ \widetilde{z}_2 \\ \widetilde{z}_3 \end{bmatrix} + \begin{bmatrix} b_0 \\ 0 \\ a_1 b_2 \end{bmatrix} \widetilde{p}(r_w, t) \tag{C.3}$$

that satisfies the block canonical form for the system in $z(t)$ and the following transformations

$$T_o A_o = A T_0, \qquad T_0 B_o = B, \qquad C_o = C T_o \quad . \tag{C.4}$$

Bibliography

[1] J. J. Azar and G. R. Samuel, *Drilling engineering*. PennWell books, 2007.

[2] C. Berg, G. A. Evjen, N. Velmurugan, and M. Culen, "The influx-management envelope considering real-fluid behavior", *SPE Drilling & Completion*, 2019.

[3] B. Rehm, J. Schubert, A. Haghshenas, A. S. Paknejad, and J. Hughes, *Managed pressure drilling*. Elsevier, 2013.

[4] U. J. F. Aarsnes, "Modeling of two-phase flow for estimation and control of drilling operations", PhD thesis, 2016.

[5] J. D. Macpherson, J. P. de Wardt, F. Florence, C. Chapman, M. Zamora, M. Laing, and F. Iversen, "Drilling-systems automation: Current state, initiatives, and potential impact", *SPE Drilling & Completion*, vol. 28, no. 04, pp. 296–308, 2013.

[6] E. Cayeux, B. Daireaux, E. W. Dvergsnes, and F. Florence, "Toward drilling automation: On the necessity of using sensors that relate to physical models", *SPE Drilling & Completion*, vol. 29, no. 02, pp. 236–255, 2014.

[7] J. Thorogood, W. D. Aldred, F. Florence, and F. Iversen, "Drilling automation: Technologies, terminology, and parallels with other industries", *SPE drilling & completion*, vol. 25, no. 04, pp. 419–425, 2010.

[8] E. Hauge, Ø. Nistad Stamnes, O. M. Aamo, and J.-M. Godhavn, "A dynamic model of percolating gas in a wellbore", *SPE Drilling & Completion*, vol. 27, no. 02, pp. 204–215, 2012.

[9] G. H. Nygaard, E. H. Vefring, K. K. Fjelde, G. Nævdal, R. J. Lorentzen, and S. Mylvaganam, "Bottomhole pressure control during drilling operations in gas-dominant wells", *SPE Journal*, vol. 12, no. 01, pp. 49–61, 2007.

[10] G. Nygaard and G. Nævdal, "Nonlinear model predictive control scheme for stabilizing annulus pressure during oil well drilling", *Journal of Process Control*, vol. 16, no. 7, pp. 719–732, 2006.

[11] C. Berg, J. Å. Stakvik, S. Kulikov, M. Badrawi, G.-O. Kaasa, A. Dubovtsev, S. Korolev, and G. Veliyev, "Automated pressure control for UBD operations: Case study and field validation", *SPE Drilling & Completion*, 2019.

[12] J. Å. Stakvik, C. Berg, G.-O. Kaasa, O. M. Aamo, and U. Lehner, "Adaptive model based choke control system for MPD operations", in *SPE/IADC Managed Pressure Drilling and Underbalanced Operations Conference and Exhibition*, Society of Petroleum Engineers, 2016.

[13] L. P. Dake, *Fundamentals of reservoir engineering*. Elsevier, 1983.

[14] G. Da Prat, *Well test analysis for fractured reservoir evaluation*. Elsevier, 1990.

[15] B. Rehm, A. Haghshenas, A. S. Paknejad, A. Al-Yami, and J. Hughes, *Underbalanced drilling: limits and extremes*. Elsevier, 2013.

[16] P. L. O'Bryan and A. T. Bourgoyne Jr, "Swelling of oil-base drilling fluids due to dissolved gas", in *SPE Annual Technical Conference and Exhibition*, Society of Petroleum Engineers, 1987.

[17] P. L. O'Bryan and A. T. Bourgoyne, "Methods for handling drilled gas in oil-based drilling fluids", *SPE drilling engineering*, vol. 4, no. 03, pp. 237–246, 1989.

[18] R. D. Grace and J. L. Shursen, "Field examples of gas migration rates", in *IADC/SPE drilling conference*, Society of Petroleum Engineers, 1996.

[19] U. J. F. Aarsnes, E. Hauge, and J.-M. Godhavn, "Mathematical modeling of gas in riser", in *SPE Deepwater Drilling and Completions Conference*, Society of Petroleum Engineers, 2016.

[20] A. B. Johnson and D. B. White, "Gas-rise velocities during kicks", *SPE drilling engineering*, vol. 6, no. 04, pp. 257–263, 1991.

[21] M. F. Jerez-Carrizales, J. E. Jaramillo, and D. A. Fuentes, "Simulation of the two phase flow in a wellbore using two-fluid model", in *11th World Congress on Computational Mechanics*, 2014.

[22] H. Linga, A. Torsvik, and A. Saasen, "Kick detection capability of oil-based muds in well control situations", in *SPE Bergen One Day Seminar*, Society of Petroleum Engineers, 2016.

[23] H. V. Nickens, "A dynamic computer model of a kicking well", *SPE Drilling engineering*, vol. 2, no. 02, pp. 159–173, 1987.

[24] H. V. Nickens, "A dynamic computer model of a kicking well: Part II - model predictions and conclusions", in *SPE Annual Technical Conference and Exhibition*, Society of Petroleum Engineers, 1985.

[25] A. L. Podio and A.-P. Yang, "Well control simulator for IBM personal computer", in *SPE/IADC Drilling Conference*, Society of Petroleum Engineers, 1986.

[26] R. Rommetveit and E. H. Vefring, "Comparison of results from an advanced gas kick simulator with surface and downhole data from full scale gas kick experiments in an inclined well", in *SPE Annual Technical Conference and Exhibition*, Society of Petroleum Engineers, 1991.

[27] R. Rommetveit and A. C. V. M. Lage, "Designing underbalanced and lightweight drilling operations; recent technology developments and field applications", in *SPE Latin American and Caribbean Petroleum Engineering Conference*, Society of Petroleum Engineers, 2001.

[28] E. H. Vefring, Z. Wang, S. Gaard, and G. F. Bach, "An advanced kick simulator for high angle and horizontal wells - Part I", in *SPE/IADC Drilling Conference*, Society of Petroleum Engineers, 1995.

[29] H. M. Santos, E. Catak, J. I. Kinder, and P. Sonnemann, "Kick detection and control in oil-based mud: Real well test results using micro-flux control equipment", in *SPE/IADC Drilling Conference*, Society of Petroleum Engineers, 2007.

[30] J. A. Tarvin, I Walton, P Wand, and D. B. White, "Analysis of a gas kick taken in a deep well drilled with oil-based mud", in *SPE Annual Technical Conference and Exhibition*, Society of Petroleum Engineers, 1991.

[31] J. A. Tarvin, "Gas rises rapidly through drilling mud", in *SPE/IADC Drilling Conference*, Society of Petroleum Engineers, 1994.

[32] D. C. Thomas, J. F. Lea Jr, and E. A. Turek, "Gas solubility in oil-based drilling fluids: Effects on kick detection", *Journal of petroleum technology*, vol. 36, no. 06, pp. 959–968, 1984.

[33] F. Di Meglio, "Dynamics and control of slugging in oil production", PhD thesis, 2011.

[34] E. Hauge, "Automatic kick detection and handling in managed pressure drilling systems", PhD thesis, 2013.

[35] E. Cayeux, B. Daireaux, E. Dvergsnes, A. Leulseged, B. Bruun, and M. Herbert, "Advanced drilling simulation environment for testing new drilling automation techniques and practices", *SPE Drilling & Completion*, vol. 27, no. 04, pp. 559–573, 2012.

[36] G.-O. Kaasa, Ø. N. Stamnes, O. M. Aamo, and L. S. Imsland, "Simplified hydraulics model used for intelligent estimation of downhole pressure for a managed-pressure-drilling control system", *SPE Drilling & Completion*, vol. 27, no. 01, pp. 127–138, 2012.

[37] W. Kneissl, "Reservoir characterization whilst underbalanced drilling", in *SPE/ IADC drilling conference*, Society of Petroleum Engineers, 2001.

[38] J. L. Hunt and S. Rester, "Reservoir characterization during underbalanced drilling: A new model", in *SPE/CERI Gas Technology Symposium*, Society of Petroleum Engineers, 2000.

[39] J. L. Hunt and S. Rester, "Multilayer reservoir model enables more complete reservoir characterization during underbalanced drilling", in *IADC/SPE Underbalanced Technology Conference and Exhibition*, Society of Petroleum Engineers, 2003.

[40] X. Kong, Y. Lin, Y. Qiu, H. Zhu, L. Dong, and Y. Chen, "A new model for predicting dynamic surge pressure in gas and drilling mud two-phase flow during tripping operations", *Mathematical Problems in Engineering*, vol. 2014, 2014.

[41] A. Van Everdingen and W. Hurst, "The application of the laplace transformation to flow problems in reservoirs", *Journal of Petroleum Technology*, vol. 1, no. 12, pp. 305–324, 1949.

[42] H. Cinco L, F Samaniego V, and N Dominguez A, "Transient pressure behavior for a well with a finite-conductivity vertical fracture", *Society of Petroleum Engineers Journal*, vol. 18, no. 04, pp. 253–264, 1978.

[43] A. C. Gringarten and H. J. Ramey Jr, "The use of source and Green's functions in solving unsteady-flow problems in reservoirs", *Society of Petroleum Engineers Journal*, vol. 13, no. 05, pp. 285–296, 1973.

[44] K. H. Guppy, H Cinco-Ley, and H. J. Ramey Jr, "Non-Darcy flow in wells with finite-conductivity vertical fractures", *Society of Petroleum Engineers Journal*, vol. 22, no. 05, pp. 681–698, 1982.

[45] G. Li, H. Li, Y. Meng, N. Wei, C. Xu, L. Zhu, and H. Tang, "Reservoir characterization during underbalanced drilling of horizontal wells based on real-time data monitoring", *Journal of Applied Mathematics*, vol. 2014, 2014.

[46] L. Larsen and F. Nilsen, "Inflow predictions and testing while underbalanced drilling", in *SPE Annual Technical Conference and Exhibition*, Society of Petroleum Engineers, 1999.

[47] S. Moi, L. A. Carlsen, H. J. Skadsem, A. Islam, and O. A. Helstrup, "Nonlinear regression analysis and system stiffness approach for formation integrity test interpretation", in *SPE/IADC Drilling Conference and Exhibition*, Society of Petroleum Engineers, 2017.

[48] E. H. Vefring, G. H. Nygaard, R. J. Lorentzen, G. Naevdal, and K. K. Fjelde, "Reservoir characterization during underbalanced drilling (UBD): Methodology and active tests", *SPE Journal*, vol. 11, no. 02, pp. 181–192, 2006.

[49] J. E. Gravdal, M. Nikolaou, Ø. Breyholtz, and L. A. Carlsen, "Improved kick management during MPD by real-time pore-pressure estimation", *SPE Drilling & Completion*, vol. 25, no. 04, pp. 577–584, 2010.

[50] A. Ambrus, U. J. F. Aarsnes, A. K. Vajargah, B. Akbari, E. van Oort, and O. M. Aamo, "Real-time estimation of reservoir influx rate and pore pressure using a simplified transient two-phase flow model", *Journal of Natural Gas Science and Engineering*, vol. 32, pp. 439–452, 2016.

[51] J. Auriol, K. A. Morris, and F. Di Meglio, "Late-lumping backstepping control of partial differential equations", *Automatica*, vol. 100, pp. 247–259, 2019.

[52] M. Abbasi, S. N. Lordejani, N. Velmurugan, C Berg, L. Iapichino, W. Schilders, and N. van de Wouw, "A godunov-type scheme for the drift flux model with variable cross section", *Journal of Petroleum Science and Engineering*, vol. 179, pp. 796–813, 2019.

[53] S. Naderi Lordejani, M. H. Abbasi, N. Velmurugan, C. Berg, J. Å. Stakvik, B. Besselink, L. Iapichino, F. Di Meglio, W. H. Schilders, and N. van de Wouw, "Modeling and numerical implementation of managed-pressure-drilling systems for the assessment of pressure-control systems", *SPE Drilling & Completion*, 2020.

[54] A. Deutschmann, L. Jadachowski, and A. Kugi, "Backstepping-based boundary observer for a class of time-varying linear hyperbolic PIDEs", *Automatica*, vol. 68, pp. 369–377, 2016.

[55] F. Di Meglio, R. Vazquez, and M. Krstic, "Stabilization of a system of $n+1$ coupled first-order hyperbolic linear PDEs with a single boundary input", *IEEE Transactions on Automatic Control*, vol. 58, no. 12, pp. 3097–3111, 2013.

[56] L. Camacho-Solorio, N. Velmurugan, F. Di Meglio, and M. Krstic, "Observer design for a coupled ODE-PDE system from a wellbore reservoir drilling model", in *2019 IEEE 58th Conference on Decision and Control (CDC)*, IEEE, 2019, pp. 3086–3091.

[57] N. Velmurugan and F. Di Meglio, "Transient modelling of influx and observer implementation for estimation while drilling", in *2018 IEEE Conference on Decision and Control (CDC)*, IEEE, 2018, pp. 2623–2628.

[58] N. Zuber and J. A. Findlay, "Average volumetric concentration in two-phase flow systems", 1965.

[59] M. Ishii and T. Hibiki, "One-dimensional drift-flux model", in *Thermo-Fluid Dynamics of Two-Phase Flow*, Springer, 2011, pp. 397–436.

[60] R. Pompilio, "Experimental analysis of air water two phase flow in vertical large pipes and development of drift flux models", 2014.

[61] S. M. Bhagwat and A. J. Ghajar, "A flow pattern independent drift flux model based void fraction correlation for a wide range of gas–liquid two phase flow", *International Journal of Multiphase Flow*, vol. 59, pp. 186–205, 2014.

[62] F. Di Meglio, G.-O. Kaasa, N. Petit, and V. Alstad, "Slugging in multiphase flow as a mixed initial-boundary value problem for a quasilinear hyperbolic system", in *Proceedings of the 2011 American Control Conference*, IEEE, 2011, pp. 3589–3596.

[63] T. Reed and A. Pilehvari, "A new model for laminar, transitional, and turbulent flow of drilling muds", in *SPE Production Operations Symposium*, Society of Petroleum Engineers, 1993.

[64] K. K. Fjelde and K. H. Karlsen, "High-resolution hybrid primitive–conservative upwind schemes for the drift flux model", *Computers & fluids*, vol. 31, no. 3, pp. 335–367, 2002.

[65] R. Courant, K. Friedrichs, and H. Lewy, "On the partial difference equations of mathematical physics", *IBM journal of Research and Development*, vol. 11, no. 2, pp. 215–234, 1967.

[66] R. J. LeVeque, *Finite volume methods for hyperbolic problems*. Cambridge university press, 2002, vol. 31.

[67] B. Van Leer, "Towards the ultimate conservative difference scheme", *Journal of Computational Physics*, vol. 135, no. 2, pp. 229–248, 1997.

[68] T. Flåtten and S. T. Munkejord, "The approximate Riemann solver of Roe applied to a drift-flux two-phase flow model", *ESAIM: Mathematical Modelling and Numerical Analysis*, vol. 40, no. 4, pp. 735–764, 2006.

[69] D. H. Cuong and M. D. Thanh, "A godunov-type scheme for the isentropic model of a fluid flow in a nozzle with variable cross-section", *Applied Mathematics and Computation*, vol. 256, pp. 602–629, 2015.

[70] D. Kröner and M. D. Thanh, "Numerical solutions to compressible flows in a nozzle with variable cross-section", *SIAM Journal on Numerical Analysis*, vol. 43, no. 2, pp. 796–824, 2005.

[71] J. E. Udegbunam, K. K. Fjelde, S. Evje, and G. Nygaard, "On the advection-upstream-splitting-method hybrid scheme: A simple transient-flow model for managed-pressure-drilling and underbalanced-drilling applications", *SPE Drilling & Completion*, vol. 30, no. 02, pp. 98–109, 2015.

[72] S. Evje and K. K. Fjelde, "Hybrid flux-splitting schemes for a two-phase flow model", *Journal of Computational Physics*, vol. 175, no. 2, pp. 674–701, 2002.

[73] P. K. Sweby, "High resolution schemes using flux limiters for hyperbolic conservation laws", *SIAM journal on numerical analysis*, vol. 21, no. 5, pp. 995–1011, 1984.

[74] M. Prebeg, T. Flåtten, and B. Müller, "Boundary and source term treatment in the large time step method for a common two-fluid model", in *The 11th International Conference on CFD in the Minerals and Process Industries*, 2015, pp. 7–9.

[75] C. Cook, S Balachandar, J. Chung, and L Vu-Quoc, "A generalized characteristic-based split projection method for Navier-Stokes with real fluids", *International Journal of Heat and Mass Transfer*, vol. 124, pp. 1045–1058, 2018.

[76] U. J. F. Aarsnes, B. Açıkmeşe, A. Ambrus, and O. M. Aamo, "Robust controller design for automated kick handling in managed pressure drilling", *Journal of Process Control*, vol. 47, pp. 46–57, 2016.

[77] F. Crouzet, F. Daude, P. Galon, J.-M. Hérard, O. Hurisse, and Y. Liu, "Validation of a two-fluid model on unsteady liquid–vapor water flows", *Computers & Fluids*, vol. 119, pp. 131–142, 2015.

[78] G. B. Wallis, "One-dimensional two-phase flow", 1969.

[79] H Bansal, W Schilders, N van de Wouw, L Iapichino, and B Koren, "Modified sound speed for the unification of single-phase and two-phase flow scenarios", 2017.

[80] C. G. da Silva Santim and E. S. Rosa, "Roe-type riemann solver for gas–liquid flows using drift-flux model with an approximate form of the Jacobian matrix", *International Journal for Numerical Methods in Fluids*, vol. 80, no. 9, pp. 536–568, 2016.

[81] C. H. Whitson and M. R. Brulé, *Phase behavior*. Henry L. Doherty Memorial Fund of AIME, Society of Petroleum Engineers, 2000, vol. 20.

[82] A. Nikoofard, T. A. Johansen, and G.-O. Kaasa, "Design and comparison of adaptive estimators for under-balanced drilling", in *2014 American Control Conference*, IEEE, 2014, pp. 5681–5687.

[83] P. V. Suryanarayana, R. N. Vaidya, and J. Wind, "Use of a new rate-integral productivity index in interpretation of underbalanced drilling data for reservoir characterization", in *Production and Operations Symposium*, Society of Petroleum Engineers, 2007.

[84] R. Dautray and J.-L. Lions, *Mathematical analysis and numerical methods for science and technology: volume 3 spectral theory and applications*. Springer Science & Business Media, 2012.

[85] R. Freeman and P. V. Kokotović, "Backstepping design of robust controllers for a class of nonlinear systems", in *Nonlinear Control Systems Design 1992*, Elsevier, 1993, pp. 431–436.

[86] M. Krstic and A. Smyshlyaev, *Boundary control of PDEs: A course on backstepping designs*. SIAM, 2008.

[87] H. Hochstadt, *Integral equations*. John Wiley & Sons, 2011, vol. 91.

[88] K. Yoshida, *Lectures on differential and integral equations*. Interscience Publishers, 1960, vol. 10.

[89] R. Vazquez and M. Krstic, *Control of turbulent and magnetohydrodynamic channel flows: boundary stabilization and state estimation*. Springer Science & Business Media, 2008.

[90] T. Kailath, *Linear systems*. Prentice-Hall Englewood Cliffs, NJ, 1980, vol. 156.

[91] R. Vazquez and M. Krstic, "Boundary control and estimation of reaction–diffusion equations on the sphere under revolution symmetry conditions", *International Journal of Control*, vol. 92, no. 1, pp. 2–11, 2019.

[92] J.-M. Coron and H.-M. Nguyen, "Null controllability and finite time stabilization for the heat equations with variable coefficients in space in one dimension via backstepping approach", *Archive for Rational Mechanics and Analysis*, vol. 225, no. 3, pp. 993–1023, 2017.

[93] A. Zettl, *Sturm-liouville theory*, 121. American Mathematical Soc., 2010.

[94] L. Camacho-Solorio, S. Moura, and M. Krstic, "Robustness of boundary observers for radial diffusion equations to parameter uncertainty", in *2018 Annual American Control Conference (ACC)*, IEEE, 2018, pp. 3484–3489.

[95] D. Kirkham, "Graphs and Formulas for Zeros of Cross Product Bessel Functions", *Journal of Mathematics and Physics*, vol. 36, no. 1-4, pp. 371–377, Apr. 1957, ISSN: 00971421.

[96] R. Vazquez, M. Krstic, and J.-M. Coron, "Backstepping boundary stabilization and state estimation of a 2×2 linear hyperbolic system", in *2011 50th IEEE conference on decision and control and european control conference*, IEEE, 2011, pp. 4937–4942.

[97] A. D. Polyanin and A. V. Manzhirov, *Handbook of mathematics for engineers and scientists*. CRC Press, 2006.

[98] U. J. F. Aarsnes, F. Di Meglio, S. Evje, and O. M. Aamo, "Control-oriented drift-flux modeling of single and two-phase flow for drilling", in *Dynamic Systems and Control Conference*, American Society of Mechanical Engineers, vol. 46209, 2014, V003T37A003.

[99] J. Auriol and F. Di Meglio, "Minimum time control of heterodirectional linear coupled hyperbolic PDEs", *Automatica*, vol. 71, pp. 300–307, 2016.

[100] M. Krstic and A. Smyshlyaev, "Backstepping boundary control for first-order hyperbolic PDEs and application to systems with actuator and sensor delays", *Systems & Control Letters*, vol. 57, no. 9, pp. 750–758, 2008.

[101] R. Vazquez and M. Krstic, "Boundary control of coupled reaction-diffusion systems with spatially-varying reaction", *IFAC-PapersOnLine*, vol. 49, no. 8, pp. 222–227, 2016.

RÉSUMÉ

Lors du forage d'un puits de pétrole, il est courant de subir un influx non désiré de fluides provenant du réservoir. Ce manuscrit porte sur l'étude de la dynamique de l'écoulement en résultant dans le réservoir et le puits, pendant les opérations de forage à pression contrôlée (MPD en Anglais). La modélisation repose sur des équations de conservation, qui débouchent sur un modèle d'écoulement biphasique appelé *modèle à dérive de flux*. Celui-ci prend la forme d'un système hyperbolique d'équations de transport, alors que l'évolution de la pression dans le réservoir suit une dynamique gouvernée par une équation parabolique de diffusion. Nous proposons des schémas numériques permettant d'approcher les solutions de ces deux systèmes dynamiques. Nous synthétisons ensuite des observateurs permettant d'estimer le débit entrant depuis le réservoir. Ces observateurs du système couplé puits-réservoir prennent des formes différentes selon que le caractère distribué de chacune des dynamiques (puits ou réservoir) est négligé ou non. Nos estimateurs reposent sur la mesure de la pression en tête du puits, où un capteur est systématiquement installé dans les opérations de forage à pression contrôlée. L'existence d'un capteur de pression installé au fond du puits, plus rare, modifie la synthèse d'observateurs, d'une manière que nous détaillons. Pour chaque observateur, nous montrons la convergence des estimations de pression et de débit distribués vers leurs valeurs théoriques.

MOTS CLÉS

Estimation de paramètres, Forage, Modèles d'écoulements multiphasiques.

ABSTRACT

While drilling an oil well, unwanted influx of fluids from the reservoir may occur. This manuscript studies the dynamics of the resulting fluid flow in the wellbore and the reservoir, during managed pressure drilling (MPD) operations. We study the phenomena using first-principle approach that leads to a modified two phase flow model called the drift-flux model (DFM). The model takes the form of a hyperbolic system of transport equations, whereas the reservoir pressure dynamics is given by a parabolic diffusion equation. We propose appropriate numerical schemes for both. Then, we propose different observer designs to estimate the influx from the reservoir into the wellbore. The observers for the coupled wellbore-reservoir system take different forms, as we combine the distributed and the reduced order models for each system. We propose to use the choke pressure as a measurement that is typically available on a MPD operational site, i.e. topside sensing. However, availability of the bottom hole pressure modifies the observer design, in ways we detail. We show convergence of the observers to the true values of reservoir pore pressure and influx, in each case.

KEYWORDS

Parameter estimation, Drilling, Multiphase flow models.